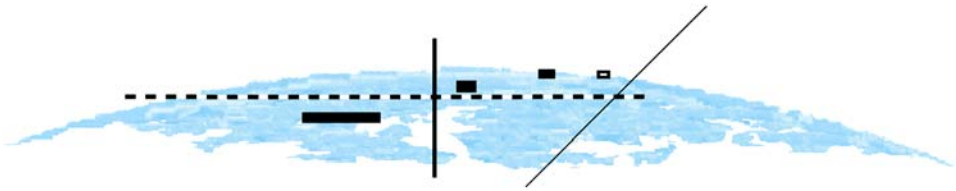

GeoForschungsZentrum Potsdam

STIFTUNG DES ÖFFENTLICHEN RECHTS

Scientific Technical Report

Advanced Algorithms of Inversion of GPS Radio Limb Sounding Data

Oleg I. Yakovlev, Alexandre G. Pavelyev, Stanislav S. Matyugov, Dmitrii A. Pavelyev, Vladimir A. Anufriev

Institute of Radio Engineering and Electronics of the Russian Academy of Scienc es

This study was carried out under the grant of the German Federal Ministry of Education and Research (BMBF) No. 01SF9922/2.

Abstract

Presently, the radio holography approach combines the radar-focused synthetic aperture principle with the perturbation method. The synthetic aperture principle is applied for constructing a reference beam using knowledge of average parameters of the atmosphere and ionosphere. The perturbation method is applied to analyze residuals in the phase and amplitude in order to find deflections in ionospheric and atmospheric parameters from expected values. As a result, radio holography proved to correspond in accuracy with the high-precision level of radio navigational GPS measurements.

The radio holographic method has a high vertical (20-30 m) and angular (8-10 micro radian) resolution. It was validated with GPS/MET and MIR/GEO data by direct observation of multi-beam propagation in the atmosphere and signals, reflected from the sea. The obtained results demonstrate the potential of the radio holography approach and open new perspectives for radio occultation experiments: measurements of the characteristics of the natural processes in the atmosphere, mesosphere and ionosphere, for observations of the state of the sea surface by measuring parameters of reflected signal simultaneously with radio occultation experiments.

Radio holography may be used also for evaluating electromagnetic fields along the trajectory of a satellite with the objective of revealing diffraction and multi-beam propagation effects to determine the location of caustic zones and to investigate various scattering phenomena (turbulence, influence of rain and convection regions, observation of wind shear regions in mesosphere, etc.). Experimental observations of these effects are important for studying telecommunication conditions in the near-Earth's space, as well as for advances in the theory of radio wave propagation in the ionosphere and atmosphere.

This study was carried out in preparation of the radio occultation measurements of the CHAMP satellite mission within the framework of the "GPS Atmosphere Sounding" strategy fund project of the German Helmholtz centers GFZ, DLR, AWI and GKSS.

CONTENTS

page

Introduction

During 1990-1998 in Institute of Radio Engineering and Electronics of Russian Academy of Sciences (IRE RAS) practical testing of radio occultation method for monitoring the atmosphere and ionosphere of the Earth was carried out using telecommunication line between the orbital station MIR and geostationary satellite [*Yakovlev et al.,* 1995a, 1995b; *Yakovlev,* 2001].

Radio occultation sounding of the Earth's atmosphere using the radio signals of Global Positioning System (GPS) can be a valuable source of information about atmospheric variables [*Ware et al.,*1996*; Rocken et al.,* 1997; *Kursinski et al.,* 1997]. Radio occultation measurements give accurate altitude distribution of electron density in the ionosphere also as it follows from results obtained by *Hajj et al*., [1994]; *Leitinger et al*., [1997]; *Hajj and Romans* [1998]; *Schreiner et al*., [1999].

Now radio occultation satellite missions are planning in different countries with aim to establish global control for the Earth's atmosphere and ionosphere. For this future missions radio occultation method must be reconstructed with accounting for experience of the first space experiments. Up to present time the main source of information for evaluation the altitude profiles was phase dependence on time in radio occultation measurements. However the amplitude data contain valuable information on the refractivity gradient altitude distribution and may be combined with phase data for achieving more vertical resolution and accuracy in atmosphere's parameters restoration. This information is important particularly for observing wave-like structures and estimation parameters of natural phenomena in the upper atmosphere. To heighten resolution in radio occultation analysis *Pavelyev* [1998] and *Hocke et al*., [1999] suggested radio holographic approach. This approach is now deriving under joint partnership relations between IRE RAS and GFZ-Potsdam.

The final report contains description of the results obtained in IRE RAS during the six stages of works owing to calendar plan of joint investigations with Potsdam Geophysical Scientific Centre (GFZ-Potsdam). The plan of the work that must be fulfilled in IRE RAS during 1999-2000 years consists in:

1. Designing unified program for derivation of bending angle.
2. Modular program structure, documentation.
3. Test and validation of program using GPS/MET data (temperature profiles, atmospheric irregularities, turbulence, inversion layers).
4. Designing program module for optimal work in anti-spoofing regime.

5. Developing program module for ionospheric correction and revealing ionospheric features (irregularities, turbulence, sharp layers).
6. Modification of program of spectral analysis for obtaining optimal resolution, diminishing errors and error estimation (contribution for receiving more information on atmospheric processes, e.g. gravity waves, features of water vapour distribution).

Optimization and validation of the program code of the radio holographic method for the operational analysis of GPS radio limb sounding data were the major tasks. Another goal of the study was look to for a possibility to obtain the new supplementary information about atmospheric and ionospheric parameters.

The aim of the work described in Chapter 1 consists in measuring degree of atmospheric inhomogeneity (corresponding to stable and perturbed atmosphere) and determining characteristics for quantitative description of atmosphere's state. Two different approaches may be used for description of atmospheric irregularities: i) using intensity of statistical irregularities of the refraction index, for example, parameter C_n^2, parameter C_T^2 or some other; ii) determining regular stable layers in the atmosphere especially at the tropopause level.

MIR/GEO radio occultation amplitude data obtained in centimetre wavelength range was used for analysis of statistical inhomogeneities of the atmosphere. The high signal to noise ratio and smaller wavelength value allow to reveal detailed vertical structure of the atmosphere with heighten spatial resolution comparing with decimetre range.

The methodology of radio occultation measurements and data handling are described in the section 1.1 and 1.2. Method for determining degree of atmospheric irregularities had been presented in the section 1.3. Connection between temporal spectrum of the amplitude fluctuations and spatial spectrum of the refraction index irregularities are analysed in the section 1.4. This results may be used for decimetre wavelength range also. The expected values of amplitude variations are estimated in the section 1.5 for wavelength $\lambda = 19$ cm using MIR/GEO data. This estimation may be used for determining turbulence effects in the atmosphere from amplitude data during CHAMP mission.

The goal of Chapter 2 is to analyse phase and frequency fluctuations stipulated both the atmospheric inhomogeneities and technical reasons.

In Chapter 3 current state of problem of accounting for for ionospheric contribution is considered and a basic methodology for designing analytical radio physical model is derived including connections between the phase path, bending angle and amplitude in radio

occultation measurements. The derived methodology has been used for developing radio physical model and program module for ionospheric correction in radio occultation experiments. The alternative methods for subtracting of the upper ionosphere contribution are also considered. Application of method of low frequency noise filtration for revealing features in E- and D- layer of ionosphere is described in the last part of this chapter.

General description of radio holographic method and its validation using GPS/MET radio occultation data contains in the fourth chapter of report.

1. Amplitude scintillation and development of technique of the atmospheric turbulence estimation

1.1. Conditions of radio occultation experiments

The radio occultation experiments were being carried out on the orbital station MIR–geo-stationary satellite link when the station was going in the Earth's shadow relative to the geo-stationary satellite. The experiment geometry is shown in Fig. 1.1. The centre of the Earth is shown in this Figure by the point O. The Earth's radius is denoted by the symbol a and the position of the station MIR, which radiated a radio signal with wavelength λ =2 cm is denoted by the point A. The maximum–gain axis of the transmitting antenna of the station MIR was oriented on a tangent to the earth surface in the direction of a geostationary satellite at radio occultation measurements. On moving the station MIR the minimal altitude of the ray H_0 in the point C that is in the perigee of the ray decreased, which provided "slit" of the atmosphere. The distortion of the ray AB because of the refraction in the atmosphere in Fig. 1.1 is not shown. The radio waves having past through the atmosphere were being received on the geostationary satellite in the point B, which had the receiving antenna with the high–gain, oriented in the direction of the station MIR. The received signal was amplified and retranslated without a phase distortion on the ground receiving station. The application of the gain antenna on the station MIR and on the geo-stationary satellite provided a high signal /noise ratio that increased the measurement accuracy of the signal amplitude.

In the experiments two geostationary satellites – retranslators (western and eastern) were used. The first geostationary satellite was over the meridian 16°W and the second was over the meridian 95°E. The orbital plane angle of the station MIR equal to 52° allowed radio occultation measurements to be carried out in the Southern and Northern hemispheres in the latitude intervals from 0 up to 52°. The research of the regions in the belt ±2.5° in relation to average meridians 60.5°E and 171.5°E was possible. The measurements have been realised over the Indian Ocean, over the northern part of the Pacific Ocean and also over the territory of Kazakhstan. The meteorological conditions in these regions strongly differ, which results in the appearance of features in experimental dependencies of the field strength E on the minimal altitude of the ray H_0. In this report we analyse dependencies $E(H_0)$ for the southern region

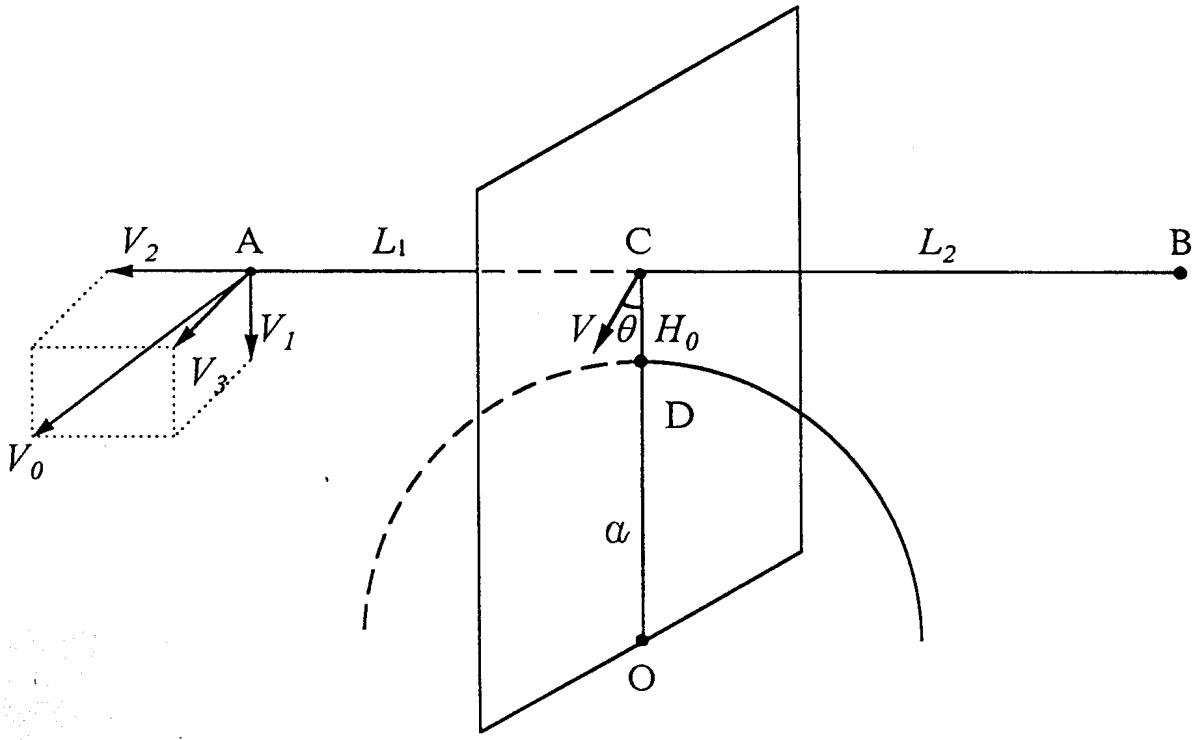

Figure 1.1 Geometry of problem. Phase screen and ray path.

of the Indian ocean with the latitudes from 40°S up to 52°S and the average longitude 60.5°E, where 24 radio occultations have been curried out.

Let us give the main parameters essential for the analysis of the amplitude scintillation: distances from the station MIR and from the geo-stationary satellite up to the probed atmospheric area AC=L_1=2100÷2500 km and BC=L_2=41700 km accordingly; the radius of the first Fresnel zone $r=[\lambda L_1L_2/(L_1+L_2)]^{1/2}\approx 0{,}2$ km. The frequency of the amplitude scintillations F depends on the crossing velocity of atmospheric inhomogeneities by a line AB and on peculiar scales of inhomogeneities. The conditional atmospheric width along the line AB is $L\approx(2aH_a)^{1/2}\approx 600$ km, where $H_a\approx 6$ km is the height of the homogeneous atmosphere. As $L_1>>L$, in the case of weak fluctuations the effect of the atmosphere on the radio wave can be considered in the approximation of the phase screen passing through points O and C perpendicularly to the line AB. This phase screen is shown in Fig. 1.1 by the rectangle. The velocity vector of the station MIR V_0 determines the velocity of the atmospheric irregularity crossing by the ray in the phase screen plane. Let's introduce the angle θ between the tangent to the point C trajectory in the phase screen plane and OC vertical. Depending on the angle value θ different cuts of the atmosphere by the ray AB are implemented: at $\theta=0$ – vertical, at $\theta=\pi/2$– horizontal cuts of the atmosphere. In the Greenwich coordinate system, in which the point B is fixed, the velocity of the station is expressed by its components: $V_0=(V_1^2+V_2^2+V_3^2)^{1/2}$, where V_1 is the velocity component in a plane AOB perpendicular to the straight line AB, V_2 is the velocity component along the straight line AB, V_3 is the velocity component perpendicular to the plane AOB (Fig. 1.1). Let's notice, that $\theta=arctg(V_3/V_1)$ and the velocity of the atmospheric inhomogeneity intersection by the line AB in the point C, without taking into account the refraction $V=(V_1^2+V_3^2)^{1/2}L_2(L_1+L_2)^{-1}\approx(V_1^2+V_3^2)^{1/2}$. During our measurements the values V_0, V_1, V_2, V_3 and θ were in the following limits: $V_0\approx 7.31$ km/s, $V_1\approx 1.8\div 2.6$ km/s, $V_2\approx 4.9\div 6.9$ km/s, $V_3\approx 1{,}0\div 4.9$ km/s and $\theta\approx 23\div 71°$.

The signal registration started 8 minutes before the ray perigee reached the altitude $H_0\approx 40$ km and finished after the miss of the signal. The changes of the signal amplitude due to the atmospheric influence were being observed for 60÷90 seconds depending on the velocity value V_1. The received signal was detected by the linear detector with a dynamic range 50 dB and time constant equal to $2\cdot 10^{-3}$ sec. The readings of the potential difference U_j, appropriate to the received signal, were carried out with the frequency 150 Hz; an analog–to–digital

converter digitised them.

After the signal registration termination the measurements of the amplitude characteristic of the communication link between the station MIR – geo-stationary satellite – ground receiving station were made. At these calibration measurements the receiving antenna of the geo-stationary satellite (GEO) were directed to the ground measuring station. The transmitter with an antenna similar to those used on the station MIR mounted on the ground station transmitted the signal in the GEO direction. Furthermore the received signal was relayed to the Earth, where its registration was established. Thus, this signal passed through the same path as at the occultation measurements. Such a calibration by the stepping of emitted power of the transmitter similar to the one set on the station MIR was made over the range of signal level changes observed at the occultation. According to the calibration data obtained the through gain characteristic of the communication link was determined which was taken into account while processing the data of radio occultation measurements.

1.2. Primary data processing

The signal $U(t)$ registered on the ground receiving station corresponds to the changes of the field strength $E(H_0)$ in the location of the GEO while the station MIR is going in the Earth's shadow. At the first stage of the data processing the measurements $U(t)$ were corrected with allowance for the through gain characteristic of the communication link. Then the dependencies of the potential on time $U(t)$ were transformed into the dependencies of the potential on the minimal altitude of the ray $U(H_0)$. For the definition of H_0 the minimal ray altitude using the MIR/GEO trajectory data was evaluated and the refraction effect on the basis of the model of the exponential altitude profile of the refractivity $N(h)$ was taken into account, where h is the altitude from the Earth surface. The model $N(h)$ parameters were selected with allowance for the available data about surface values of the refractivity. In our estimations the errors of altitude binding can reach ±1 km in the stratosphere and ± 0,5 km in the troposphere. On the measurement space appropriate to altitudes H_0 =50÷70 km the mean value of potential U_0 proportional to the field strength in the free space E_0 was determined. The U_j readings normalisation to the value appropriate to the radio wave propagation in the absence of refraction $E_j = U_j / U_0$ was effected further. So the field strength normalised to level of the radio wave propagation in the absence of refraction $E(H_0)=E_j / E_0$ was determined, therefore $E(H_0 >40)=1$. At the analysis of $E(H_0)$ changes the altitude dependencies of the

fluctuation dispersion σ^2 and the spectra of the field strength fluctuations *G(F)*, (here *F* is the frequency of amplitude scintillation) were determined.

The field strength fluctuation dispersion was calculated as

$$\sigma^2 = \frac{1}{m}\sum\left[\frac{E_j - \langle E\rangle}{\langle E\rangle}\right]^2, \qquad (1.1)$$

where E_j is a measured value, $\langle E\rangle$ is its average , *m* is the number of samples. At the σ^2 definition the number of E_j value indications depended on the time interval Δt. The time interval was selected under the condition that the minimal ray altitude varies on ΔH_0 =2 km in the Δt time. At ΔH_0 =2 km the number of *m* samples at the σ^2 calculation varied from 150 – at stratosphere probing – up to 2000 at the troposphere bottom probing. The spectrum of the scintillations *G(F)* was determined according to the program of the fast Fourier transform, thus the data observed at the intervals $\Delta t \approx 2\div4$ s, appropriate to the altitude intervals $\Delta H_0 \approx 3\div5$ km were used. The regular decrease of the field strength average level at the Δt intervals was taken into account at σ^2 and *G(F)* definition with the help of a linear approximation. The obtained values of spectral density *G(F)* were smoothed on the rectangular window, which width meets the condition $F/\Delta F$=2.

The typical dependencies of the field strength *E* on the ray altitude H_0 are shown in Fig. 1.2. Curves 3 in Fig. 1.2 show a fragment of typical measurements of the signal amplitude at the altitude interval from 50 up to 85 km, where the atmospheric influence was absent; they give a representation about small *E* fluctuations due to equipment factors. When the station MIR is going in the Earth's shadow the field strength mean value decreases and the scintillation due to the atmosphere start to show themselves simultaneously. The $E(H_0)$ dependencies in Fig. 1.2 represent a typical pattern of the radio wave fluctuations with strong spikes (focusings) and deep fadings. The decrease of an average $\langle E\rangle$ level is determined by refractive attenuation and absorption of centimetre radio waves; these effects were analysed in *Yakovlev et al,* [1995a], therefore they are not considered here.

In view of the diversity of meteorological conditions in different regions we have conditionally divided the $E(H_0)$ dependencies into two qualitatively different groups. The

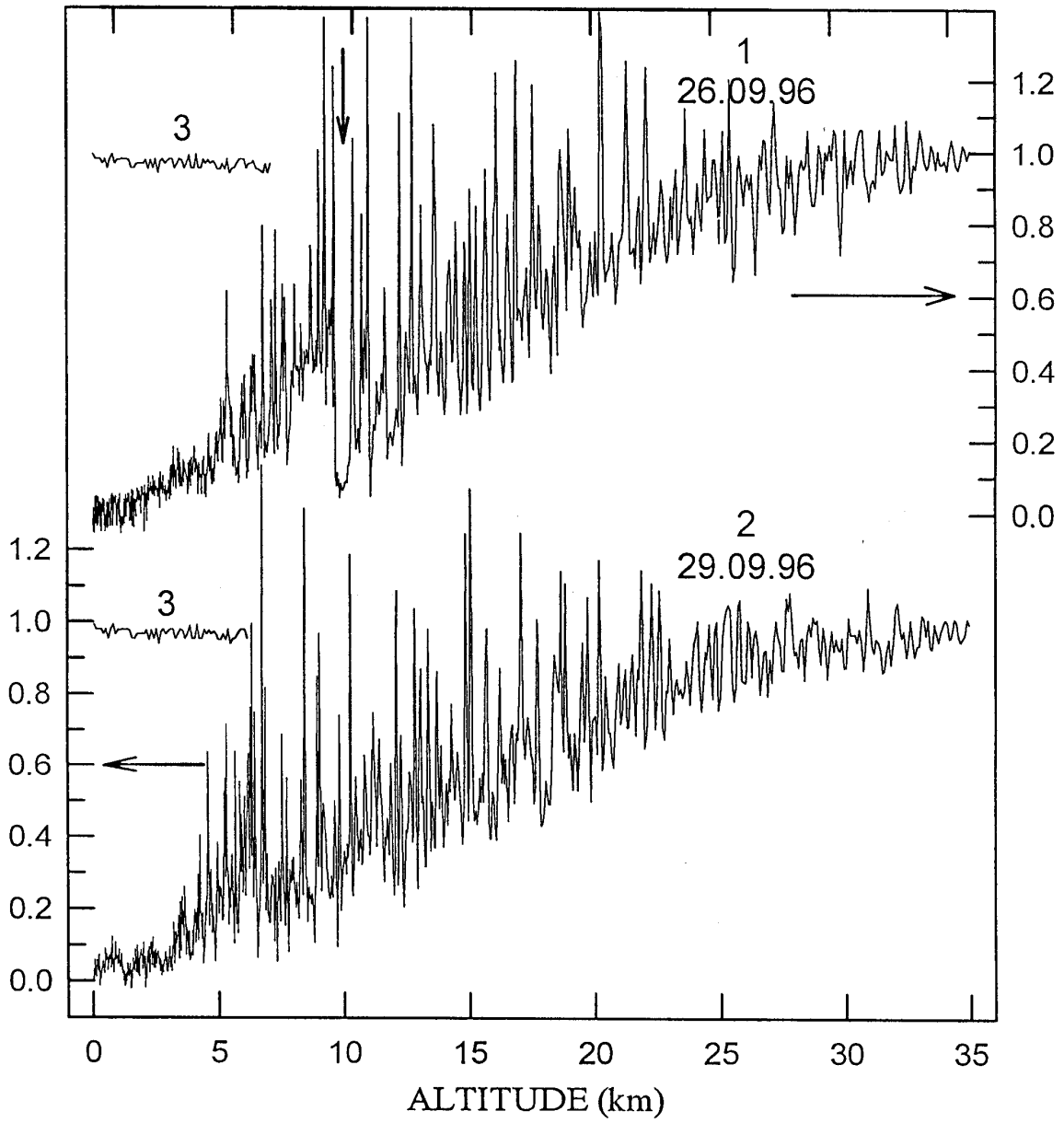

Figure 1.2. Typical dependences of field strenght
from the minimum altitude of ray path.

first group included measurement sessions in which the sharply expressed regular $E(H_0)$ change is observed in the field of the tropopause, i.e. in the interval of the altitudes $H_0 \approx 9 \div 13$ km. Curve 1 in Fig. 1.2 belongs to this group, where the vertical arrow indicates strong E change in the field of the tropopause. In Fig. 1.3 the examples, typical of the first group, of the $E(H_0)$ dependence are shown in the field of the tropopause; the stretched horizontal scale allows to see a thin structure of the E change in this area. In Fig. 1.3 the E=1 values correspond to the condition of the radio wave distribution in the absence of the refraction, when the atmospheric influence is absent, and E=0.5 corresponds to the average refractive weakening for H_0=9÷14 km are visible. Sharp changes of the field strength from $E \approx 0.2$ up to $E \approx 1.5 \div 2$ due to focusing by thin stratified inhomogeneities of the atmosphere are seen on curves 1 and 2 in Fig. 1.3. The absence of the influence of the obviously expressed stratified structures is characteristic for the second group of dependencies $E(H_0)$ not only in the interval of 10÷13 km, but also in the troposphere at the altitudes lower than 7 km. The measurement sessions with a higher level of random fluctuations on the altitudes more than 13 km and the absence of a strong focusing effect in the field of a tropopause were ganged in the second group. The dependence $E(H_0)$, shown in Fig. 1.2 curve 2 represents this group.

1.3. RMS amplitude fluctuations and degree of atmospheric turbulence

At first we shall consider dependencies of the rms amplitude fluctuations on a minimal altitude of the ray $\sigma(H_0)$. In Fig. 1.4 σ values obtained at the processing of the dependencies $E(H_0)$ for six measurement sessions included in the first group are shown by different symbols. In this Figure a strong dispersion of the σ values on the altitudes from 0.5 up to 13 km, connected with the fact that both random oscillations and regular spikes and fadings E contribute to σ. In the stratospheric area at H_0 >15 km the values σ are not large and they decrease with increasing the altitude H_0. Fig. 1.5 gives the dependence $\sigma(H_0)$, obtained according to the data of six measurement sessions included in the second group. The regular increase σ with decreasing H_0 from 35 up to 14 km, a relative persistence of fluctuation intensity in the altitude interval from 14 up to 8 km and the decrease σ in the troposphere at decreasing H_0 from 8 up to 0.5 km are characteristic for this group. In measurement sessions, shown in Fig. 1.5, the main contribution to the field strength scintillation is made

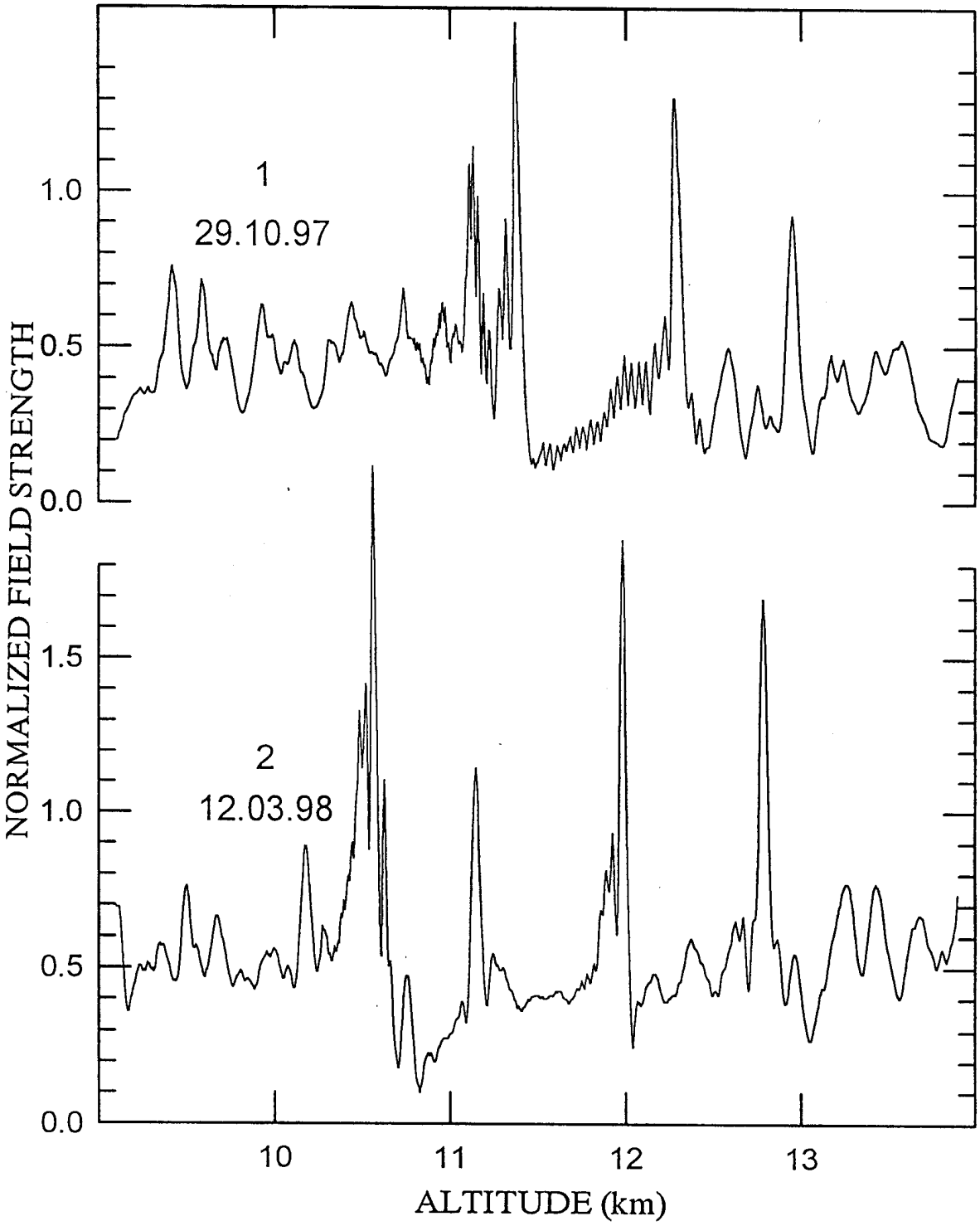

Figure 1.3 Examples of field focusing by layered formations to the tropopause.

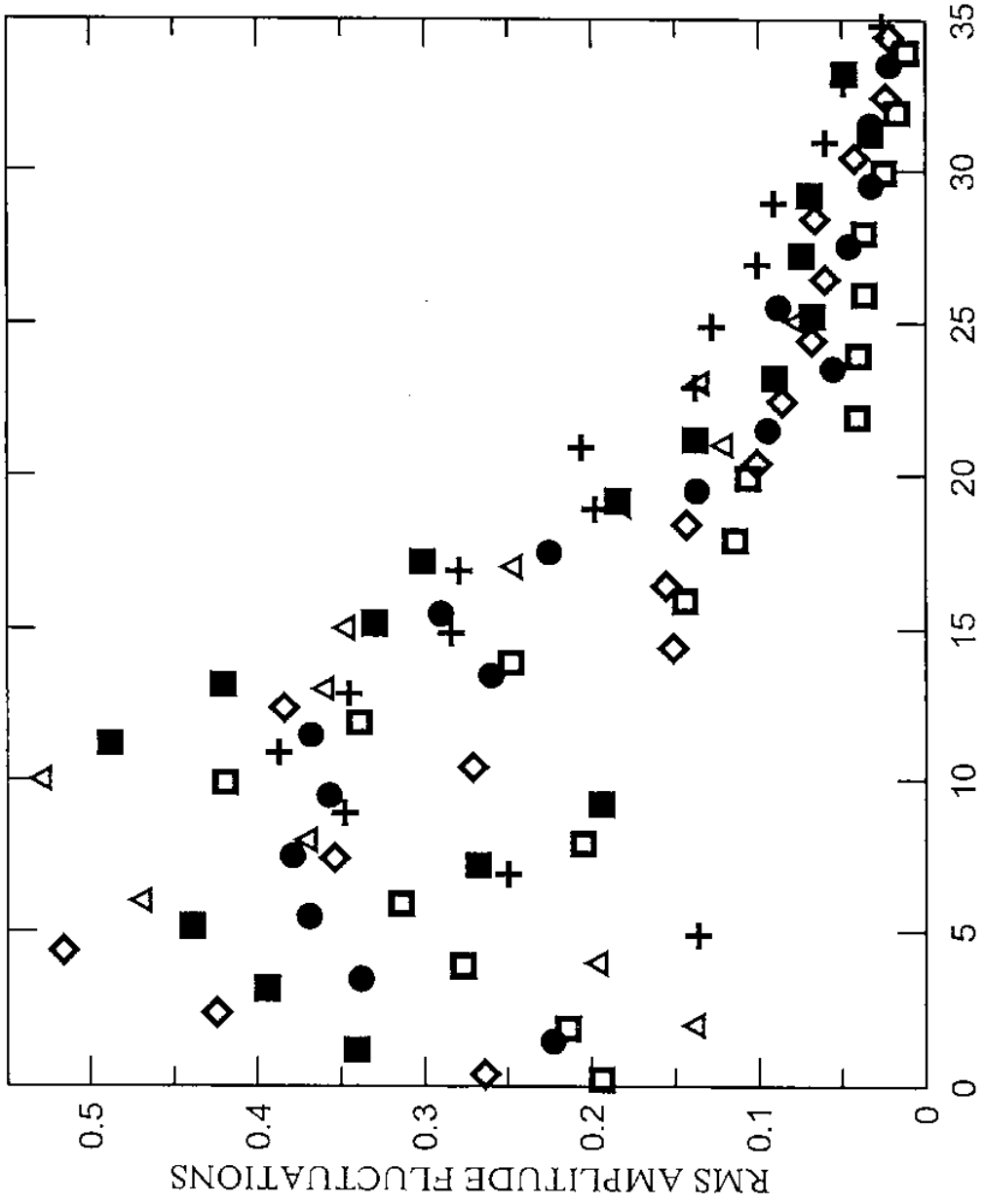

Figure 1.4. RMS amplitude fluctuations as a functions of altitude H_0 for first group of measurements: + – 26 Sep 1996, 45°S, 58.2°E; ● – 11 Mar 1998, 50.8°S, 59.6°E; □ – 12 Mar 1998, 41.7°S, 62.1°E; △ – 17 Mar 1998, 52.0°S, 59.2° E; ◇ – 16 July 1998, 46.3°,60.8°E; ■ –17 July 1998, 49.1°S, 60.3°E.

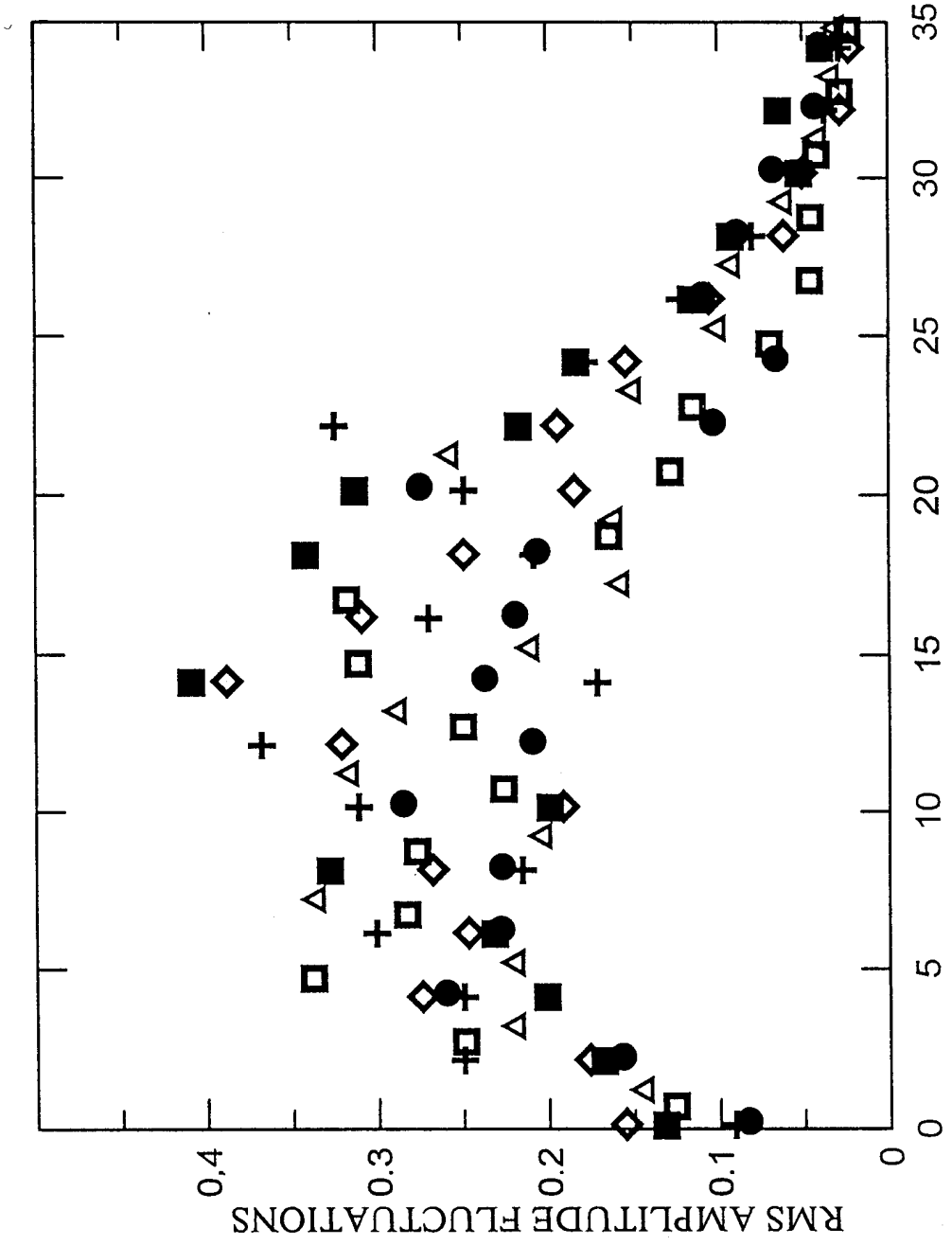

Figure 1.5. RMS amplitude fluctuations as a functions of altitude H_0 for second group of measurements: ● – 28 Nov 1997, 47.9°S, 61.2°E; □ – 01 Dec 1997, 48.4°S, 61.2°E; Δ – 02 Dec 1997, 43.2°S, 62.3°E; ◇ – 03 Dec 1997, 46.5°, 61.7°E; ■ – 04 Dec 1997, 40.1°S, 62.9°E; + – 05 Dec 1997, 44.1°S, 62.3°E.

by random inhomogeneities of the refractive index, and the contribution of stratified structures is negligible here. By comparing Fig. 1.4 and 1.5 we get that in the second group of measurements a higher intensity of amplitude fluctuations in the stratosphere is regularly observed. For example, at H_0 =20 km for the first and second groups the values σ are accordingly equal 0.14 and 0.23.

Let's analyse the dependencies $\sigma(H_0)$ and reveal the features, which can be used at the estimation of the atmospheric turbulence degree by the radio occultation technique. Two factors, not connected with the turbulence immediately, affect the dependence $\sigma(H_0)$. They are the mean altitude profile of the refractivity $N(h)$ and the refractive attenuation of the field strength X. We shall take into account the influence of the first factor – $N(h)$, considering relative fluctuations of the refractivity $\Delta N/N$. The values $\langle E\rangle$ differ from X only by radio wave absorption therefore it is possible to consider that $\langle E\rangle=X$ at $H_0 \geq 5$ km. From the wave propagation theory in a random medium it follows, that σ is proportionally rms deviation ΔN, therefore relative discontinuity of the environment in our problem can be characterised by the factor $\Delta N/N \sim \sigma/N$ [*Ishimaru,* 1978]. It is the second factor, i.e. the influence of the refractive attenuation on the scintillation intensity that we shall take into account according to [*Woo et.al*., 1980b; *Gurvich,* 1989]. According to the data of these publications in the case of the isotropic Kolmogorov spectrum the refractive attenuation decreases the fluctuations as consistent with a relation

$$\sigma=\sigma_1 X^{5/6}. \qquad (1.2)$$

Here σ_1 is rms values of the amplitude scintillations, which would take place if a statistically isotropic medium without refraction were present instead of the real atmosphere with a strong refraction, X being refractive attenuation of the field strength. The experimental dependence $\sigma(H_0)$, shown in Fig. 1.5, confirms this theory conclusion. In fact, the decrease of the fluctuation intensity of the field strength with dropping the altitude H_0 is observed for $H_0<$ 8 km. The same tendency is also seen in Fig. 1.4, though the influence of stratified inhomogeneities of the troposphere results in a strong dispersion of experimental values of σ. Thus, as the characteristic of the turbulence degree of the atmosphere at radio occultation monitoring one can take the dependence

$$\Phi(H_0)=\sigma(H_0)\langle E(H_0)\rangle^{-5/6}[N(H_0)]^{-1}. \qquad (1.3)$$

For the characterisation of $\Phi(H_0)$ we use our experimental dependencies $\sigma(H_0)$, $X(H_0)$ and the known altitude profile of the refractivity $N(H_0)$. In Fig. 1.6 the results of the definition

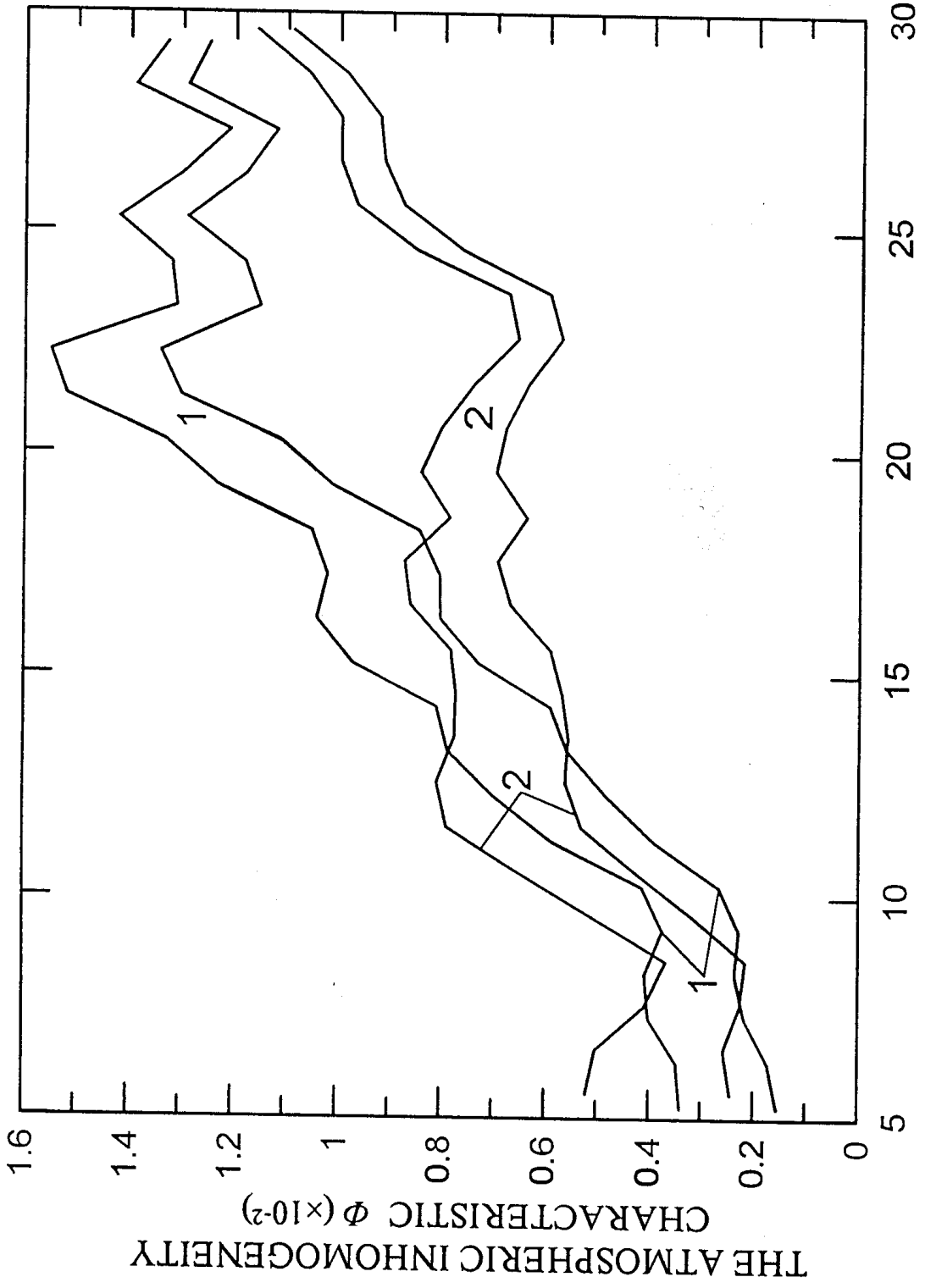

Figure 1.6. Typical dependences of value Φ on altitude Ho.

of the $\Phi(H_0)$ dependence are presented: curve 1 corresponds to average values of σ according to the data of Fig. 1.5, and the dependencies 2 are obtained for σ in Fig. 1.4. While making use of the dependence $\sigma(H_0)$ the averaging of the σ values at the altitude intervals ΔH_0 =1 km was realised. In Fig. 1.6 solid curves correspond to the dependence σ/N, when the influence of the refractive attenuation on the fluctuation intensity is not taken into account, and the dotted curves correspond to (1.3), i.e. the influence of refractive attenuation is taken into consideration.

From the comparison of curves 1 and 2 in Fig. 1.6 it follows, that the values of the atmospheric inhomogeneity characteristic Φ for the first and second measurement groups for the stratospheric area differ strongly enough. For the second measurement group, when there are no explicitly defined focusing or decreasing the field strength caused by the stratified structures, when they are destroyed by the increased atmospheric turbulence, $\Phi(H_0)$ has an increased value in the stratosphere, i.e. at the altitudes of 22 ÷30 km. In this interval of altitudes Φ does not depend on H_0, but at H_0 < 20 km the monotonous decrease of Φ is seen with the decrease of the altitude H_0. The fast decrease of Φ while changing the altitude from 30 up to 23 km, small values at H_0 =22÷24 km and, practically, the persistence Φ in the interval of altitudes H_0 =13÷22 km are peculiar for the first group of measurements. Apparently, rather weak atmospheric turbulence was at the altitudes of 24÷18 km in this case. For H_0 <13 km in the first group Φ has a greater value than in the second measurement group. It is connected with the fact that the stratified structures present in the first group give the considerable contribution to the experimental values of σ. Thus, the characteristics $\sigma(H_0)$ or $\Phi(H_0)$ for H_0<13 km do not give any objective information about the atmospheric turbulence in this case. In the case of the stable atmosphere, when the turbulence is not large and the inversion stratified structures appear, one should eliminate the contribution of such structures into σ and, therefore, in the characterisation of the turbulence $\Phi(H_0)$.

1.4. Amplitude spectra and spectra of the refractive index fluctuations

We shall consider the behaviour of the amplitude scintillation spectra $G(F)$ for different altitudes H_0. In Fig. 1.7 the examples of spectra $G(F)$, observed at the radio

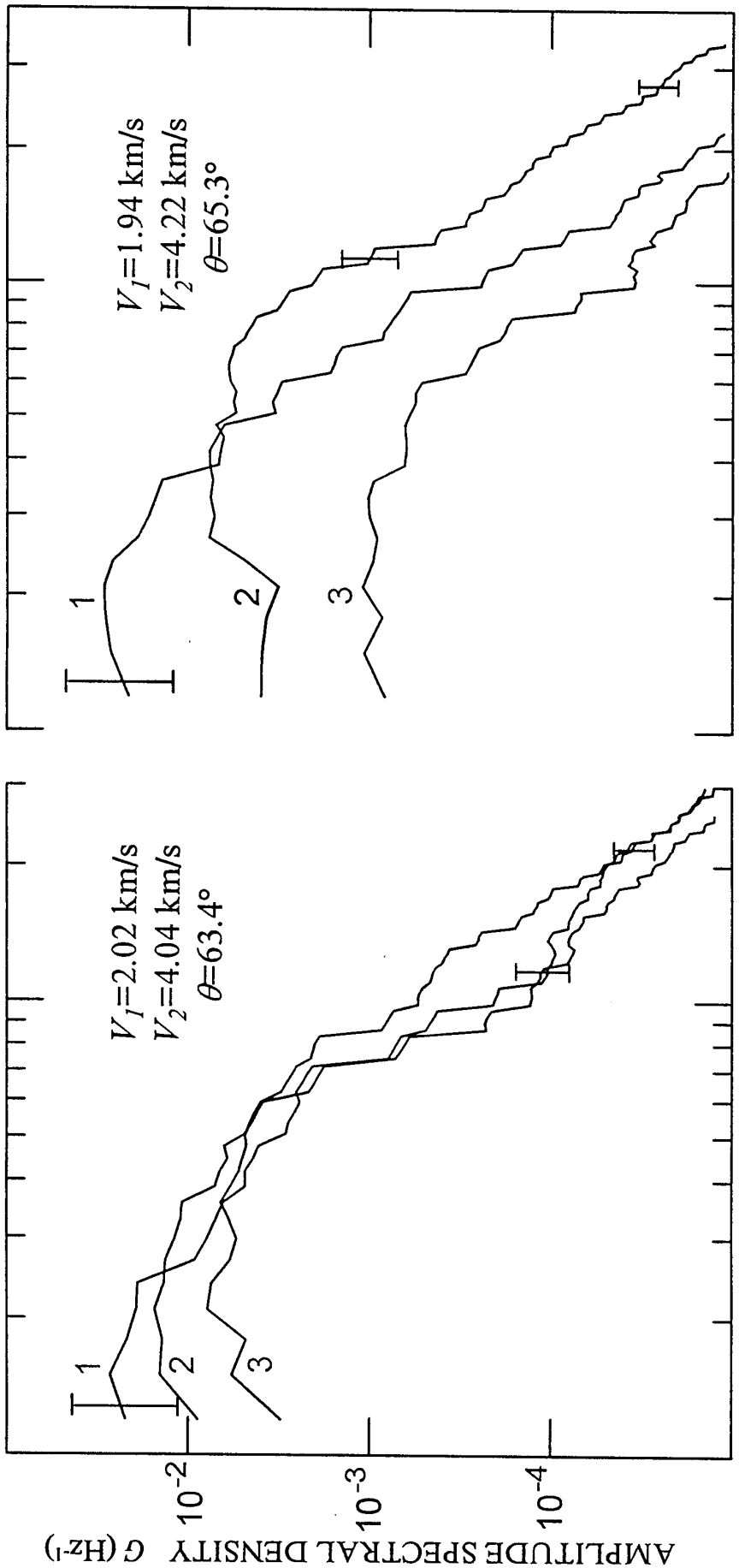

Figure 1.7. Examples of amplitude scintillation spectra.
1 - Ho=7 km; 2 - Ho=22 km; 3 - Ho=26 km.

occultation measurements in two regions are shown, were F is the scintillation frequency. The conditions of measurements in these experiments were approximately identical. The angle of setting θ was equal to 63,4° in measurements above Kazakhstan, and the values of vertical, horizontal and complete velocity of the inhomogeneity transfer without taking into account the refraction were V_1=2.02 km/s, V_3=4.04 km/s and V=4.47 km/s. For measurements in a region of the Indian Ocean we had θ=65.4° , V_1=1.94 km/s, V_3=4.22 km/s and V=4.60 km/s. Spectra 1, 2 and 3 correspond to the average altitudes H_0 =7; 22 and 26 km. Vertical segments in Fig. 1.7 show 90% confidence intervals.

From the wave propagation theory in random media with a power law of the refractive index spectrum it follows that the spectrum $G(F)$ can be described by the characteristic frequency F_0 and by the law of spectral density change $G \sim F^{-n}$ at $F >> F_0$ [*Ishimaru,* 1978]. The frequency F_0 is a boundary between two areas of the dependence $G(F)$. In the first area at $F < F_0$ spectral density of fluctuations depends slightly on F and in the second area at $F > F_0$, G diminishes as $G \sim F^{-n}$ with elevation of F. The frequency F_0 is determined as a cross point of a low–frequency asymptote $G(F \to 0)$ for the first area and high–frequency asymptote $G(F>>F_0)$ for the second area. For the turbulent medium with a power law of spatial spectrum of the refractive index fluctuations the theory [*Ishimaru,* 1978] in the approximation of weak fluctuations yields the following relations:

$$F_0 \approx \gamma V (\pi \lambda L)^{-1/2}, \tag{1.4}$$

$$n = p - 1, \tag{1.5}$$

where p is the spectral index, V is the velocity of inhomogeneity intersection by the ray; $L=L_1L_2\,(L_1+L_2)^{-1}$; γ is a coefficient of the order of unity.

The atmosphere cannot be considered as a homogeneous isotropic medium at radio occultation measurements on the satellite to satellite link. The vertical gradient of the refractive index results in a form deformation of the first Fresnel zone and in decreasing the transverse velocity of ray moving in the atmosphere. It is also known that the refractive index inhomogeneities are strongly horizontally prolated in the stratosphere. These reasons should result in the change of the radio wave fluctuation spectra. The analysis of the effect of regular refraction and inhomogeneity anisotropy at radio occultation measurements was carried out in [*Woo et al.,* 1980a]. Let's further take advantage of the results of this work. According to [*Woo et al.,* 1980a] the regular refraction and inhomogeneity anisotropy do not change the spectrum form in the high–frequency area at $F > F_0$, where $G \sim F^{-n}$, which allows to

determine the values of the index n and, according to (1.5), spectral index p from the experimental dependencies $G(F)$. At the same time the effect of defocusing and anisotropy of irregularities give rise to the change of value F_0 depending on the setting angle θ.

We shall consider the dependence n and p on the altitude. The n and p values have been defined according to the results of the analysis of 214 amplitude fluctuation spectra obtained for different regions while changing the minimal altitude of the ray H_0 from 35 up to 0.3 km. The mean values of the coefficient n (left axis of ordinates) and spectral index p (right axis of ordinates) for different altitudes H_0 are shown by dots in Fig. 1.8. Each dot in Fig. 1.8 has been obtained as a result of data averaging for 15÷18 spectra and the vertical segments characterise a rms deviation of n, connected with variations of this value in the regions investigated, the broken dashed line describing the averaged experimental dependence $n(H_0)$. Three intervals can conditionally be selected in this dependence. In the troposphere at $H_0 \leq 7$ km the index n undergoes slight changes with the altitude and its average value n=2.5±0.2 corresponds well to the spectral index of the Kolmogorov spectrum $p=n+1=11/3$. In the stratosphere at H_0=15÷30 km experimental n=3.5 ± 0.2, it practically does not depend on the altitude. The spectral index p=4.5± 0.2 appropriate to this n differs essentially from the theoretical value p=11/3. At the altitudes from 7 up to 15 km n values, according to the measurement results in different regions, vary over a wide range, which is in generally caused by a different altitude of the tropopause in these regions. The linear dependence $n(H_0)$, shown in Fig. 1.8 for this altitude interval is conditional. The difference between meteorological conditions in the regions investigated and the errors of defining n stipulate a random character of the index n changes with the same H_0 value. In this connection we shall consider empirical probability density functions of n values, shown in Fig. 1.9. In Fig. 1.9 n are indicated on the horizontal axis and a relative observation frequency of n value in the interval Δn=0.3 expressed in percentage is shown on the vertical axis. The width of an interval Δn, shown in the figure by horizontal segments, corresponds to an empirical error of n definition estimated by us. In Fig. 1.9a the n distribution in the troposphere is shown by the results of the analysis of 86 amplitude scintillation spectra obtained for altitudes H_0 from 0.3 up to 8 km. The distribution of n values in the stratosphere constructed according to the data of the 96 spectra analysis, obtained at the mean H_0 values in the interval from 15 up to 35 km, is shown in Fig. 1.9b.

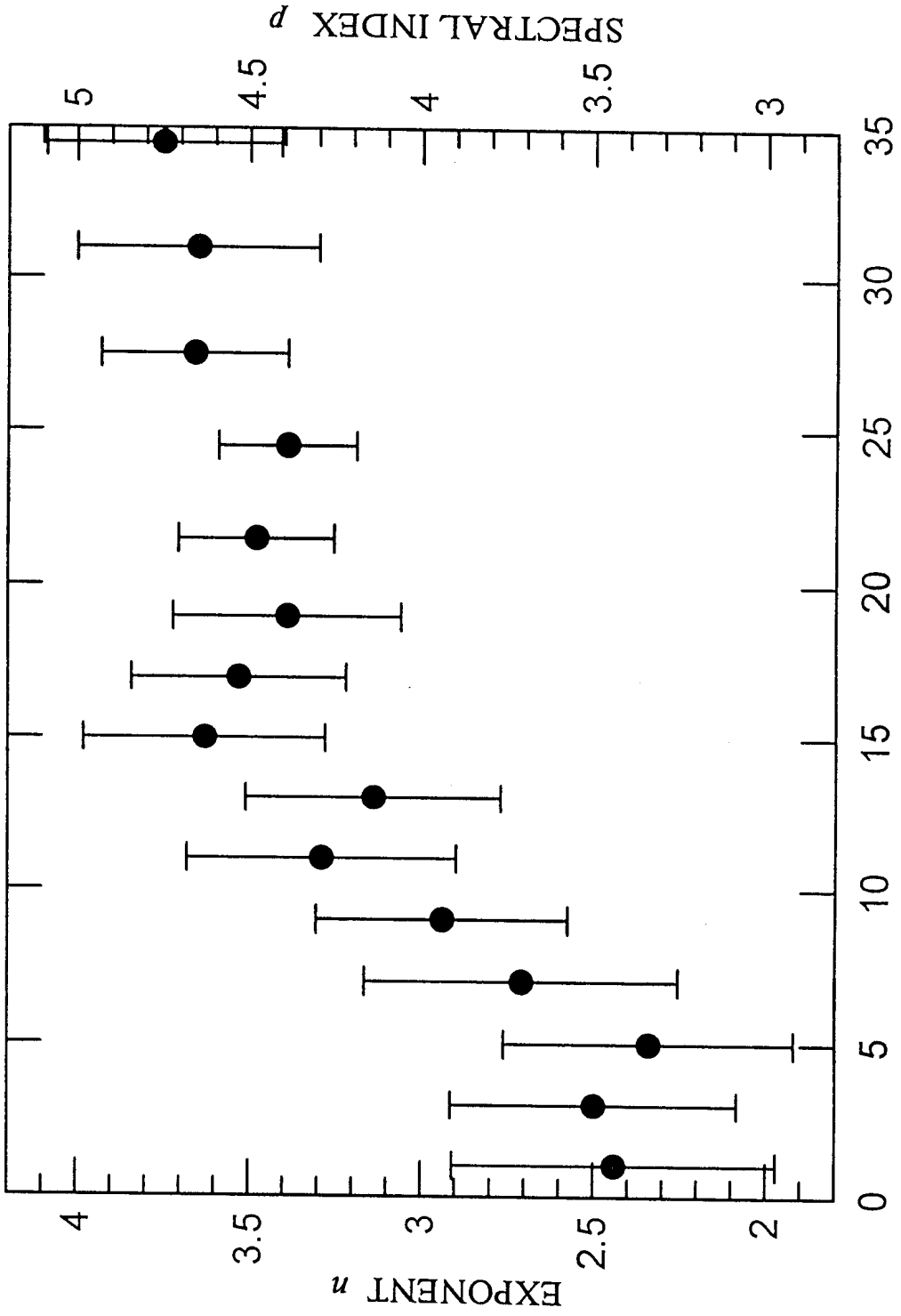

Figure 1.8. Dependence of average value of exponent n and spectral index p on the minimum ray path altitude.

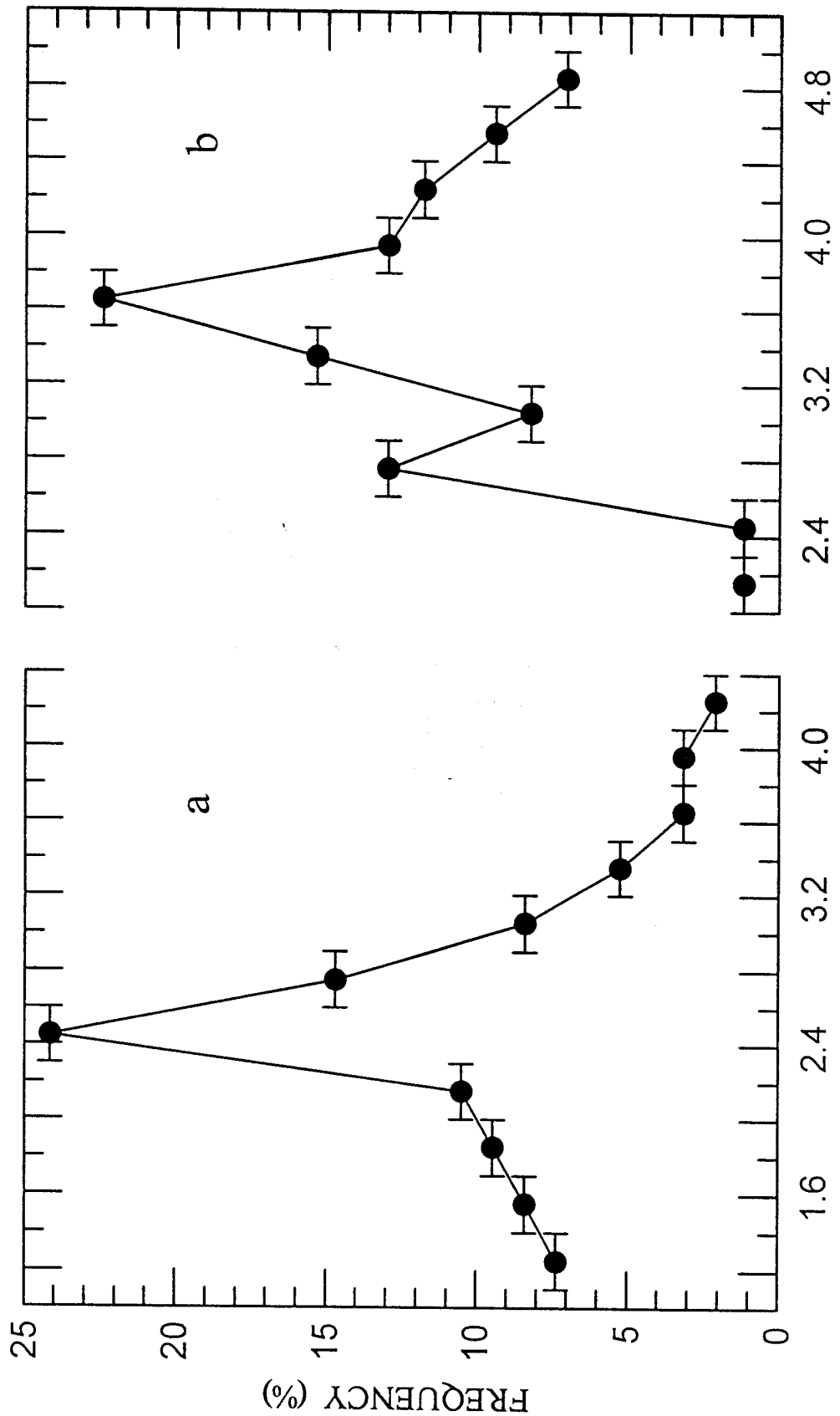

Figure 1.9. Distribution of exponent n for the troposphere (a) and for the stratosphere (b).

From Fig. 1.9 it follows, that distribution of the index n in the troposphere and stratosphere differ essentially. For the troposphere in 50% of cases n=2.5± 0.5 and the spectral index $p=n+1$=3.5± 0.5, appropriate to this value, is close to p=11/3, describing classical turbulence obeying to the Kolmogorov law. For the stratosphere in 50% of cases n=3.6± 0.5; besides an additional maximum is observed at n=2.7 in n distribution. Thus, n, corresponding to the Kolmogorov spectrum are observed only in 13% implementations.

Let's consider the other parameter describing the amplitude fluctuation spectrum, i.e. frequency F_0. The range of the F_0 variations at the radio occultation measurement of the atmosphere at altitudes from 0.3 up to 35 km has constituted from 1.2 up to 30 Hz with changing the inhomogeneity intersection velocity V by the ray in the point C (Fig. 1.1) from 2.5 up to 5.2 km/s. Formula (1.4) evaluations for such measurement conditions give the range of F_0 change from 4.7 up to 10 Hz. The reasons of experimental and theoretical difference of F_0 values are explained by the following. The spectra $G(F)$, in which the experimental F_0 values are more than theoretical ones, are observed in the troposphere, when rms fluctuations of the field strength $\sigma \geq 0.3$. In this case amplitude fluctuations cannot be considered weak any more and, as it follows from [*Fante,* 1975] the spectrum $G(F)$ broadening occurs and the characteristic fluctuation frequency F_0 does not meet the relation (1.4). At σ<0.3 the experimental F_0 values obtained by us are equal or less than theoretical ones. In the work [*Woo et al.,* 1980a] it is shown, that the atmospheric inhomogeneity anisotropy and regular refraction change F_0 values. The inhomogeneity anisotropy is characterised by anisotropy coefficient $\eta \geq 1$, determined as the ratio of a characteristic horizontal scale of the irregularities to a vertical scale. The calculations made by *Woo et al.* [1980a] show, that in that specific case $\eta = X^{-1}$ the shape of the spectrum $G(F)$ will be the same as one at the isotropic irregularities of the refractive index, nevertheless, the characteristic frequency of fluctuations F_0 thus varies. The F_0 change occurs because of a size decrease of the first Fresnel zone in the vertical direction

$$r \approx X(\lambda L)^{1/2} \tag{1.6}$$

and a decrease of the transverse ray path velocity in a point C (Fig. 1.1) due to refraction influence

$$V^* = [(XV_3)^2 + (X^2 V_1)^2]^{1/2}. \tag{1.7}$$

The difference between V^* and V (formula 1.4) is due to the regular refraction influence.

Let's discuss the relation between the spectrum $G(F)$ and spatial spectrum of refractive

index fluctuations W. The frequency spectra $G(F)$ can be conversed into one–dimensional spatial spectra of refractive index fluctuations $W(æ)$, where $æ=2\pi/l=2\pi F/V^*$ is a spatial number, l is a scale of inhomogeneity, on the basis of the "freezing" hypothesis, assuming that while cutting the area containing inhomogeneities by the ray, their spatial distribution does not vary. In this case the one–dimensional spatial spectrum of refractive index fluctuations is possible to present as:

$$W(æ)=(4\pi)^{-1}V^*G(æ\ V^*/2\pi), \qquad (1.8)$$

where V^* is determined according to (1.7). If the inhomogeneities of the refractive index are statistically isotropic, the spatial spectra $W(æ)$ should not depend on the angle θ (Fig. 1.1). The dependence of spectra $W(æ)$ on θ is observed in our measurements. In the case of the inhomogeneities, strongly prolated on the horizontal, i.e. stratified structures, the frequency spectra of the amplitude scintillations $G(F)$ should, in general, be determined by vertical velocity V_1 and the spectra measured will be similar while converting them to vertical wave numbers $æ_1=2\pi F/V_1$. In this case the one–dimensional spatial spectra $W(æ_1)$ along the vertical are also determined by (1.8) while substituting $V^* = X^2V_1$ in it, *i.e.* the vertical velocity with allowance for the refraction.

In Fig. 1.10 the examples of spectra $W(æ_1)$, obtained at measurements 01.12.1997 (dark symbol) and 26.05.1998 (light symbol) are shown. The values of the vertical scale of inhomogeneity $l_1=2\pi/æ_1$ are laid off as abscissa and the $W(æ_1)$ value as ordinates. In Fig. 1.10 spectra $W(æ_1)$, observed on the average altitude H_0=20 km are marked by squares, by triangles – at H_0=25 km, and by circles and diamonds – at H_0=30 km. Despite the difference of climatic conditions, coordinates, time of day and trajectory, on which "slit" of the atmosphere was made, the spectra $W(æ_1)$ in Fig. 1.10 demonstrate a good recurrence. The spectra $W(æ_1)$ have a maximum spectral density at sizes $l_1=2\pi/æ_1$=300 ÷ 800 m in the stratosphere in the altitude range from 15 up to 35 km. At sizes $l_1\leq$ 200 m the spectral density $W(æ_1)$ diminishes as $æ_1^{-4.5}$, at least to $l_1 \approx 40$ m.

1.5. Expected scintillations of the decimetre waves and technique of analysis of the atmospheric irregularities

Experimental data of scintillations of the centimetre wave (λ=2 cm) can be used for calculation of fluctuation characteristics of the decimetre wave (λ=19 cm). Scintillations

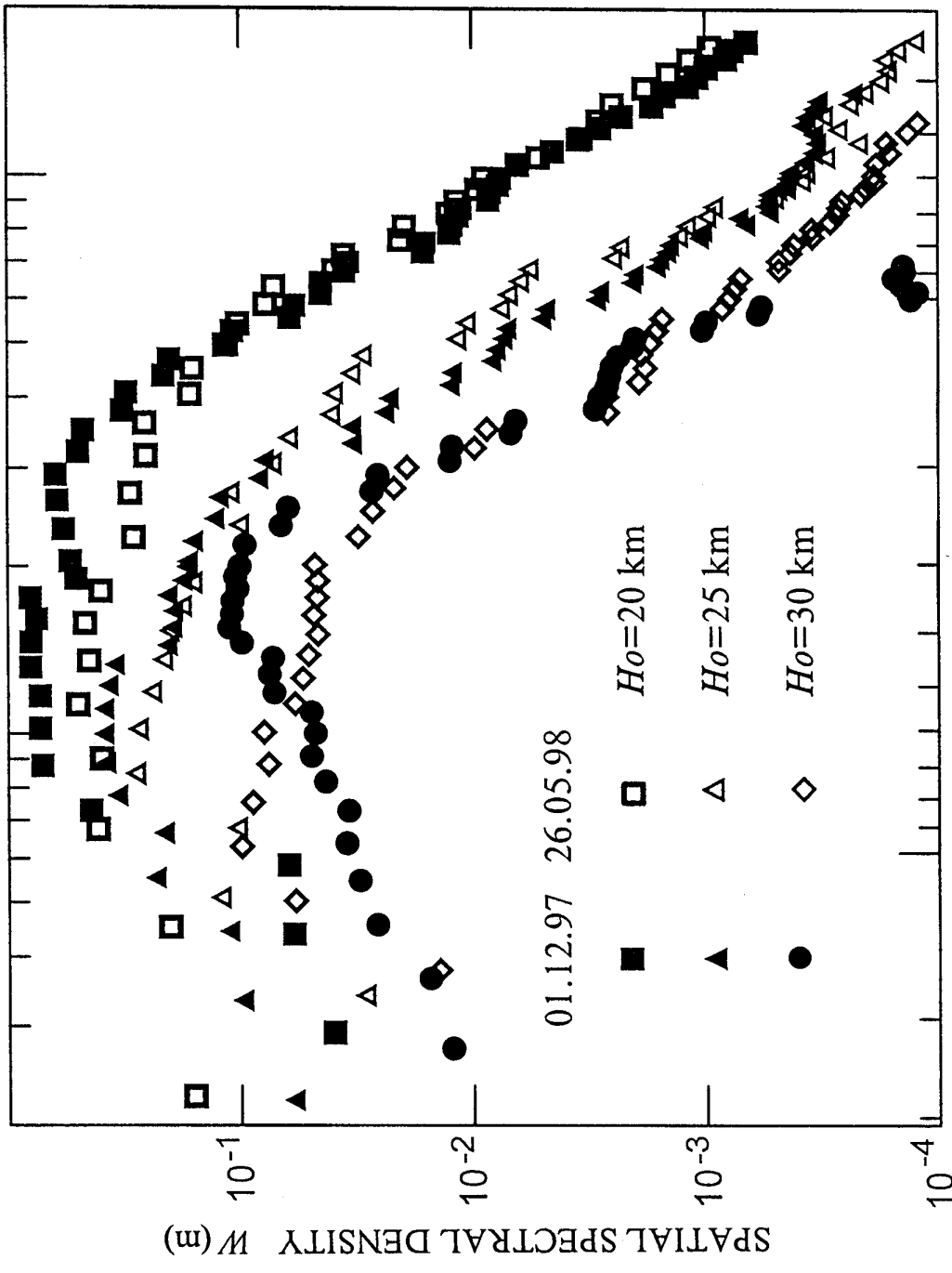

Figure 1.10. Spatial spectra of refractive index fluctuations for the stratosphere leaded to vertical spatial scales.

are defined by the parameter n (1.5), characteristic scintillation frequency F_o and dispersion σ^2. In accordance with (1.5) the parameter n depend only on the spectral index p of spatial spectrum of the refractive index. The characteristic frequency of scintillations F_o and dispersion σ^2 depend on wave length and geometry of radio occultation. The frequency F_o is expressed by a relation (1.4) and dispersion of scintillation can be expressed as [*Ishimaru*, 1978]

$$\sigma^2 \sim \lambda^{(p-6)/2} (L_1 L_2 / (L_1 + L_2))^{(p-2)/2} \qquad (1.9)$$

where L_1 and L_2 are distances from the receiver and the transmitter up to the probed atmospheric area (Fig.1.1). The parameter $L = L_1 L_2 / (L_1 + L_2)$ is the same for MIR/GEO and GPS/CHAMP radio occultation measurements. One can obtain expected values of the characteristic frequency F_o and rms amplitude fluctuations σ for λ = 19 cm using relations (1.4), (1.5) and (1.9) and the experimental data for λ = 2 cm presented on Fig. 1.4, 1.5 and 1.8.

The expected rms amplitude fluctuations σ_{19} for λ = 19 cm at the altitudes of 15÷35 km can be expressed as (if p = 4.6):

$$\sigma_{19} = \sigma_2 (19/2)^{(p-6)/4} = 0.455\ \sigma_2 \qquad (1.10)$$

where σ_2 is the rms amplitude fluctuations for λ = 2 cm. For H_o < 7 km σ_{19} is equal to 0.26 σ_2, if p = 3.6.

Thus the rms amplitude fluctuations in decimetre range are expected by 2÷4 times smaller than in centimetre range. The characteristic frequency of the amplitude scintillations are expected by 3 time lower than in centimetre range.

The calculations show that the level of the expected amplitude fluctuations of the decimetre radio waves is sufficient to analyse the intensity of the atmospheric irregularities for the heights between 1 and 25 km. The carried analysis allows to propose the technique for definition of the intensity of the atmospheric irregularities from results of measurement of the scintillations on board CHAMP. This technique consist of next stages:

The dispersion σ_n^2 of the scintillations for a interval of the minimal altitude of the ray between 35 and 65 km is calculated in accordance with formula (1.1).

The dispersion σ_S^2 is calculated for six altitude intervals with thickness $\Delta H_o \approx 4$ km :

- in the troposphere between ~0 and ~4 km and between ~4 and ~8 km,
- in the tropopause area between ~8 and ~12 km and between ~12 and ~16 km,
- in the stratosphere between ~16 and ~20 km and between ~20 and ~24 km.

The change of the average signal level $<E>$ due to defocusing of the radio wave was accounted for calculation σ_S^2 by a line approximation of the dependence $E(H_o)$ on the altitude interval ΔH_o.

Six values of the rms field strength fluctuations $\sigma_i = (\sigma_s^2 - \sigma_n^2)^{1/2}$ for chosen height intervals are calculated. If the dependence $E(H_o)$ have a sharp changes of the field strength in the tropopause area for the heights between 8 and 16 km, the values σ_3 or σ_4 are expelled from analysis.

In accordance with formula (1.3) the values Φ_i are calculated for a chosen height intervals. This six values Φ_i are a quantitative estimation of stability or perturbation (strong turbulence) of the atmosphere. The values Φ_i for the different degree of atmosphere turbulence can be determined by empirically from comparison with data of the meteorological temperature measurements and it is possible from comparison with altitude profile of the refractive index structure parameter, C_n^2. The completed criterion of the atmosphere stability (weak turbulence) in the tropopause area and in the stratosphere may be effect of the sharp change of the field strength in the tropopause.

2. Phase fluctuations from radio occultation data

2.1. Preliminary description program module for antispoofing regime

First radio occultation experiments revealed two important things. First, the real atmosphere produces effects that idealized theoretical models were able to describe only approximately. Second, it became necessary to make systematic experimental studies into the propagation of radio waves along a satellite-satellite link. The first series of radio occultation experiments concerned with the above phenomena are reported in [*Yakovlev et al.,* 1995a; *Yakovlev et al.,* 1995b; *Yakovlev,* 2001]. In this works a description of experimental and theoretical dependencies of changes in the amplitude of decimeter and centimeter radio waves in radio occultation experiments carried out on the radio link that joined the *Mir* space station and a geo-stationary satellite is given. The possibility of inferring the parameters of layered formations and atmospheric turbulence as well as the altitude distribution of humidity from amplitude data is demonstrated. In [*Yakovlev et al.,* 1995b], an experimental pattern of regular changes in frequency due to the influence of atmosphere is analyzed and it is shown that frequency data can serve as a source from which one can deduce altitude profiles of the refraction angle and of the refractive index of the atmosphere, as well as, subject to certain constraints, the behavior of temperature with respect to altitude. The multipath propagation and scattering of radio wave by the Earth's surface was discussed by *Rubashkin et al.*[1993] and *Pavelyev et al.*[1996].

In addition to regular changes in frequency and phase, radio occultation experiments often reveal random fluctuations that can be attributed to atmospheric inhomogeneities. Inhomogeneities refer random changes in the refractive index caused by atmospheric turbulence and by large-scale local entities, such as clouds, layers, and inversions that do not obey a spherically symmetric distribution. The random fluctuations of radio wave frequency and phase thus caused introduce a kind of interfering noise and thus limit the accuracy of determining temperature altitude profiles. On the other hand, the same fluctuations serve a useful purpose – they are a source of information about atmospheric inhomogeneities and thus supplement the capabilities of the radio occultation method in atmospheric monitoring. Influence of the receiver noise or antispoofing regime of the GPS introduce out the supplementary phase and frequency fluctuations. In this case the accuracy of determination of

the atmospheric parameters is lowered.

The aim of this section is to describe features of GPS signal in antispoofing regime and to give first recommendation for designing antispoofing program module. This module may diminish the negative influence of antispoofing regime on determination of atmospheric and ionospheric parameters from radio occultation data.

GPS resides on two L-band frequencies: L1 at 1575.42 MHz and L2 at 1227.6 MHz [*Hofmann-Wellnhof et al.,*1992]. The L1 frequency consists of two spread-spectrum biphase shift keyed (BPSK) modulated signals in phase quadrature: the precise (P)-code, with a 10.23 MHz chipping rate, and the coarse/acquisition (C/A)-code, with a 1.023 MHz chipping rate. The P-code is usually denoted P(Y), since it can be (and currently is) encrypted for antispoofing and military exclusivity. The C/A-code is unencrypted and is used by military receivers for initial acquisition and by civil receivers as the primary navigation signal. The L2 frequency currently has only one signal, which can be either C/A- or P(Y)-code, but not both. Currently the P(Y)-code is broadcast on L2. The C/A-code is placed on the L1 carrier in phase quadrature (i.e., 90° offset) with the P-code. Denoting unmodulated carrier by $L_i(t) = a_i \cos (F_i t)$ and the state sequences of the P-code, the C/A-code, and the navigation message by P(t), C/A(t), and D(t), respectively, the modulated carriers are represented by the equations [*Hofmann-Wellnhof et al.,* 1992]:

$$L1(t) = a_1 P(t) D(t) \cos (F_1 t) + a_1 C/A(t) D(t) \sin (F_1 t)$$
$$L2(t) = a_2 P(t) D(t) \cos (F_2 t).$$

The P-code is not classified and originates from a combination of two bit sequences, each generated by two registers. The first bit sequence repeats every 1.5 second and, because of the fundamental frequency f_0=10.23 MHz, has a length of $1.5345 \cdot 10^7$ bits. The second sequence has 37 more bits. The combination of both sequences thus results in a code with approximately $2.3547 \cdot 10^{14}$ bits which corresponds to a time span of approximately 266.4 days. The total code length is partitioned into 37 unique one-week segments and each segment is assigned to a satellite defining its PRN number. The codes are restarted at the beginning of every GPS week at Saturday midnight. The chip length of the P-code is about 30 m. The reading of the satellite clock at any time is obtained by adding the number of chips within the actual 1.5-second interval to the so-called Z-count which is transmitted in the navigation message and represents a multiple number of 1.5-second intervals since the beginning of the

current GPS week. In order to protect the P-code against spoofing (i.e., the deliberate transmission of incorrect information by an adversary), the code can be encrypted by invoking antispoofing. This procedure converts the P-code to the Y-code which is only useable when the secret conversion algorithm is accessible. There are basically two methods for denying civilian users full use of the system. The first is Selective Availability (SA) and the second method is antispoofing (A-S).

Selective availability. Primarily, this kind of denial has been accomplished by "dithering" the satellite clock frequency in a way that prevents civilian users from accurately measuring instantaneous pseudoranges. This form of accuracy denial mainly affects any one-receiver operation. When pseudoranges are differenced between two receivers, the dithering effect is largely eliminated, so that this navigation mode proposed for example by the U.S. Coast Guard will remain unaffected. The SA has only been implemented in Block II satellites and has been in force intermittently since April 1990 at various level of accuracy denial.

Antispoofing. The design of the GPS system includes the ability to essentially "turn off" the P-code or invoke an encrypted code (Y-code) as a means of denying access to the P-code to all but authorized users. The rationale for doing this is to keep adversaries from sending out false signals with the GPS signature to create confusion and cause users to misposition themselves. Under present policy, the A-S is scheduled to be activated when the system is fully operational. When this is done, access to the P-code is only possible by installing in each receiver channel an Auxiliary Output Chip (AOC) which will be available only on an authorized basis. Thus, antispoofing regime will affect many of the high accuracy survey uses of the system.

The influence of antispoofing regime on measured height dependencies of the phase path F1, F2 and amplitude A1, A2 corresponding to frequencies L1, L2 in GPS/MET radio occultation experiment (begin of this event is 06 August 1996 07h 47m 44s) is shown in Fig. 2.1-2.4. The amplitude dependencies A1, A2 (H) on perihelion ray height H are shown in Fig. 2.1. It follows from analysis of Fig. 2.1 that antispoofing regime does not effect the amplitude A1 data. The dependence of A1 on H has usual features connected with D-layer of ionosphere (short spike at 76-78 km level) and reveals fine structure of the tropopause. Energy of the A1 amplitude is as usual near signal/noise level 300 - 400 v/v. The amplitude A2 has drastically smaller signal/noise level ~ 10-15 v/v and does not shows any features connected with ionosphere and troposphere influences. Thus in the first approximation the only A1 data may be used for ionospheric and atmospheric investigation in antispoofing regime. The

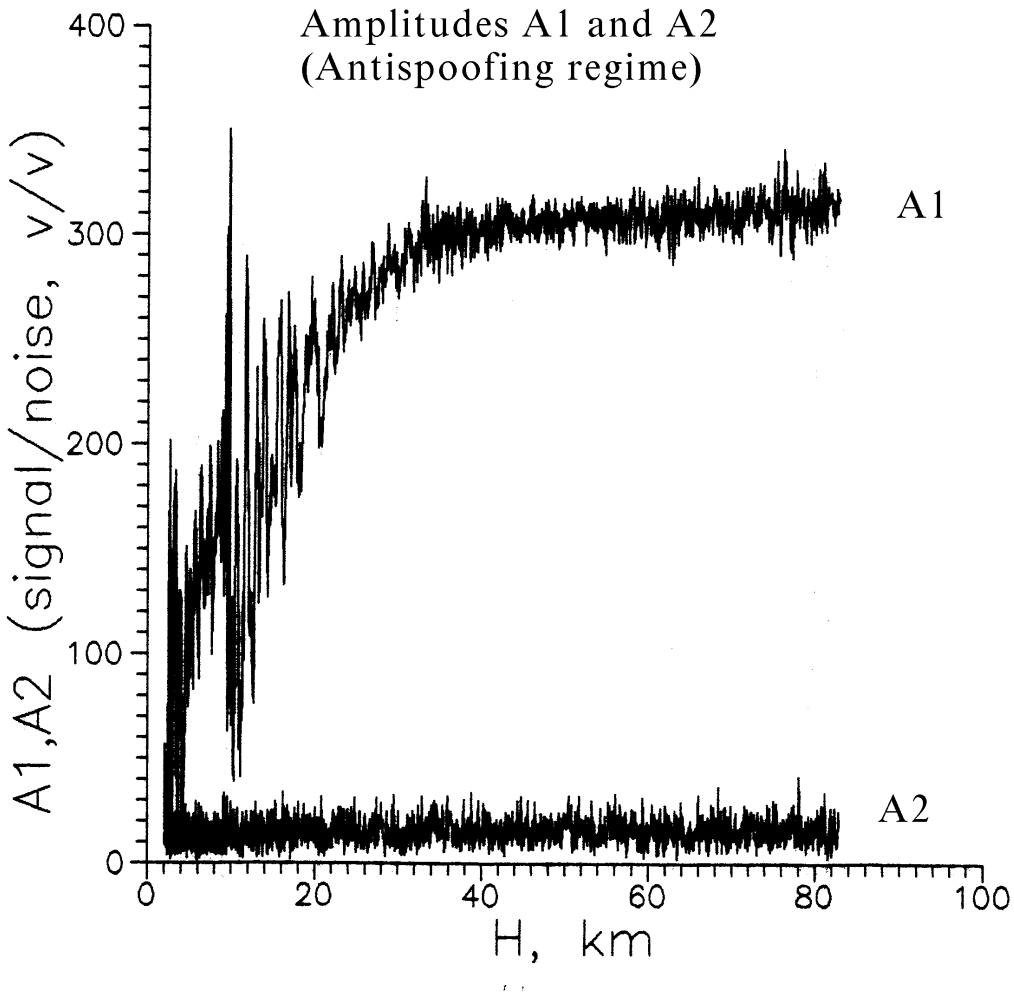

Fig. 2.1. Influence of antispoofing on radio occultation amplitudes A1,A2.
(GPS/MET, 06 August 1996, 07 h 44 m 02 s).

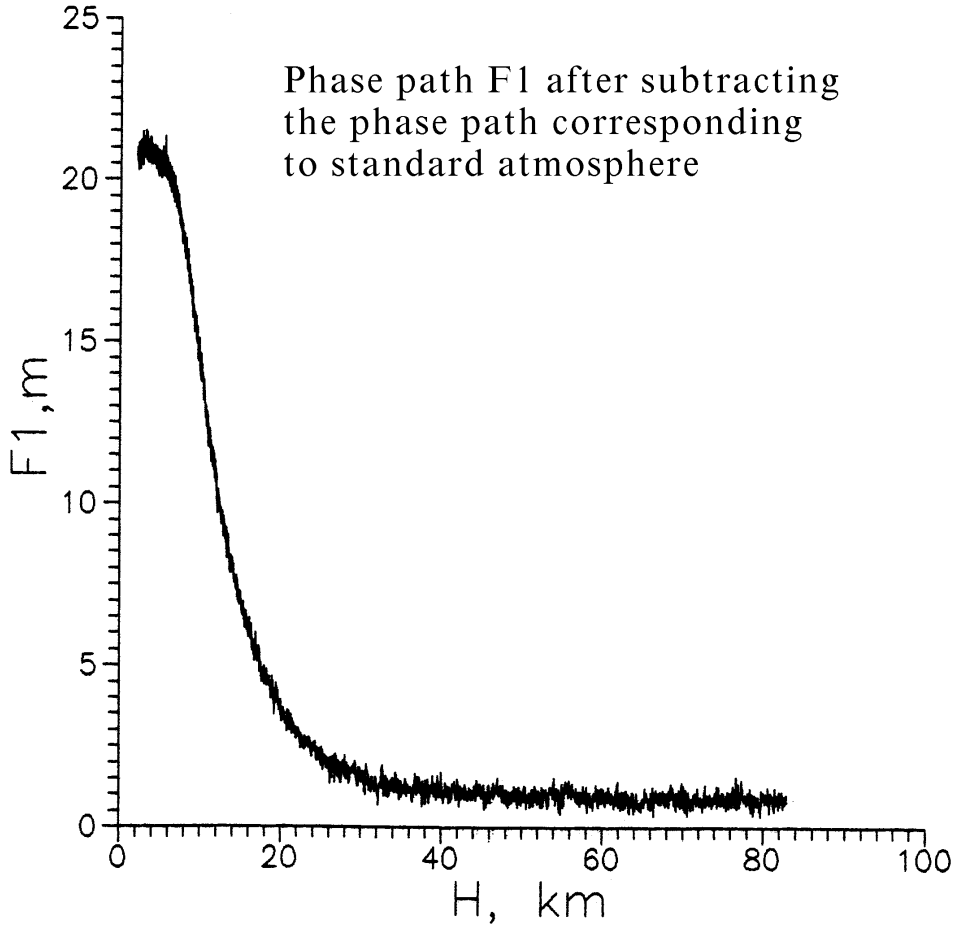

Fig. 2.2. Phase path residuals F1-$F1_s$ in antispoofing regime from GPS/MET radio occultation data. (GPS/MET, 06 August 1996, 07 h 44 m 02 s).

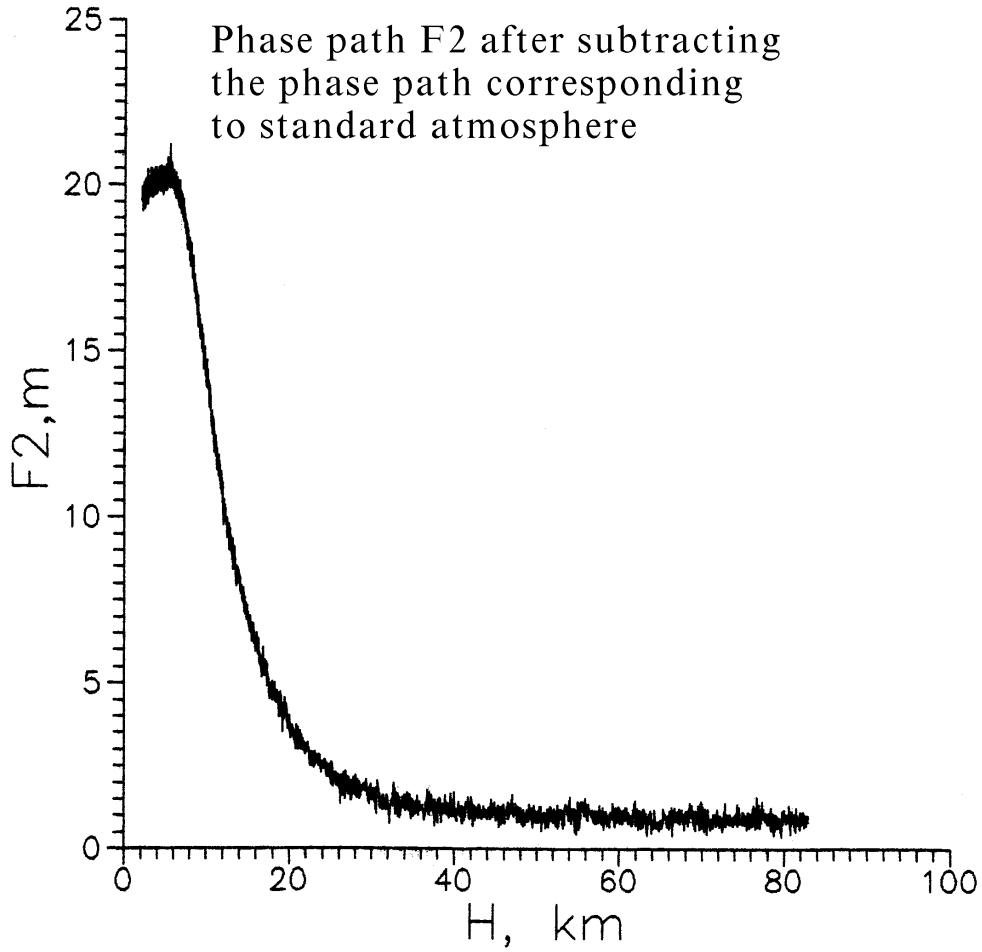

Fig. 2.3. Phase path residuals F2-F1$_s$ in antispoofing regime from GPS/MET radio occultation data. (GPS/MET, 06 August 1996, 07 h 44 m 02 s).

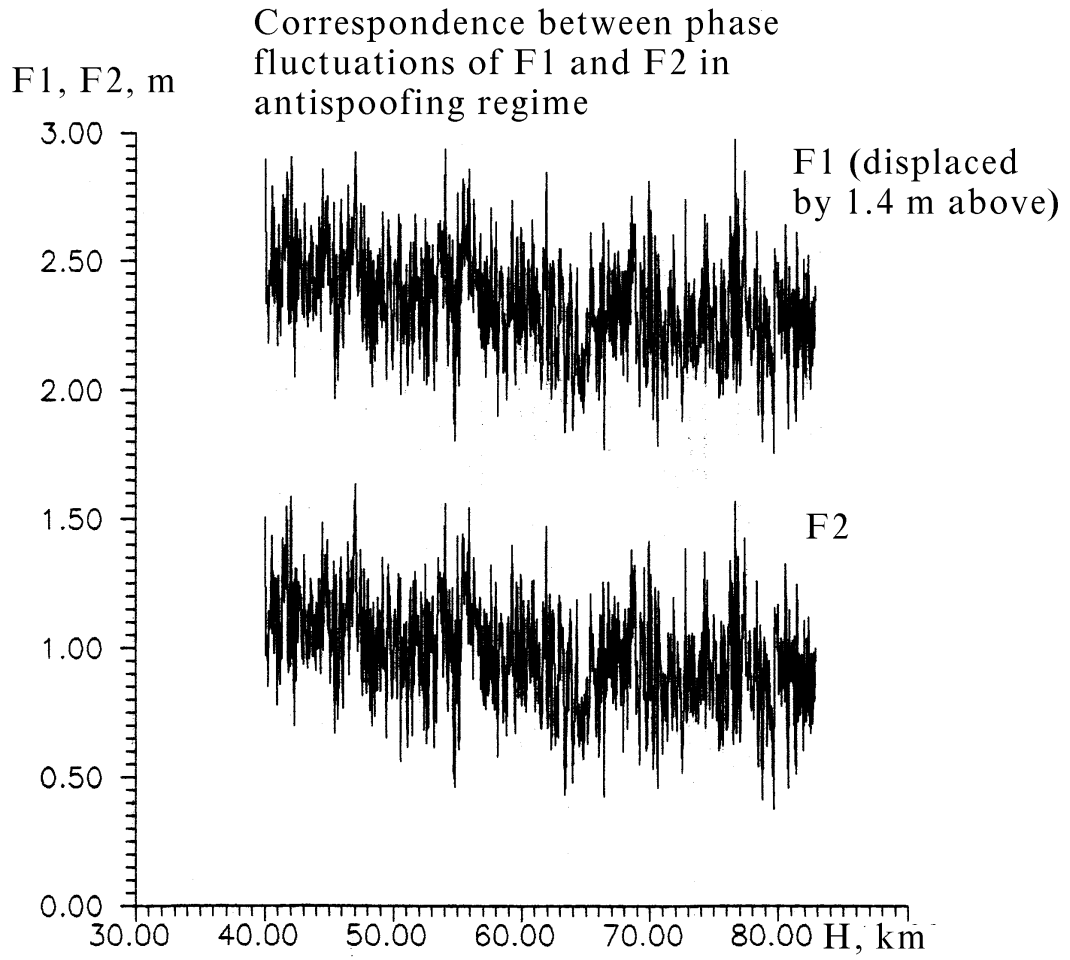

Fig. 2.4. Antispoofing phase modulation of frequencies L1 and L2 (GPS/MET, 06 August 1996, 07 h 44 m 02 s).

changes of the phase data F1 and F2 in antispoofing regime are shown in Fig. 2.2-2.4.On the vertical axis in Fig. 2.2-2.4 are shown the values of the phase paths F1, F2 (expressed in meters) obtained after subtraction the phase path $F1_s$ and $F2_s$ corresponding to standard atmosphere influence. The phase path excess connected with the troposphere influence is seen in the both dependencies and changed from values near 1 m (corresponding to possible ionospheric contribution) up to magnitude of 20-23 metres at the 2-4 km. However dispersion of the phase paths F1 and F2 is very high comparing with absence of antispoofing regime. Usually the instrumental error in the phase path in the case without antispoofing is very near to 1-2 mm level. However in the antispoofing regime the statistical variance of the phase paths F1, F2 is more higher. This level may be estimated using data shown in Fig. 2.4. In Fig. 2.4 dependencies of the phase paths in antispoofing regime on height in interval 40-80 km are

shown. For comparing the dependence F1(H) is displaced. The variance of the both dependencies is very near and is about 0.2-0.3 meters. This variance is higher by factor 200-300 than usual dispersion in high quality phase measurement without antispoofing. Thus measurements of ionospheric and atmospheric parameters using single F1 and F2 phase data are very difficult. However some possibilities are existing for using radio occultation phase data in antispoofing regime. This possibilities are connected with high level of correlation between phase variation F1 and F2 caused by antispoofing modulation.

The dependence of phase path difference F1-F2 (expressed in metres) on height *H* is shown in Fig. 2.5. The statistical variance of the phase F1-F2 is smaller than variations of both F1 and F2 by factor ~ 10. This conclusion may be supported by more detailed analysis of the difference phase variations F1-F2 shown in Fig. 2.6. The amplitude of this variations is about 2-3 cm. Thus for designing program module for work in antispoofing conditions one may use high correlation between phase changes at both frequencies.

From this consideration the next recommendation for elaboration of program module in antispoofing regime may be indicated. For this aim the radio holographic program module described in this report may be used. Instead F1 and F2 phase data this module must use the phase difference F1-F2 as function of time for finding dependence of refraction angle difference ξ_1-ξ_2 on the height in the ionosphere region. For measuring atmospheric parameters this module must use the amplitude A1(t) temporal dependence and method proposed by *Kalashnikov et al.,*[1986] for restoration the refractivity altitude profile on the radio occultation amplitude data. The phase difference F1-F2 may be used in the neutral atmosphere region for estimation ionospheric influence that caused different height of ray perihelion at frequency F1 and F2 in the troposphere. The accuracy of this approach in general depends on the statistical error in the phase difference F1-F2. This error in antispoofing regime is by factor 20-30 greater than without antispoofing. However antispoofing does not effect the amplitude temporal dependence A1(t). So the possibility exists for working in antispoofing regime without special receiver. The practical accuracy and instrumental error of this approach may be found in future work using GPS/MET or CHAMP data.

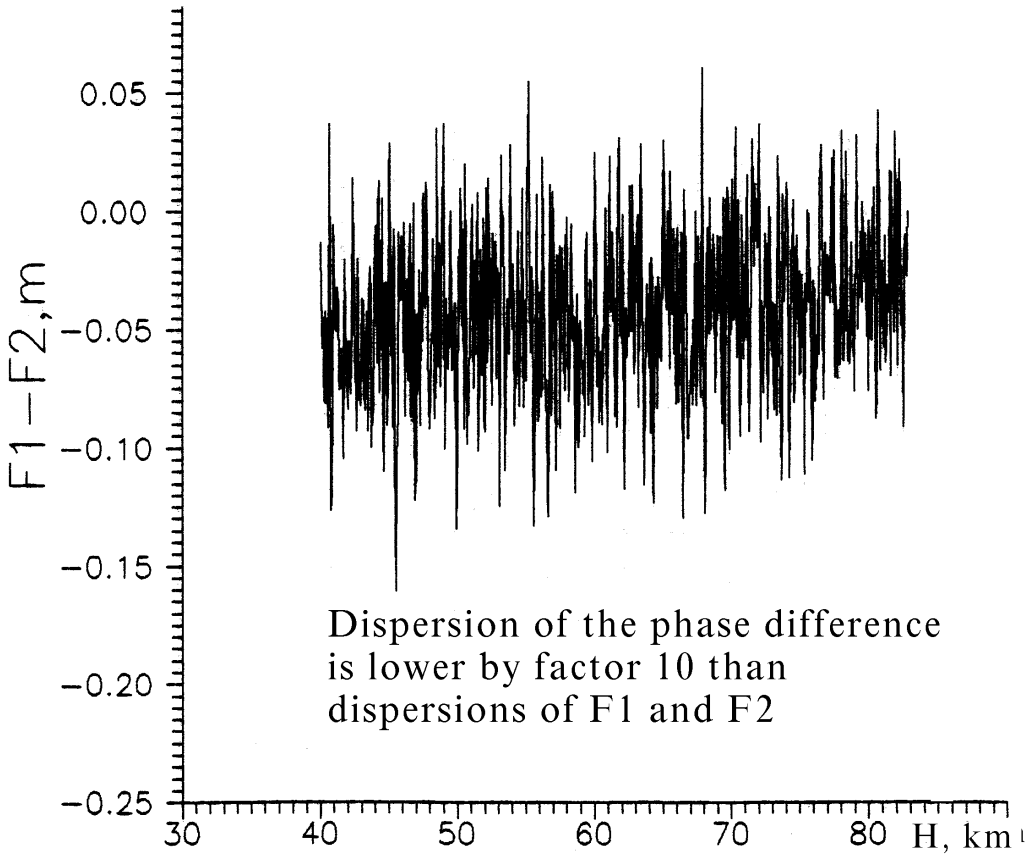

Fig. 2.5. Diminishing antispoofing effect by subtracting F1-F2.

(GPS/MET, 06 August 1996, 07 h 44 m 02 s).

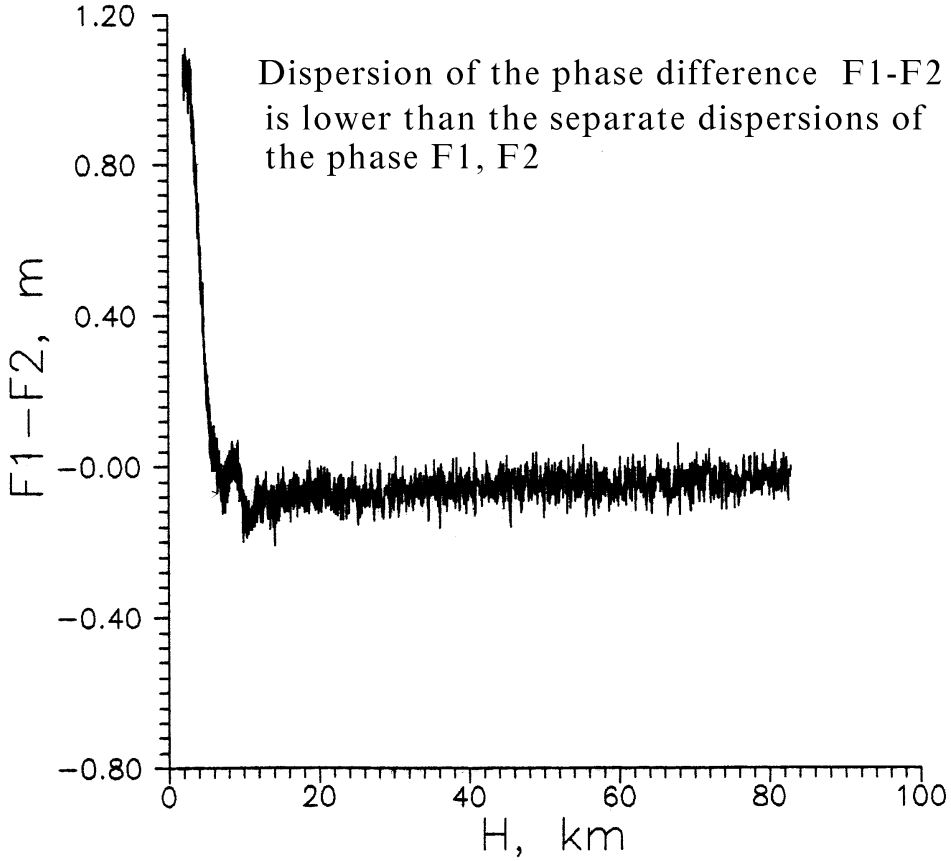

Fig. 2.6. Phase residuals F1-F2 as means against antispoofing.

(GPS/MET, 06 August 1996, 07 h 44 m 02 s).

2.2. Phase fluctuations from GPS/MET data

We consider the phase fluctuations from data GPS/MET in sessions of measurements without antispoofing. As phase path length in neutral atmosphere does not depend from a wave length, we analyze only fluctuations of a phase for L1 (λ=19 cm). The results of measurements in this range are more reliable because of a greater ratio signal to noise, than for L2 (λ=24 cm). For the analysis of influence irregularities of the refractive index on a phase fluctuations it is necessary from residual atmospheric phase to exclude contribution connected with a regular altitude structure of the refractive index, *N(h)*. The regular change of a phase can be determined or with the help of calculation phase for model atmosphere with given parameters, or by approximation of regular phase change on temporary intervals Δt by an analytical function. The analysis has shown, that both approaches lead to close results. We have chosen variant division of the measurement sessions on temporary intervals Δt=2 s and approximated average change residual atmospheric phase in limit of each interval by a power function of the second degree on a method of the least squares. In result we have received dependence casual variations of a phase from time with zero average meaning

$$\delta F1(t) = F1(t) - F_p(t),$$

where δF1 is phase fluctuation, F1 is residual atmospheric phase for L1 and F_p is average atmospheric phase.

On Figures 2.7, 2.8 and 2.9 examples of dependencies δF1 from height of a ray in measurement sessions of № 21 05 February 1997, № 216 02 February 1997 and № 426 10 February 1997 are given, respectively. From these Figures it is visible, that at $Ho > 35$ km statistical variations of a phase do not exceed 0.2 cm. Fluctuations of a phase are increased at decrease of height ray and directly before the discontinuance of radio connection at H_0=1 to 4 km they reach at 2 to 3 cm. Except casual changes δF1 are observed quasi-periodical variations of it caused apparently layered structures and diffraction effects at a level of tropopause. The example of influence tropopause on the phase variations is shown on Fig. 2.7 by an arrow.

Analysis of data has shown that phase variations for L2, δF2 at $H_0 > 35$ km have more than for L1. It is explained by smaller ratio signal/noise and large influence ionospheric irregularities. Variations δF1 and δF2 at altitudes $H_0 < 20$ km are correlated.

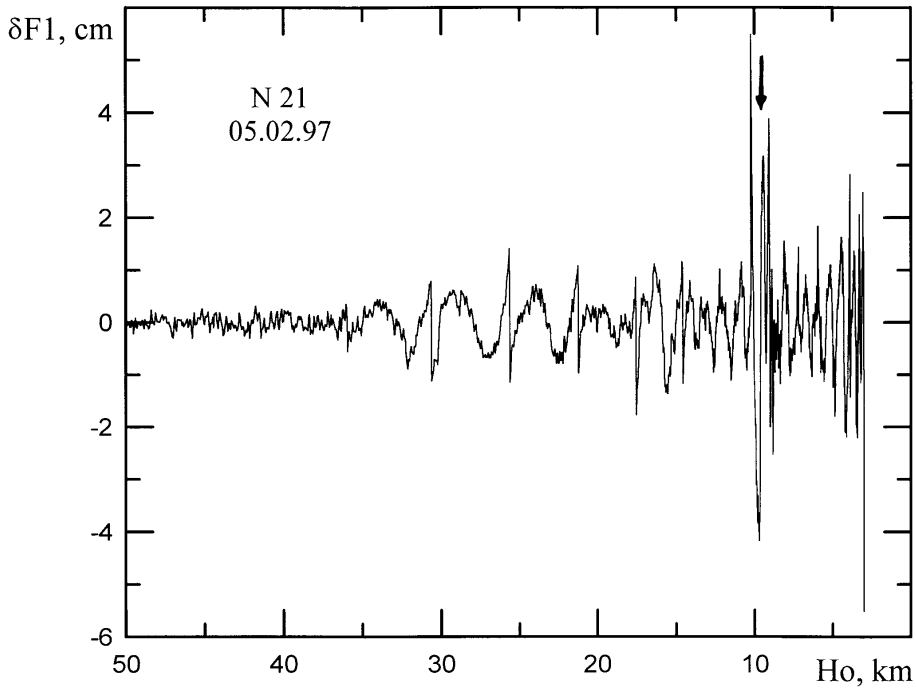

Fig.2.7. Fluctuations of phase, δF1 plotted as function of the minimum ray altitude H_0 from MIR/GEO occultation N 21, 05 February 1997.

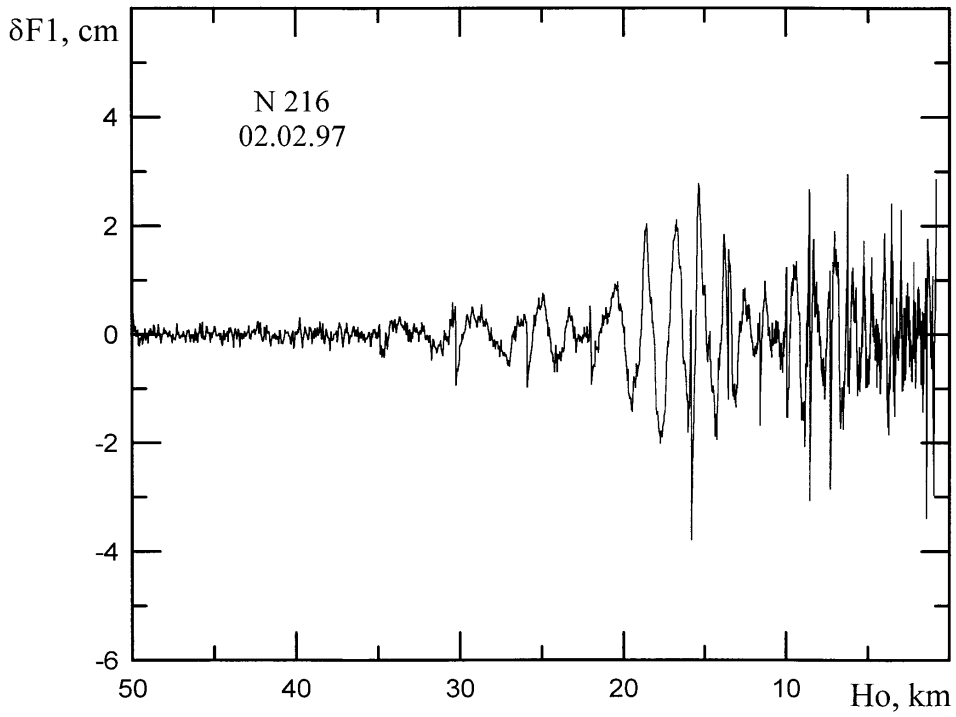

Fig. 2.8. Fluctuations of phase, δF1 plotted as function of the minimum ray altitude H_0 from MIR/GEO occultation N 216, 02 February 1997.

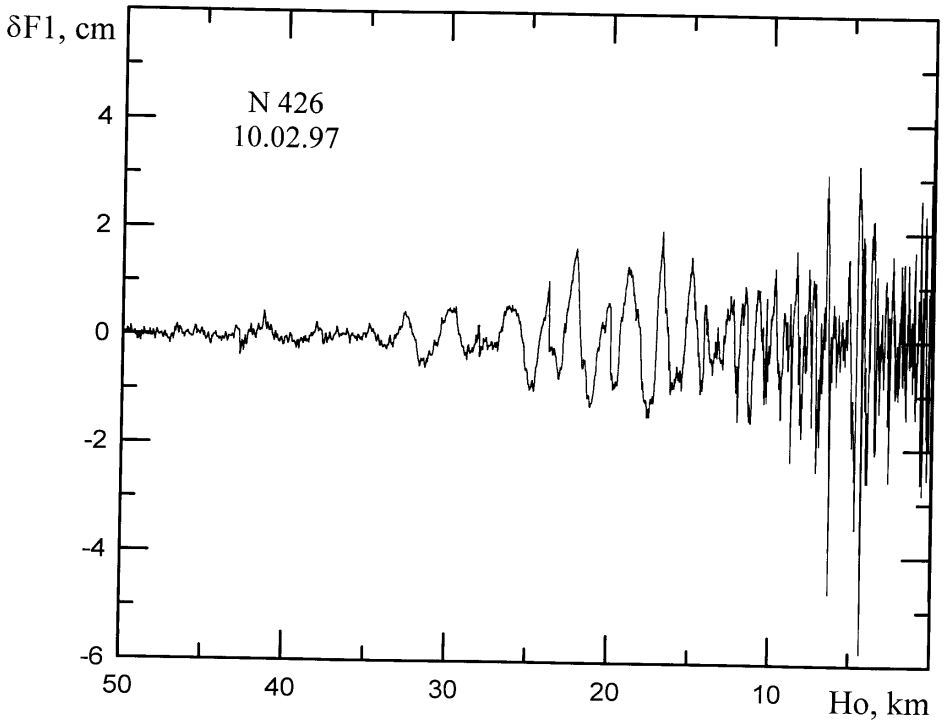

Fig.2.9. Fluctuations of phase, δF1 plotted as function of the minimum ray altitude H_0 from MIR/GEO occultation N 426, 10 February 1997.

The complete similarity of dependencies δ F(H_0) for both ranges is caused by insignificant distinction of the sizes of the first Fresnel zone.

A quantitative estimation phase fluctuations is dispersion σ_L^2 or root-mean-square deviation σ_L. We have determined σ_L for temporary intervals Δt=2 s. On Fig. 2.10 meanings σ_L are resulted at different minimum heights of a ray for three sessions of measurements. From Fig. 2.10 follows, that at H_0 < 35 km of meaning σ_L do not exceed errors of measurements. At 30> *Ho* > 10 km σ_L is equal 0.5 cm, and at heights *Ho*=2 to 5 km of meaning σ_L have large variability and on the average are equal 1 cm. Fig. 2.10 describes phase fluctuations caused as casual isotropic irregularities of the refractive index (turbulence), and anisotropic by layered structures, which have not of spherical symmetry. Therefore, at further for determination of parameters of atmospheric turbulence it is necessary to develop criteria for exception of influence of regular layered formations.

We now proceed to sum up our analysis of radio-wave frequency and phase fluctuations . As showed above, rms phase and frequency fluctuations are reverse proportional to the wavelength λ, and they are independent from geometrical parameters L_1 and L_2. The phase path length of radio wave and its fluctuations in the neutral atmosphere is independent from the wavelength. Therefore we can compare experimental data received for the wavelength 32 cm on link station *Mir* – geo-stationary satellite and data for the wavelengths 19 cm and 24 cm on link GPS – Microlab 1. Comparison of the data show satisfactory agreement between them.

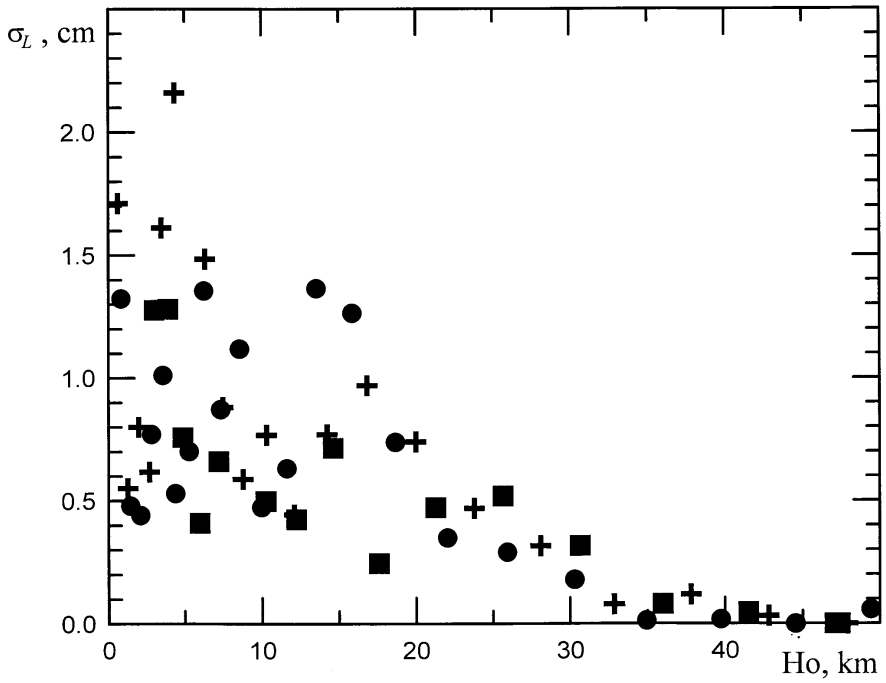

Fig. 2.10. RMS fluctuations of phase path length, σ_L, plotted as function of the minimum ray altitude H_0 from GPS/MET data.

2.3. Theoretical relations for phase and frequency fluctuations

Consider the influence of atmospheric turbulence on the phase of a radio wave in radio occultation measurements. Suppose that refractive index inhomogeneities have a spatial spectrum of the form

$$\Phi_n(\kappa) = 0.033 C_n^2 (\kappa^2 + 1/L_0^2)^{-11/6}, \tag{2.1}$$

where κ is the spatial wavenumber, C_n^2 is the structural characteristic of the refractive index, and L_0 is the external inhomogeneity scale. According to *Ishimaru* [1978], the variance of phase fluctuations may then be written as

$$\sigma_\varphi^2 = 0.39\, k^2\, L_0^{5/3} \int_0^L C_n^2\, dx = 15.38\, \lambda^{-2}\, L_0^{5/3}\, G, \tag{2.2}$$

where

$$G = \int_0^L C_n^2\, dx.$$

Here, $k = 2\pi/\lambda$ is the wavenumber, λ is the wavelength, dx is an element of the ray line length, and G is the integral whose value depends on the minimum altitude of the ray line ACB (Fig. 1.1) and the altitude profile of C_n^2. As equation (2.2) implies, σ_φ^2 is function of both the integral G and the rather arbitrary external inhomogeneity scale L_0.

As follows from *Fante* [1980], at h= 0 to 12 km, C_n^2 only slightly varies with h, whereas at h > 12 km it rapidly decreases with increasing altitude. We will describe the altitude profile $C_n^2(h)$ by model relation of the form

$$\begin{aligned} C_n^2(h) &= C_0^2 \quad \text{for } 0 < h < h_1, \\ C_n^2(h) &= C_0^2 \exp[-\beta(h-h_1)] \quad \text{for } h > h_1. \end{aligned} \tag{2.3}$$

For an approximate evaluation of the integral G, we assume that the Ox axis is tangent to the ray line and that the origin of reckoning coincides with the point C (Fig. 1.1). Under this assumption, we integrate over a straight line. For the relation in (2.3), the integral G takes the form

$$\begin{aligned} &G = 2\, C_0^2 \{[2\alpha(h_1-H_0)]^{1/2} + (\pi\alpha/2\beta)^{1/2} \exp[-\beta(H_0-h_1)]\{1-\Phi[\beta(h_1-H_0)^{1/2}]\}\} \quad \text{for } H_0 < h_1, \\ &G = 2\, C_0^2 (\pi\alpha/2\beta)^{1/2} \exp[-\beta(H_0-h_1)] \quad \text{for } H_0 > h_1. \end{aligned} \tag{2.4}$$

Here α is the Earth's radius and Φ(x) is the error function. The results calculated for $\sigma_\varphi(H_0)$ and $\sigma_L(H_0)$ at λ = 32 cm are shown as dashed lines in Fig. 2.11. In calculations we assumed that $C_0^2 = 1.5 \times 10^{-15}$ m$^{-2/3}$, $h_1 = 7$ km, and $\beta = 0.2$ km^{-1}. Curves 1,2, and 3 correspond to an external inhomogeneity scale L_0 of 5, 3, and 1 km, respectively. Equations (2.4) and these theoretical curves imply that $H_0 > h_1$, the rms fluctuations σ_φ and σ_L decrease exponentially as H_0 increases. At $H_0 < h_1$, the influence of the exponential factor is negligible, so σ_φ and σ_L vary as $(h_1 - H_0)^{1/2}$. Comparison of the calculated functions $\sigma_\varphi(H_0)$ with experimental σ_φ reveals a satisfactory agreement between them. At $H_0 < 4$ km, the highest values of σ_φ can be twice or even three times as great as the theoretical ones, apparently due to the influence of local layered formations.

A theory explaining frequency fluctuations when radio waves propagate in statistically inhomogeneous medium is set forth in [*Armand,* 1982*; Armand et al.,* 1988]. In comparing experiments with theory, we will draw upon the analysis reported by *Yakovlev* [2001] with reference to frequency fluctuations of radio waves in a medium whose refractive index fluctuation spectrum is given by

$$\Phi_n(\kappa) = 0.033\, C_n^2\, \kappa^{-\alpha}, \tag{2.5}$$

where α is the exponent of the spatial refractive index fluctuation spectrum. It is legitimate to invoke this spectrum representation, because the external inhomogeneity scale affects the frequency fluctuations variance only slightly. As is proved in [*Yakovlev,*2001], in the case of the spectrum defined in (2.5), the frequency fluctuations variance may be written as

$$\sigma_f^2 = 1.3k^2 \frac{\Gamma\left(\frac{1}{2}\right)}{\Gamma\left(\frac{\alpha}{2}\right)} \Gamma\left(\frac{\alpha-1}{2}\right) V_2^{\alpha-2} \int_0^L C_n^2 dx \int_{\nu_1}^{\nu_2} \nu^{3-\alpha} d\nu, \tag{2.6}$$

where $V_2=(V_1^2+V_3^2)^{1/2}$ is the speed at which inhomogeneities were carried across the radio link near the point C (see Fig. 1.1), Γ is the gamma function, and ν is the frequency of fluctuations. Formally, in calculating the frequency fluctuation variance, all components of the frequency fluctuation spectrum must be taken into account, which is why the integral of ν in (2.6) must be evaluated from zero to infinity. In real measurements, fluctuations of the signal frequency may be evaluated only in the interval bounded by the lowest and highest observed frequencies ν_1 and ν_2, respectively.

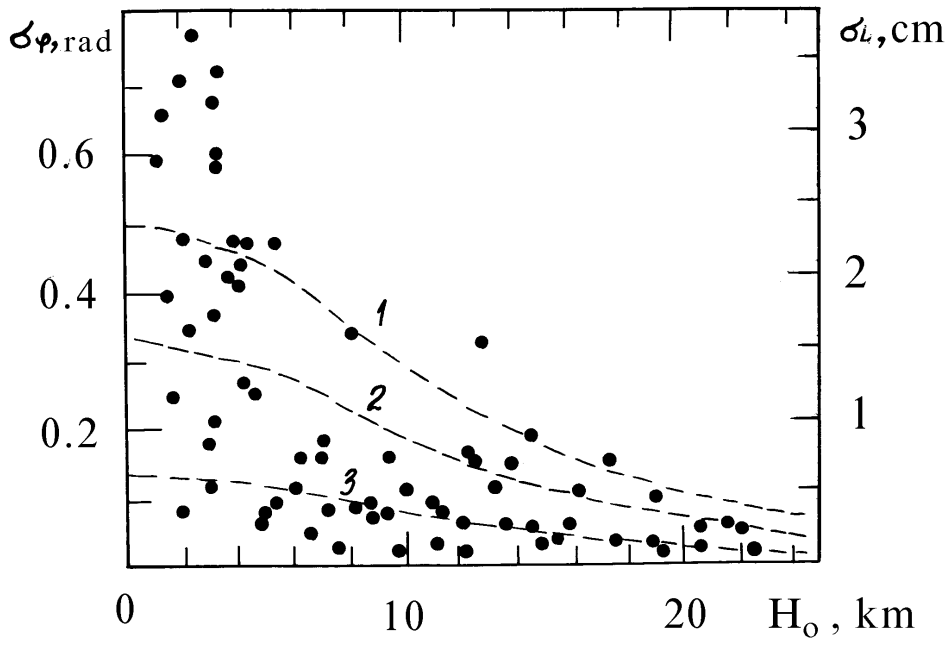

Fig. 2.11. RMS fluctuations of phase, σ_φ, and of phase path length, σ_L, plotted as function of the minimum ray altitude H_0 from MIR/GEO data.

Accordingly, in (2.6), we take the integral of ν between the limits ν_1 and ν_2. We also set $\alpha =$ 11/3. As a result, we get

$$\sigma_f^2 = 20.2 V_2^{5/3} \lambda^{-2} (\nu_2^{1/3} - \nu_1^{1/3}) G. \qquad (2.7)$$

The signal frequency is usually measured at equal time intervals Δt. In MIR/GEO measurements was Δt = 0.125 s. The highest frequency was ν_2 =1/(2Δt) = 4 Hz. The lowest credible observed frequency of fluctuations is determined by the duration ΔT of a realization having a certain variance σ_f^2. In our case, ΔT = 2 s, that is, ν_1 =0.5 Hz. Equation (2.7) implies that the behavior of the frequency fluctuation variance with the minimum beam-line altitude, $\sigma_f^2(H_0)$, is a function of the integral G and of the behavior of $V_2(H_0)$. For the function $C_n^2(h)$ defined in (2.3), the factor G is determined by equation (2.4). In MIR/GEO measurements, V_2 varied from 2.5 to 6 km/s. A graph of the function $\sigma_f(H_0)$ found theoretically by equations (2.7) and (2.4) for V_2 = 1 km/s is shown as a solid curve in Fig. 9. Comparison of experiment and calculations reveals that the theoretical values of σ_f are higher than the experimental ones.

A different approach may be taken to analyze the frequency fluctuations of radio waves in radio occultation experiments. Lying at its basis is the relation between changes in radio wave frequency, ΔF, and the angle of regular or irregular refraction ξ in the atmosphere. According to [*Yakovlev,* 2001], for a weakly refractive medium, this relation takes the form

$$\Delta F \approx \frac{V_1}{\lambda} \xi, \qquad (2.8)$$

where V_1 is the radio-wave source velocity component perpendicular to the ray line. Inhomogeneities in the refractive index give rise to irregular variations in the arrival angle $\delta\xi$ of radio waves. Therefore, the signal frequency experiences random variations

$$\delta F \approx \frac{V_1}{\lambda} \delta\xi. \qquad (2.9)$$

Equation (2.9) makes it possible to relate the frequency fluctuation variance σ_f^2 to the radio-wave arrival angle variance σ_ξ^2

$$\sigma_f^2 = \left(\frac{V_1}{\lambda}\right)^2 \sigma_\xi^2. \qquad (2.10)$$

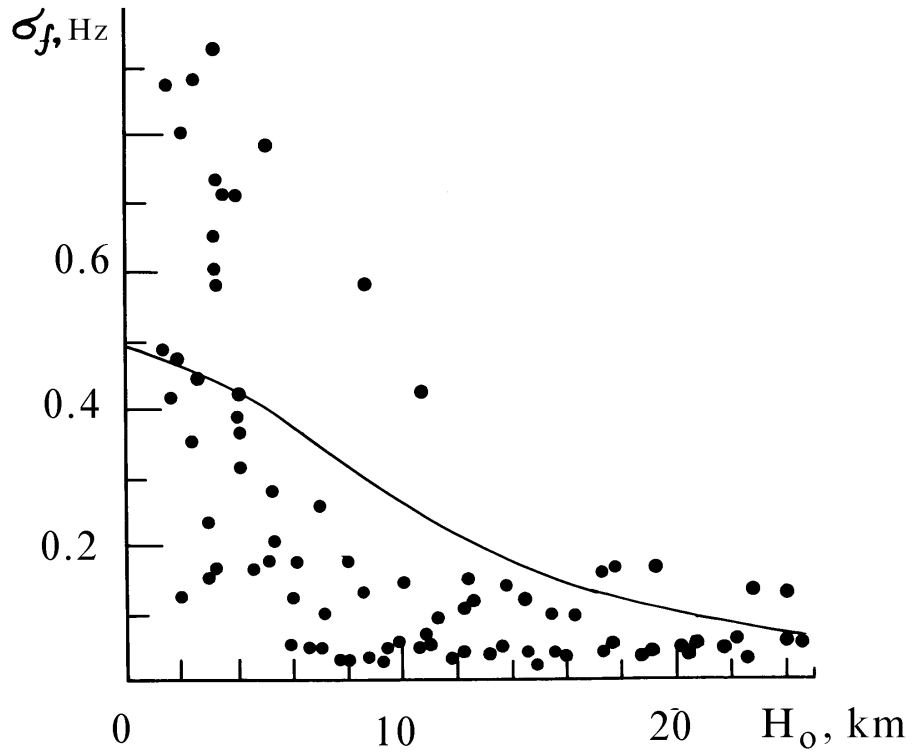

Fig. 2.12. RMS frequency fluctuations σ_f, plotted as function of the minimum ray altitude H_0 from MIR/GEO data.

If the size of first Fresnel zone is many times the internal turbulence scale and is a small fraction of the external turbulence scale, then, according to *Ishimaru* [1978], the variance σ_ξ^2 may be written as

$$\sigma_\xi^2 = 1.46\ \rho_0^{-1/3} \int_0^L C_n^2(x)dx. \quad . \tag{2.11}$$

In our case, the effective synthesized aperture size was $\rho_0 = V_1\Delta T$, where ΔT is the duration of a realization as adopted in the determination of σ_f. From equations (2.10) and (2.11) the following relation for the frequency fluctuation variance may be written:

$$\sigma_f^2 = 1.46\ \lambda^{-2}\ V_1^{5/3}\ \nu^{1/3}\ G. \tag{2.12}$$

Here, $\nu = 1/\Delta T$. Equations (2.7) and (2.12) are identical in structure and only differ in the constant coefficients and in the meaning of speeds V_1 and V_2 that occur in them. In equation (2.7), V_2 is the speed at which inhomogeneities are carried across the radio link near the point D. In equation (2.12), V_1 is the radio-wave source velocity component transverse to the case of weak regular refraction and a plane wave, $V_1 \approx V_2$.

As equations (2.2), (2.7), or (2.12) imply, the experimental function $\sigma_\varphi^2(H_0)$ or $\sigma_f^2(H_0)$ may well serve to deliver the function $G(r_0)$ defined as

$$G(r_0)=2a\int_{r_0}^{\infty}\frac{C_n^2 r dr}{\sqrt{r^2-r_0^2}}, \tag{2.13}$$

where $r = a + h$ and $r_0 = a + H_0$. By taking the Abel transform of (2.13), we get

$$C_n^2(r_0)=\frac{1}{\pi}\int_{r_0}^{\infty}\frac{dG}{dr}\frac{dr}{\sqrt{r^2-r_0^2}}. \tag{2.14}$$

As follows from equation (2.14), the experimental function $G(r_0)$ may well serve to derive the altitude profile $C_n^2(h)$. The function $C_n^2(h)$ describes the altitude distribution of atmospheric turbulence. Note that the function $G(r_0)$ deduced from phase or frequency fluctuation data may show a considerable scatter of experimental values. It is possible to determine $C_n^2(h)$ if smoothed experimental function $G(H_0)$ has been obtained. We found a suitable analytical relation $C_n^2(h)$ represented by equations (2.3) and evaluated $\beta < h_1$, and C_0^2. In [*Yakovlev et al.,*1995a], it is pointed out that in the case of radio occultation measurements, atmospheric turbulence can be assessed from radio wave amplitude scintillations. In this work we have demonstrated that atmospheric turbulence can be monitored and assessed from radio wave phase and frequency fluctuations.

3. Ionospheric correction and revealing ionospheric features

3.1. Current state of the problem and the task formulation

Problem of accounting for ionospheric contribution now is under investigation. This problem has been thoroughly considered by *Melbourne et al.,* [1994], *Kursinski, E.R. et al*., [1997]*, Rocken C. et al.,* [1997], *Hocke, K.,* 1997, *Hocke, K. et al,* [1999]. Other references may be seen in the list of the some radio occultation and radio holographic publications in the end of report. However the problem is still open due its complexity and high diversity of ionospheric conditions in different regions of the Earth.

The goal of this division is to develop analytic radio physical model that may be used for subtracting ionospheric influence from radio occultation data. This model may be applied to description ionospheric contribution in the phase and amplitude of radio occultation signal by using special ionospheric correction program tool. We also analyzed phase and amplitude data for revealing thin features in E- and D-layers of the ionosphere.

The Earth's ionosphere, which extends from about an 80-km altitude upward, acts as a lens that overlays the neutral atmosphere [*Melbourne et al.,* 1994]. In an occultation geometry, the signal must pass through the ionosphere on its way into and out of the neutral atmosphere below a 100-km altitude. This implies that a removal of this ionospheric effect on the signal is necessary before we can accurately deduce the neutral atmospheric profile. The dispersive nature of the ionosphere causes the two GPS signals to travel at different speeds. A simple linear combination of the L1 and L2 signals can be formed to subtract out most of the ionospheric delay. This commonly used simple linear combination, however, assumes that the two GPS signals are travelling along exactly the same paths. Moreover, it also ignores higher order terms in the expansion of the ionospheric refractive index. This residual ionospheric effects, if left uncalibrated, act as an error source that maps into neutral atmospheric profile errors. In this section we will examine these problem in some detail.

1. The most simple way of the ionospheric correction provided under assumption that L1 and L2 signals are propagating along the same path. In this case the phase paths of the

`signals L1 and L2 are equal to:

$$\rho_1 = \int_{GPS}^{LEO} (1 + N - 40.3\frac{N_e}{f_1^2})ds \qquad (3.1)$$

$$\rho_2 = \int_{GPS}^{LEO} (1 + N - 40.3\frac{N_e}{f_2^2})ds \qquad (3.2)$$

where N is the refractivity of the neutral atmosphere, N_e is the electron density distribution [m^{-3}], f_1, f_2 are the signals frequency [Hz], ds is element of a ray trajectory. Combining results of measurements L1, L2 at the same time instant one may exclude the ionospheric influence and find the length of the phase path in the neutral ionosphere ρ_a.

$$\rho_a = \int_{GPS}^{LEO} (1 + N)ds \approx [\rho_1 f_1^2 - \rho_1 f_1^2]/[f_1^2 - f_1^2] \qquad (3.3)$$

2. The second way of ionospheric correction have been suggested by *Vorob'ev and Krasilnikova,* [1994]. This method accounts for distinction of ray trajectories and impact parameters of signals L1, L2. This method may be applied under assumptions of local spherical symmetry of the ionosphere and linear dependence of the refractive bending angle on the refractivity. Also the influence of magnetic field is neglected in this approach. This method gives the bending angle corresponding to neutral atmosphere in the form:

$$\xi(p) = [f_1^2\ \xi_1(p) - f_2^2 \xi_2(p)]/[f_1^2 - f_2^2] \qquad (3.4)$$

where magnitudes $\xi_1(p)$, $\xi_2(p)$ are estimated at the same value of the impact parameter p. For practical implementation of the second method one must find from the experimental data the dependencies of the refractive bending angles $\xi_1(p_1)$, $\xi_2(p_2)$ at the frequencies L1, L2 on impact parameters p_1 , p_2. Then the interpolation of the function $\xi_1(p_1)$ may be used to find $\xi_1(p_2)$ in any instant of time and then formula (3.4) may be applied using relation $p=p_2$. Nowadays this method is successfully applied to analysis of radio occultation data for measuring the temperature altitude profiles in the atmosphere under spherical symmetry assumption. However to find the influence of the horizontal gradients and magnetic field one may use more general approach.

3. Basic methodology (calculus of variations) for this approach have been introduced by *Gu and Brunner* [1990], *Melbourne et al.,* [1994]. According to *Melbourne et al.,* [1994],

the phase delay of a signal passing through the ionosphere and atmosphere is given by

$$\rho_i = \int n_i ds_i \qquad (3.5)$$

where i=1,2 for L1,L2 respectively; ds_i is an element of length along the curved path that the i-th signal travels (Fig.3.1). The value of ionospheric effect on determination the refractivity, pressure and temperature vertical profiles depends on ionospheric state that is temporally and geographically different and may have various type of horizontal gradients according to level of solar activity and magnetosphere's interaction. Ionospheric influence on the phase excess may be described according to *Melbourne et al.,* [1994], for the case where $n<<1$ and where the gradient of the refractive index is slowly varying along the path, using the stationary phase property. For this case the phase path ρ_i can be written with sufficient accuracy as

$$\rho_i = \int_0^{R_{LG}} n_i dx - \frac{1}{2}\int_0^{R_{LG}} \frac{1}{x^2}\left[\left(\int_0^x \frac{\partial n_i}{\partial z} x' dx'\right)^2 + \left(\int_0^x \frac{\partial n_i}{\partial y} x' dx'\right)^2\right] dx \,, \qquad (3.6)$$

where dx and dx' are elements along the straight line connecting the transmitter and the receiver (OX axis). All integrations in eq.(3.6) are carried out along this line. The coordinates y (horizontal, perpendicular to OX axis) and z form a mutually orthogonal set with x. The partial derivatives $\partial n_i/\partial y$, $\partial n_i/\partial z$ are evaluated at $(y,z)=0$. For more accuracy, they should be evaluated at (y,z) of the curved path at given x. Equation (3.6) describes the phase path as a perturbation relative a stationary path (straight line LEO-GPS). All atmospheric and ionospheric influence including effect of regular refraction in the spherical symmetric media and possible action of two horizontal gradients are described by equation (3.6) as a perturbation relative to the free space case. For practical use it is convenient to have a formula similar to equation (3.6) describing perturbations according to horizontal gradients relative to spherical symmetric model of the ionosphere. The straight line path LEO-GPS may be replaced in this case by the stationary curved path LEO-GPS corresponding to local spherical symmetric model of the ionosphere (different at LEO-atmosphere and atmosphere - GPS parts of the path). Evaluation similar to the variations method applied by *Melbourne et al.,* [1994], to solution of this problem gives the equation:

$$\rho_i = \int_0^L n_i \, dl_i - 1/2 \int_0^L n_i \, dl_i \; l_i^{-2} \left[\left\{\int_0^{l_i} \partial n_i/\partial\zeta \, l'_i dl'_i\right\}^2 + \left\{\int_0^{l_i} \partial n_i/\partial\eta \, l'_i dl'_i\right\}^2\right] \qquad (3.7)$$

where dl_i, dl'_i are elements along the stationary curve in the locally spherical symmetric

ionosphere and atmosphere, L is the length of the stationary ray path. All integrations are carried out along this curve. The coordinates ζ, η form a mutually orthogonal set with the current unit vector $\mathbf{r_1}$ describing local vertical direction. The coordinate ζ corresponds to horizontal direction in the plane LEO-GPS satellites and the center of the Earth, the coordinate η corresponds to the direction perpendicular to this plane. The partial derivatives $\partial n_i/\partial\eta$, $\partial n_i/\partial\zeta$ are evaluated at a current point of the stationary curve. For spherical symmetric case the horizontal gradients are absent, the partial derivatives $\partial n_i/\partial\eta$, $\partial n_i/\partial\zeta$ are equal to zero and equation (3.7) coincides with (3.5). In general equation (3.7) may be used to account for the influence of distinction from spherical symmetric case.

As it follows from this consideration the necessity exists to have a local spherical symmetric model of the ionosphere in the radio occultation region because influence of the horizontal gradients and magnetic field may be evaluated using perturbation method relative to this model.

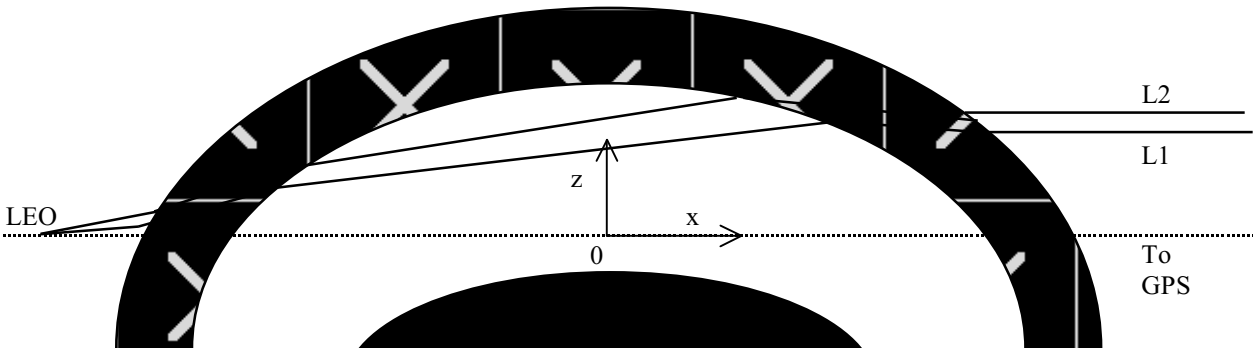

Fig. 3.1. Ray diversity due to ionospheric influence in radio occultation experiments.

L1 and L2 ray splitting due to dispersive ionospheric refraction using a simple spherically symmetric shell model [*Melbourne et. al.,* 1994]. The emitting GPS satellite is assumed to be at an infinite distance. Differential bending through the atmosphere by the L1 and L2 signals is suppressed for clarity. Special geometry results in non-parallel paths shown in the atmosphere. The z=0 line corresponds to the ionospheric-free stationary phase path for L1 and L2.

3.2. Possibility of the experimental radio occultation measurement of an ionospheric contribution

In this section the possibility of the experimental radio occultation measurement of ionospheric contribution will be described. The main assumption is global spherical symmetry of the ionosphere in the radio occultation region. Despite this the methodology may be used in practice for the first approximation of the ionospheric contribution.

Propagation of radio waves between GPS and LEO may be happened on trajectories of two type. The trajectory of the first type is shown in Fig. 3.2 by line TP, this line is characterized by absence of turning point E. This situation arises some time before radio occultation and the path TP do not have points disposed below the LEO altitude. For this case important property of the ray trajectory TP consists in growing of the impact parameter p when the LEO satellite is approaching to the radio occultation region. The maximum of the impact parameter p is achieved at the time instant t_x when the ray TP is perpendicular to the direction TO and the turning point E appears on the trajectory TP. The impact parameter p is diminishing after the time instant t_x. The point E exists for trajectory of the second type T′P′. The distance of the point E from the Earth's surface is minimal for ray trajectory T′P′ and equal to r_o. In this point the relation is fulfilling:

$$n(r_o)\, r_o = p, \tag{3.8}$$

where $n(r_o)$ is the refractive index at the level r_o, p is impact parameter. The connection between the refractive bending angle ξ, impact parameter $p=n(r)r \sin \varphi(r)$ (φ is the ray's zenith angle) and the angle θ_1 may be described for trajectory TP by equation

$$\theta_1 = \arccos[p/(n(R_T)R_T)] - \arccos[p/(n(R_P)R_P)] + \xi_1(p), \tag{3.9}$$

where $R_T=a+H_T$, $R_P=a+H_P$, a is the Earth's radius. Trajectory of the second type is described by relation

$$\theta_2 = \arccos[p/(n(R_T)R_T)] + \arccos[p/(n(R_P)R_P)] + \xi_2(p). \tag{3.10}$$

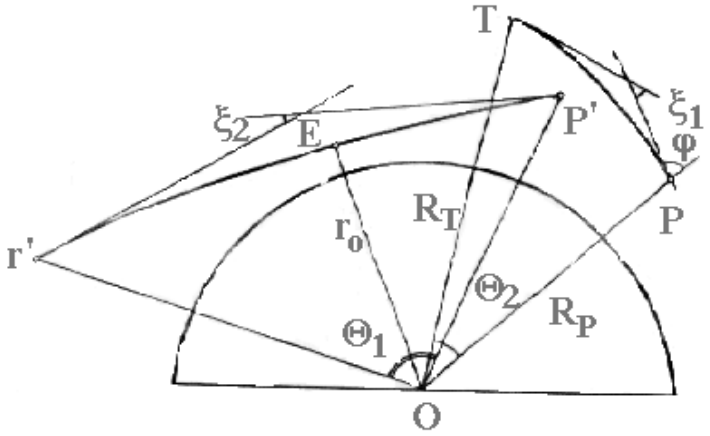

Fig. 3.2. Geometrical relations in radio occultation experiments

The next equations may be revealed for the bending angles $\xi_1(p)$, $\xi_2(p)$:

$$\xi_1(p) = -p \int_{R_P}^{R_T} dn/dr \, (n^2 r^2 - p^2)^{-1/2}/n dr \qquad (3.11)$$

$$\xi_2(p) = -p \int_{r_o}^{R_T} dn/dr \, (n^2 r^2 - p^2)^{-1/2}/n dr - p \int_{r_o}^{R_P} dn/dr \, (n^2 r^2 - p^2)^{-1/2}/n dr, \qquad (3.12)$$

where $p = n(r_o) r_o$. Thus if we have measurements of the bending angles $\xi_1(p)$, $\xi_2(p)$ which are corresponding to trajectories TP and T′P′ we may combine the functions $\xi_1(p)$, $\xi_2(p)$ under the same values of the impact parameter p for subtracting the ionospheric contribution corresponding to the layers disposed higher than the altitude of the LEO satellite. This way of subtracting of the upper layers influence was suggested by *Gaikovich, Gurvich and Naumov* [1982] for solution of the problem of determining meteorological parameters for the case of receiver disposed in the atmosphere. The necessity of measurements of the refractive bending angles for positive and negative values of elevation angles with equal magnitudes of corresponding impact parameters was established. So the difference $\xi(p) = \xi_2(p) - \xi_1(p)$ may

be found and then using Abel's transformation the dependence $N(h)$ may be restored. Subtraction (3.11) from (3.12) gives for the case $R_P < R_T$:

$$\xi(p) = \xi_2(p) - \xi_1(p) = \int_{r_o}^{R_P} dn/dr \, (n^2 r^2 - p^2)^{-1/2}/n dr \, . \qquad (3.13)$$

According to (3.13) the bending angle $\xi(p)$ depends on values R_P, r_o. In the case of spherical symmetry the Abel's transformation may be used for determining $n(r)$ from known dependence $\xi(p)$:

$$n(r) - 1 = N(p) \approx ln(n) = \pi^{-1} . \int_{p}^{n_P R_P} \xi(p') dp' / (p'^2 - p^2)^{1/2} \, . \qquad (3.14)$$

The next equation may be obtained after integration by part from (3.14):

$$N(p) = \pi^{-1} \xi(n_P R_P) \ln[n_P R_P / p + ((n_P R_P / p)^2 - 1)^{1/2}] - \pi^{-1} \int_{p}^{n_P R_P} d\xi(p')/dp' \ln [p' / p + (p'^2/p^2 - 1)^{1/2}] dp' . \qquad (3.15)$$

After differentiating (3.15) relative to parameter p the connections between dN/dr and the function $d\xi/dp$ may be obtained:

$$(dN/dr)/(n + r dN/dr) = -\pi^{-1} \xi(n_P R_P) n_P R_P / [(n_P R_P)^2 - p^2)^{1/2}] + \pi^{-1} \int_{p}^{n_P R_P} d\xi(p')/dp' [(p'^2 - p^2)^{1/2}] p' / p dp' \qquad (3.16)$$

The distance R_P, the refractive index at the receiver installation n_P must be known for evaluation the altitude profile $N(h)$ on the measured functions $\xi(p) = \xi_2(p) - \xi_1(p)$ and $d\xi(p)/dp = d[\xi_2(p) - \xi_1(p)]/dp$.

For determination of connection between changes in frequency and in bending angle the next formulas for variation of phase $\Phi_{1,2}$ of radio waves corresponding to trajectories of the first and the second type may be used:

$$\Phi_1 = k\int_{R_P}^{R_T} (n^2 r^2 - p^2)^{1/2}\, r^{-1}\, dr + kp\theta_1\,, \quad k=2\pi/\lambda\,, \tag{3.17}$$

$$\Phi_2 = k\int_{r_o}^{R_T} (n^2 r^2 - p^2)^{1/2}\, r^{-1} dr + k\int_{r_o}^{R_P} (n^2 r^2 - p^2)^{1/2}\, r^{-1}\, dr + kp\theta_2. \tag{3.18}$$

The Doppler frequency after propagation of radio wave through the atmosphere may be found by differentiating (3.17) and (3.18) on time using (3.9) and (3.10):

$$F_1(t) = (2\pi)^{-1}\, d\Phi_1/dt = \lambda^{-1}\{\, pd\theta_1/dt + (dR_T/dt)/R_T\, [n^2(R_T)\, R_T^2 - p^2\,]^{1/2} - (dR_P/dt)/R_P [n^2(R_P)\, R_P^2 - p^2\,]^{1/2}\}\,, \tag{3.19}$$

$$F_2(t) = (2\pi)^{-1}\, d\Phi_2/dt = \lambda^{-1}\{\, pd\theta_2/dt + (dR_T/dt)/R_T [n^2(R_T)\, R_T^2 - p^2\,]^{1/2} + (dR_P/dt)/R_P [n^2(R_P)\, R_P^2 - p^2\,]^{1/2}\}\,. \tag{3.20}$$

The magnitudes $F_{1,2}(t)$ are describing the influence of the atmosphere and displacements of transmitter and receiver. It follows from (3.19) and (3.20) that impact parameter $p(t)$ as function of time may be retrieved from dependencies $F_{1,2}(t)$. The most simple case is when the parameters R_P, R_T do not change with time:

$$p_{1,2} = \lambda\, F_{1,2}(t)/(d\theta_{1,2}/dt). \tag{3.21}$$

The restored from (3.19), (3.20) or (3.21) impact parameter p may be used in (3.9), (3.10) for determination the refractive bending angles $\xi_{1,2}(p)$ if the coordinates of the transmitter and receiver $\theta_{1,2}$, R_T, R_P and the refractive index $n(R_T)$, $n(R_P)$ are known. The refractivity profile $N(h)$ may be found then by after substitution $\xi_{1,2}(p)$ in (3.13) and (3.14). The instrumental accuracy in this case is determined by errors in frequency measurements.

The described methodology may be used in the case when the time of radio occultation measurements are prolonged by factor 2-3 to obtain data for evaluation $\xi_1(p)$. However usually the beginning of radio occultation measurement is disposed after the time instant t_x and the need is existing for subtracting the upper ionosphere contribution by means of an appropriate model.

3.3. Connections between the phase path, refractive bending angle and amplitude in radio occultation measurements

The aim of this section is to obtain connection between the phase path excess, impact parameter, bending angle and amplitude for developing a radio physical model of the ionosphere. For the spherical symmetry case we may use as basic the connection (3.18) which may be transformed by means of relation

$$r^{-1} = (n\,r)'_r/(nr) - n'_r/n \tag{3.22}$$

to the form that describes connection between the phase excess Φ_e, impact parameter p and bending angle $\xi(p)$:

$$\Phi_e = (n^2(R_P)R_P^2 - p^2)^{1/2} + (R_T^2 - p^2)^{1/2} - (R_P^2 - p_b^2)^{1/2} - (R_T^2 - p_b^2)^{1/2} + p\theta(p) + \kappa(p) \tag{3.23}$$

$$\kappa(p) = -\int_{r_o}^{R_T} n'_r/n\,(n^2 r^2 - p^2)^{1/2}\,dr - \int_{r_o}^{R_P} n'_r/n\,(n^2 r^2 - p^2)^{1/2}\,dr, \quad \xi(p) = -d\kappa(p)/dp \tag{3.24}$$

where p, p_b are the impact parameters corresponding to the ray path in the ionosphere and atmosphere and to the straight path.

The phase excess Φ_e is given in raw occultation data for two frequency L1 and L2 as function of time. It may be easily shown for the case of circular orbits of LEO and GPS that

$$d\Phi_e/dt = p\,d\theta/dt \tag{3.25}$$

$$\theta = \pi + \xi(p) - \arcsin[p/R_T] - \arcsin[p/(n(R_P)R_P)], \tag{3.26}$$

where θ is the angle between directions TO and PO.(Fig. 3.2)

Connections between the bending angle and amplitude data may be found from expression derived by *Pavelyev and Kucherjavenkov* [1978]

$$X = [pn(R_P)R_{TP}^2]/\{R_T R_P n(R_T)\{\sin\theta[n^2(R_T)R_T^2 - p^2]^{1/2}[n^2(R_P)R_P^2 - p^2]^{1/2}\,|\,\partial\theta/\partial p\,|\}, \tag{3.27}$$

where X is the power attenuation owing to refraction relative to free space; R_{TP} is the distance

TG along direct path, θ is given by equation (3.26). The partial derivative $\partial\theta/\partial p$ must be evaluated under condition R_P, R_T =const. Using equations

$$dp/dt\ \partial\theta/\partial p = d\theta/dt - \partial\theta/\partial R_T\, dR_T/dt - \partial\theta/\partial R_P\, dR_P/dt = D_\theta(t,p);$$
$$\partial\theta(p)/\partial p = d\xi/dp - (R_T^2 - p^2)^{-1/2} - (R_P^2 - p^2)^{-1/2}, \qquad (3.28)$$

the next formula may be obtained from (3.27):

$$R_T R_P R_{TP}^{-2} T_n(t) D_\theta(t,p) X(t) \sin\theta = -pdp/dt/\{[n^2(R_T)R_T^2 - p^2]^{1/2}[n^2(R_P)R_P^2 - p^2]^{1/2}\}, \qquad (3.29)$$
$$T_n(t) = n(R_T)/n(R_P). \qquad (3.30)$$

It follows from (3.29) for the free space when refraction is absent:

$$R_T R_P R_{TP}^{-2}\, D_\theta(t,p_b) \sin\theta = p_b dp_b/dt/[(R_T^2 - p_b^2)^{1/2}(R_P^2 - p_b^2)^{1/2}],$$
$$\partial\theta(p_b)/\partial p_b = -(R_T^2 - p_b^2)^{-1/2} - (R_g^2 - p_b^2)^{-1/2}. \qquad (3.31)$$

The connection between p, $X(t)$ and p_b may be obtained from (3.29), (3.31):

$$p(dp/dt)/\{T_n(t)[n^2(R_T)R_T^2 - p^2]^{1/2}[n^2(R_P)R_P^2 - p^2]^{1/2}\} =$$
$$= X(t)p_b(dp_b/dt)/[(R_T^2 - p_b^2)^{1/2}(R_P^2 - p_b^2)^{1/2}]. \qquad (3.32)$$

In general case (3.32) gives connection between derivatives dp/dt and dp_b/dt and allows to find using experimental function $X(t)$ the temporal dependence of impact parameter $p(t)$ if some initial condition is given. Under assumptions $p \approx p_b$, $n(R_P)=1$, $n(R_T)=1$ (3.29) may be simplified

$$dp/dt = X(t)dp_b/dt, \qquad p(t) - p(t_o) = \int_{t_o}^{t} X[t(p_b)]\, dp_b\,. \qquad (3.33)$$

Equation (3.33) gives using the experimental refraction attenuation $X(t)$ the temporal dependence of the impact parameter $p(t)$ if initial value $p(t_o)$ in the time instant t_o and ballistic impact parameter p_b as function of time are known. Similar way may be applied to find the temporal dependence of $d\xi/dp$ on time. For this aim it may be noted that formula (3.27) is described also the case when the refraction is absent (free space case). From comparing the

free space case and refraction case and supposing $p \approx p_b$ one may obtain using (3.27), (3.28), (3.31):

$$X(t) \approx [\partial\theta(p_b)/\partial p_b]/\partial\theta(p)/\partial p,$$
$$d\xi/dp=[1-1/X(t)][(R_T^2-p_b^2)^{-1/2}+(R_g^2-p_b^2)^{-1/2}]. \quad (3.34)$$

Equation (3.34) gives the temporal dependence $d\xi/dp$. Thus the amplitude data may be used for restoration impact parameter $p(t)$, bending angle $\xi(t)$ and $d\xi/dp(t)$. This temporal dependencies may be used for finding the vertical distributions of the refractive index and electron density. For revealing gradient of electron density distribution from the amplitude data the equations derived by *Kalashnikov et al.,* [1986] may be used

$$dN(h)/dh_{1,2} \approx C_{a1,2}/[(a+h)\pi] \int_{a+h}^{\infty} pdp\, d\xi_{1,2}(p)/dp[p^2-(a+h)^2]^{-1/2}, \quad C_{a1,2}=f_{1,2}^2/40.3, \quad (3.35)$$

$$d\xi_{1,2}(p)/dp= (X_{1,2}-1)/X_{1,2}\,[(R_T^2-p^2)^{-1/2}+(R_P^2-p^2)^{-1/2})],$$
$$X_{1,2}= A_{1,2}^2/A_{1,2o}^2; \quad h= p-a, \quad (3.36)$$

where a is the Earth's radius, $A_{1,2}$ is the amplitude of the radio occultation signal, $A_{1,2o}$ is the amplitude before radio occultation, $C_{a1,2}$ is a scaling factor depending on frequency. Expressions (35), (36) give the dependence $dN(h)/dh_{1,2}$ on the height h separately for each frequency *f1, f2*. For diminishing influence of the random noise the next formula may be applied for the gradient evaluation:

$$dN(h)/dh=[dN(h)/dh_1 + dN(h)/dh_2]/2. \quad (3.37)$$

Combined analysis of the results obtained separately from the phase and amplitude data is needing for removing systematic errors that may arise due to inaccuracies in subtracting of low frequency trends.

3.4. Development model and program module for correction of ionospheric influence

Radio physical model uses equations (3.23), (3.24), (3.26)-(3.32) for description ionospheric contribution at low altitudes. For practical applications it is needing to describe dependence of the refractive index and its gradient in the ionosphere. For this aim the existing models of the ionosphere may be applied, for example, published in *Orlyanskii et al.,* [1997].

The dependence of the refractive index may be used in the Fourie form

$$N(H)=A(H-H_o)^n \exp[-(H-H_o)/\Delta H][1+\sum_{j=0}^{M} a_j \exp[-(H-H_o)/\Delta H_j]\cos(2\pi j(H-H_o)/D+\varphi_j)], \quad (3.38)$$

$$H>H_o$$

where $N(H)$ is the refractivity, A is the coefficient depending on frequency, H_o is initial height of the ionosphere, D is the vertical size of the ionosphere, $\Delta H, \Delta H_j$ are correspondingly the general width and the spatial dimension of the j-th wavelet in the electron density distribution of the ionosphere, a_j, φ_j are the amplitude and phase of j-th wavelet, M is general number of Fourie components in the altitude electron density distribution, n is a parameter of model, n >2. Factor ΔH_j may be negative, in this case the condition must be satisfied: $|\Delta H_j| > \Delta H$.

The parameters A, D, n, M, $H_o, \Delta H, \Delta H_j, a_j, \varphi_j$ may be defined using existing models of the ionosphere and may be different for the first path (LEO-atmosphere) and for the second path (atmosphere-GPS) (Fig.3.1). However this parameters do not depend on horizontal distance. Equation (3.38) is convenient for description the ionospheric influence because the dependencies of the phase path, bending angle and amplitude on the impact parameter have simple analytical form.

Radio physical model (3.38) has been used for developing preliminary program module for calculation ionospheric contribution in the low altitude radio occultation data. Examples of preliminary calculations are shown in Fig. 3.3 – 3.5 for the case n=10; 16; M=2; ΔH=500 km; $\Delta H_{0,1}=\infty$; H_o=250 km; $\varphi_{0,1}=0$ $a_{0,1}=1$ D=100 km. The electron density altitude distribution corresponding to n=10 (a) and n=16 (b) is shown in Fig. 3.3. This distributions have maximums of electron density equal to 600 and 1300 thousands electron per cubic centimeter at heights near 340 and 390 km. This distributions may describe influence of the F-layer of the ionosphere. For calculating the influence of broad ionospheric tail one may chose in (3.38) additional terms with corresponding tail's parameters. In the Fig. 3.4 (b) are given results of evaluation phase excess as function of the height for electron density distribution shown in Fig. 3.3 (b). For comparing in the upper part of Fig. 3.4 are given experimental altitude dependence of the phase path excess at frequency L1 for GPS/MET occultation event № o0460406. The behavior of the slopes of both curves is similar, the difference in the magnitudes is connecting with 2π uncertainty in GPS/MET phase path measurements. In Fig. 3.5 (b) the impact parameter computed from (3.38) for n=10 is compared with experimental

dependence of the impact parameters obtained from GPS/MET radio occultation data (a). The maximum (at the height near 95 km) in the experimental data is corresponding to E-layer of the ionosphere, which influence have not been accounted for in calculations. The influence of the upper ionosphere is seen in the Fig. 3.5 (a) as a constant displacement equal to 260 and 410 m at frequencies L1 and L2. The modeled dependence of the impact parameters have more lower value due to small magnitude of total electron concentration chosen in calculation. Preliminary results of examination of program module shown the effectiveness of developed radio physical model for description of the influence of the upper ionosphere. This module may be elaborated further for description in full volume the influence of the upper ionosphere using existing ionospheric models.

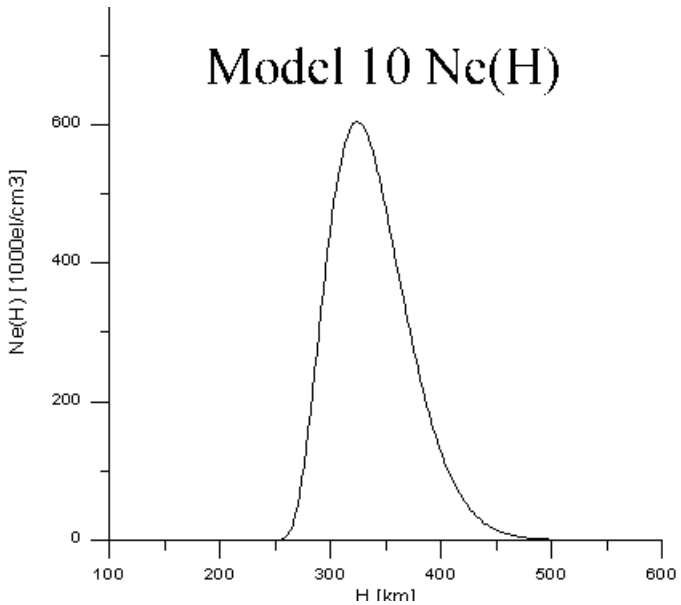

(a)

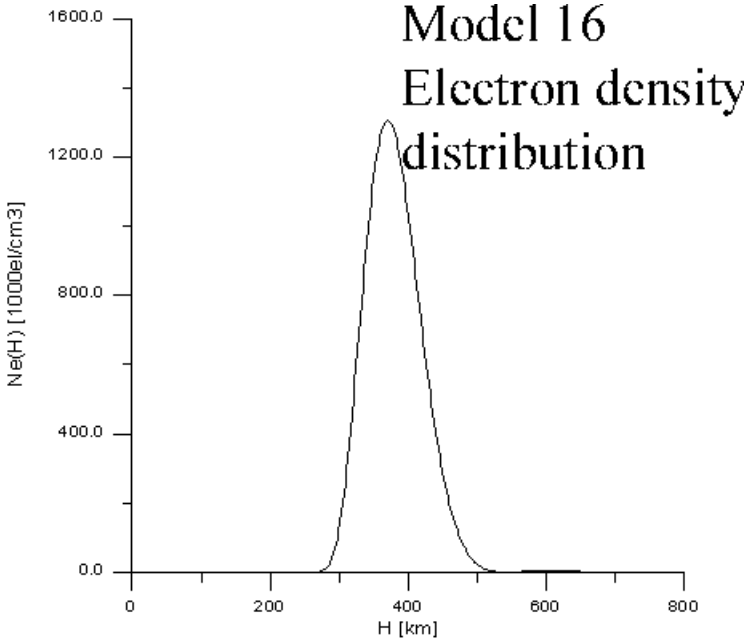

(b)

Fig. 3.3. Examples of model of F-layer of the ionosphere, corresponding to n=10 (a) and n=16 (b).

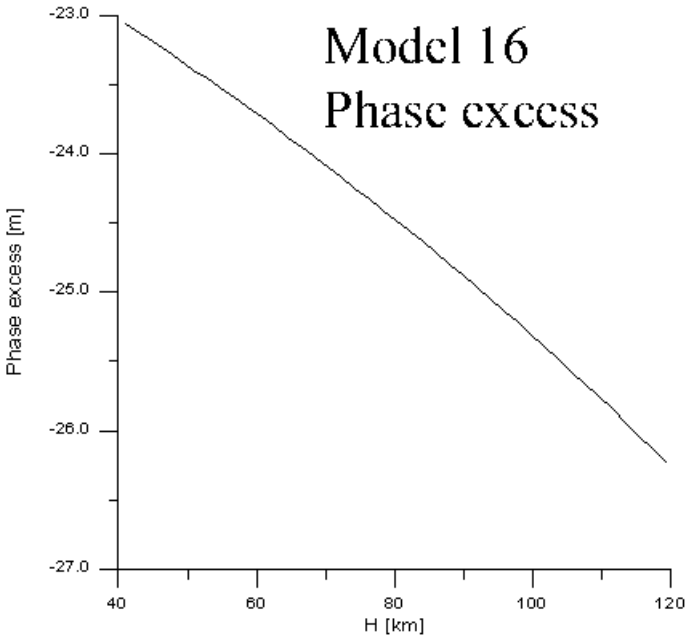

(a)

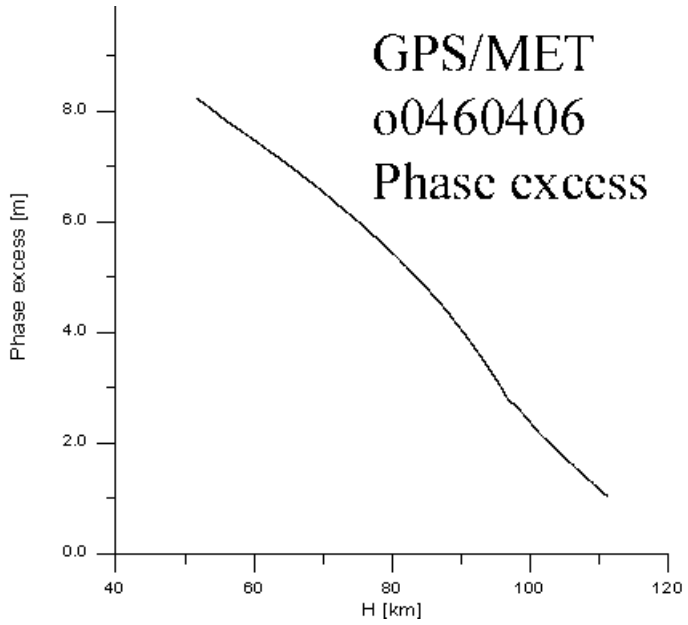

(b)

Fig. 3.4. Theoretical model with n=16 (a) and experimental (b) phase excess altitude dependence. The behaviour of both curves are similar. The difference in the magnitudes is due to uncertainty in initial GPS/MET data.

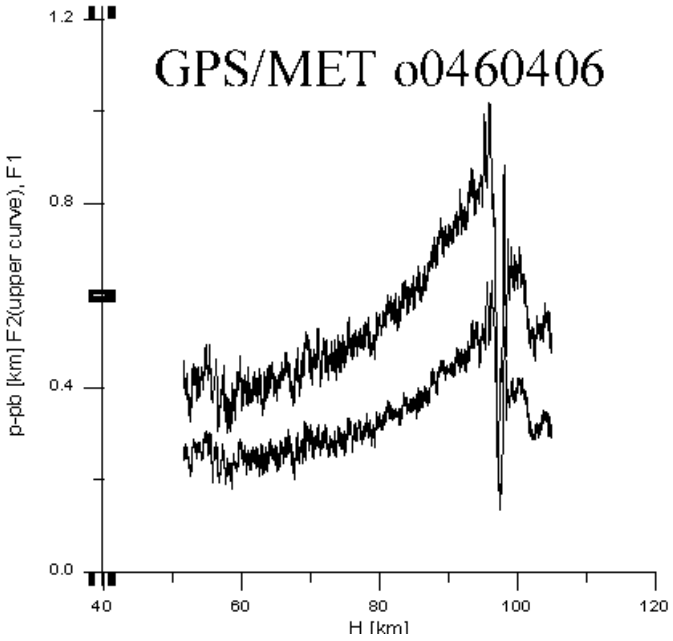

(a)

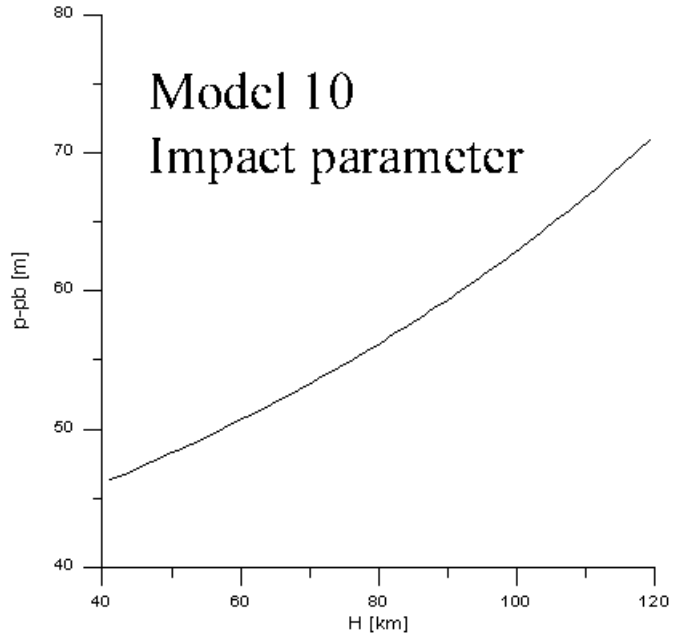

(b)

Fig. 3.5. Dependence of impact parameters at frequencies *F1, F2* (a) and theoretical dependence (b) corresponding to model with n=10. Experimental impact parameter is greater by factor 3..5 due to higher value of total electron concentration in the real ionosphere.

3.5. Revealing features in E- and D- layer of the ionosphere

Processes in the upper atmosphere (height interval 60-120 km) now are staying outside of attention of the most radio occultation works besides some rare publications, for example, [*Vorob'ev et al.,* 1999], applied the phase screen theory for deriving electron density distribution in the E-layer of ionosphere from amplitude GPS/MET data. However, phenomena in the upper atmosphere can be analyzed more carefully using high-precision GPS/MET radio occultation data. Comparing may be done with results of Earth-based observations for validation [*Igarashi et al.* 1999]. Wave structures in the upper atmosphere are producing short-period changes both in the phase and amplitude radio occultation data at frequencies L1 and L2. The phase changes are hidden under the more intense low-frequency phone arising owing to the ionospheric F-layer. The corresponding amplitude variations are visible more clearly, however interference of low-frequency noise must be removed also. In this case the radio holography may be applied in a form of perturbation method that use filtration of low frequency and high frequency components separately for the phase and amplitude radio occultation signals to retrieve electron density altitude profiles in the upper atmosphere. For the phase channel it is convenient to use the phase difference *F1-F2* for estimation refractivity profile because existing systematic error in the phases *F1, F2* connected with 2π and initial uncertainties in the *F1, F2* data (usually in the raw radio occultation data $F1_o = F2_o = 1$ m in the beginning of a measurement session). After removing the low frequency noise (or trends) from the phase and amplitude data (this may be achieved by means of the appropriate model of the upper ionosphere) it is possible to apply two inversion formula separately for the phase and amplitude channels. For the phase channel the Abel's inversion formula may be applied:

$$N(h) \approx -C/\pi \int_{a+h}^{\infty} d\kappa(p)/[p^2 - (a+h)^2]^{1/2}, \quad \kappa(p) = (F1-F2)_r, \quad C = f_1^2 f_2^2 /[40.3(f_1^2 - f_2^2)], \tag{3.39}$$

where $(F1-F2)_r$ is the phase residuals after subtracting the F-layer's trend, p is ballistic impact parameter, h is the height above the Earth's surface, $N(h)$ is the perturbation part of the electron density altitude distribution (el/m^3), C is the scaling factor, f_1, f_2 are the frequencies L1, L2 [Hz].

The results of the application of radio holographic analysis and low noise filtration

method to two GPS/MET occultation event (07 February 1997, No. 0447, 0158), D-region of the ionosphere, are shown in Fig. 3.6. The occultation event No. 0447 took place near Japan (Okinawa) during the local winter mid-nighttime. For the data given in Fig. 3.6 the time-spatial coordinates of ray perihelion height H was near 25.5^o N 231.7^o W, H=95 km, 15 h 53 m 23 s UT. The three right curves in Fig. 3.6 correspond to the experimental phase (upper curve) and amplitude (curve L1 and L2) data. Upper curve describes phase difference *F1-F2* [m] between carriers L1 and L2 that shows slow trend from +1 to –4 cm and small high-frequency residuals variations in the interval ±5 mm. Curves L1 and L2 show the height dependence of the normalized amplitudes at frequencies L1 and L2. Some correspondence may be seen from the *F1-F2* small high-frequency changes and amplitude *A1, A2* variations in the height interval 62-81 km. This variations may correspond to wave structures in the D-layer of the ionosphere. This structures are more clearly seen in the both amplitudes *A1* and *A2*. The electron density vertical gradient distribution $dN_a(H)/dH$ restored from the amplitude data is shown by lower curve in Fig. 3.6 (left). The middle curve in the left side of Fig. 3.6 corresponds to the electron density distribution $N_a(H)$ (amplitude data) found by integration of the gradient $dN_a(H)/dH$ on height. The upper left curve in Fig. 3.6 describes $N_p(H)$ distribution found using the phase residuals data. Both $N_a(H)$, $N_p(H)$ curves show correspondence in high spatial frequency variations (spatial periods 1-2 km) despite some differences in the low frequency domain (spatial periods 10-15 km). This fact shows that the systematic errors is greater in low frequency domain and low in high frequency region. This conclusion is suggested by analysis of the data of the second event. The results for the another GPS/MET occultation event (07 February 1997, No. 0158), E-region of the ionosphere, are shown in Fig. 3.7. The studied occultation event took place during the local summer daytime in the Antarctic region. For the data given in Fig. 3.7 the time-spatial coordinates of ray perihelion height H changed from 71.2^o S 18.2^o W, H=95 km, 14 h 51 m 05 s UT to 70.5^o S 16.4^o W, H=60 km, 14 h 51 m 25 s UT. The raw amplitude corresponding to frequencies *F1* and *F2* and phase path difference *F1-F2* are given in Fig. 3.7 (left). A general coincidence between phase and amplitude changes in the altitude interval 102-108 km may be seen. After removing trends from phase path data caused by interference of the upper part of the ionosphere, the influence of wave part of electron density distribution on the phase data may be seen (Fig. 3.7, right). For comparison, the ratio *A2/A1* is also shown. The value of the phase path connected with

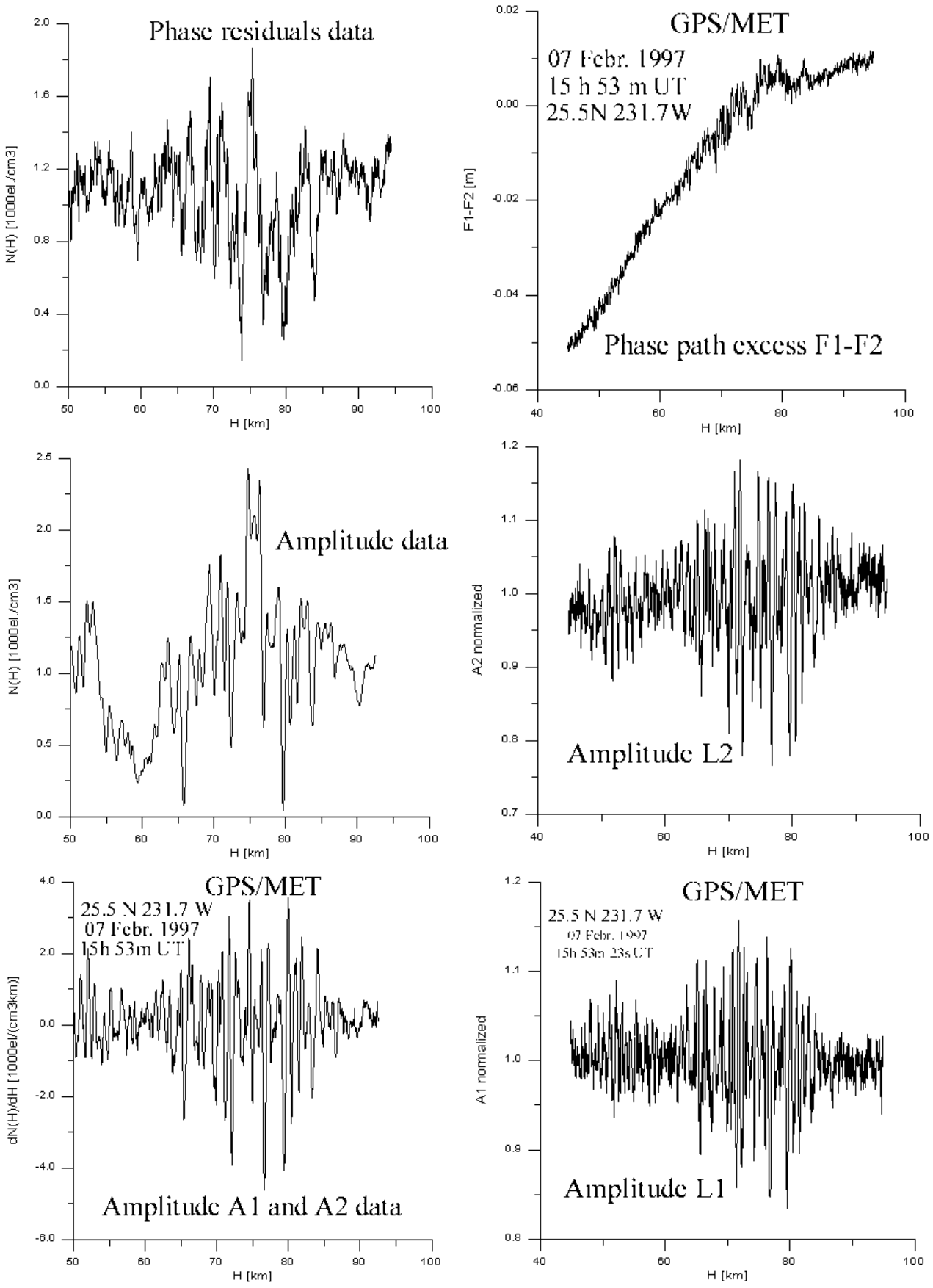

Fig. 3.6. Observation of wave structures in D-region of the ionosphere using phase and amplitude GPS/MET radio occultation data.

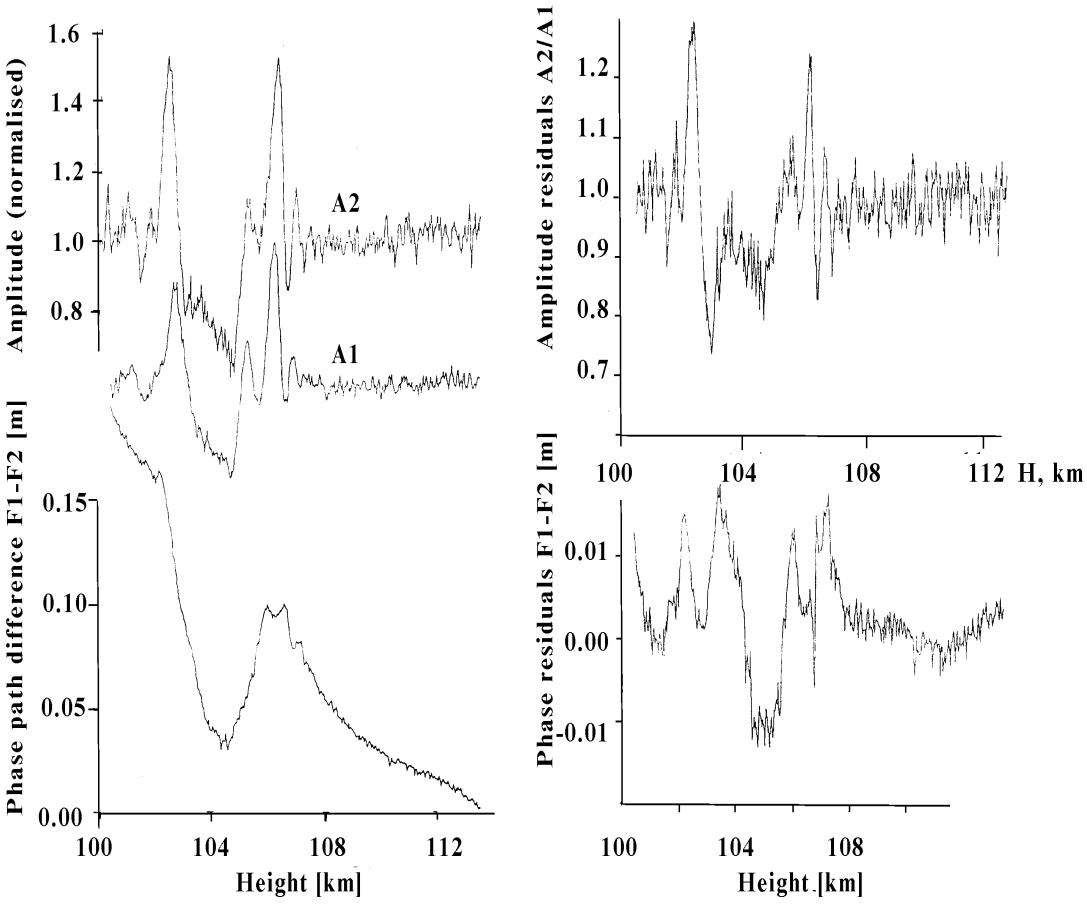

Fig. 3.7. Connection of the phase path difference *F1-F2* and amplitude variations in E-layer.

wave structures changes in the interval ±1 cm, this is lower by a factor 10 than the whole contribution of the E-layer. The amplitude ratio also followed phase path changes with some delay. In Fig. 3.8, the results of restoration of the electron density altitude profile $N_e(H)$ from phase data and gradient $dN_e(H)/dH$ from amplitude data are shown (left). The maximum in electron density distribution equal to $6.1 \cdot 10^4$ el/cm^3 corresponds to height 104 km. The maximum gradient of the electron density distribution $dN_e(H)/dH = 6.8 \cdot 10^4$ el/(cm^{3}km)) corresponds to a height 103 of km. The forms of features seen in the electron density distribution may be revealed in perturbed part of the phase path and amplitude using Abel' inversion. The wave structure in the electron density distribution $N_e(H)$ from phase data and gradient $dN_e(H)/dH$ from amplitude data is shown in Fig. 3.8 (right). The vertical period of the

wave changed from 2 km to 0.5 km. The amplitude of the wave structures is 2 to 3 $\cdot 10^3$ el/(cm^3). The origin of wave structures may be connected with gravitational waves and wind shears existing in the ionospheric E-layer as it has been observed by *Igarashi et al.,* [1998]), *Yamamoto et. al.,* [1998].

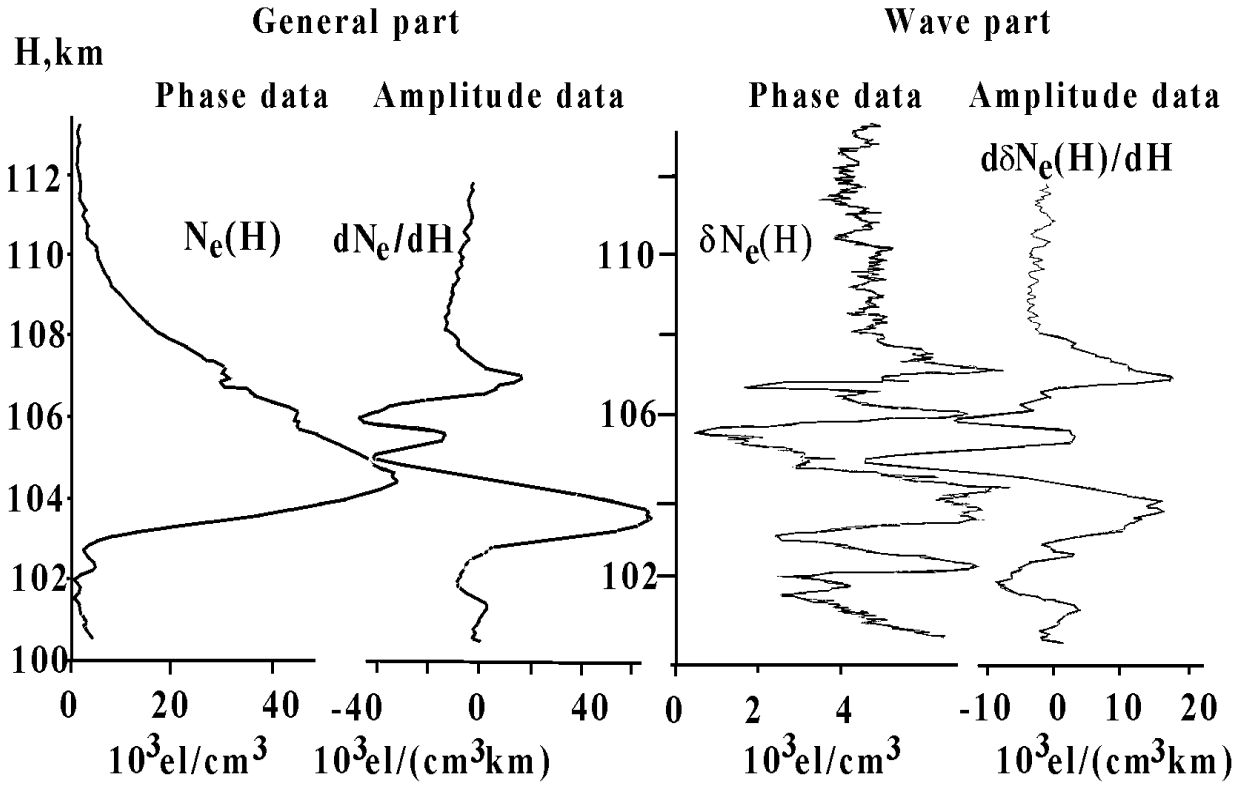

Fig. 3.8. $N_e(H)$ (phase data), $dN_e(H)/dH$ (amplitude data) (left) and wave structures (right) in ionospheric E-layer.

4. Radio holographic technique: applying to radio occultation data analysis and validation using GPS/MET data

4.1. Current state of radio occultation problem

The high accuracy of the radio occultation sounding was demonstrated using the Global Positioning System (GPS) at wavelengths 19 and 24 cm [*Ware et al*., 1996; *Kursinski et al.,* 1996, 1997; *Rocken et al.,* 1997; *Feng and Herman*,1999; *Schreiner et al.,*1999]. First experiments in another frequency bands have been provided in 1989-1998 years at wavelengths 2 and 32 cm as described by *Yakovlev et al.* [1995a].

Now the first stage of investigating of the Earth's atmosphere and ionosphere has been accomplished using this method and new radio occultation missions are under elaboration (see, for example, *Anthes et al.,* [2000]). The results of this stage of radio occultation investigations show the need to design a new radio occultation methodology that includes combined amplitude and phase data analysis for achieving better spatial resolution and accuracy in vertical profiles of atmospheric and ionospheric parameters. Some basic approaches of the technology have been developed early during Viking, Voyager, Pioneer Venus missions [*Marouf et al.,* 1986; *Tyler et al.,* 1989]. *Lindal et al.* [1987] applied some methods of radio holography for observing multibeam propagation in Uranus atmosphere. They derived the power spectra as a function of time and revealed multibeam propagation caused by a methane cloud layer in the atmosphere of Uranus. *Lindal* [1992] applied multibeam approach to interpret Voyager Neptune occultation data. However, up to now the phase dependence on time in radio occultation measurements has been the main source of information for evaluating the vertical profiles of atmospheric and ionospheric parameters. It may be noted that amplitude data contain valuable information on the refractivity gradient altitude distribution. This information is important for observing wave structures and estimating the parameters of natural phenomena in the upper atmosphere. Attempts to combine phase and amplitude information by applying a backward method have been made by *Gurvich, Gorbunov, and Bengtsson* [1996]; *Karayel and Hinson* [1997]; *Mortensen and Hoeg* [1998]; *Mortensen et al.,* [1999]. An attempt to apply a method of deciphering the ray structure in regions of multipath propagation based on diffraction theory and the principles of

synthesized aperture has been described by *Gurvich and Gorbunov* [1998]. They provided numerical modeling of the method and shown the possibility for the refinement of the vertical resolution beyond the Fresnel scale up to value ~ 100 m at wavelength 19 cm. Radio holographic approach was suggested for this aim also by *Pavelyev et al.* [1998, 1999]; *Hocke et al.* [1999] on the basis of the fundamental theoretical radio optics approach derived by *Zverev* [1975]. Main task of both backward propagation and radio holographic methods consists in developing algorithms that using full precision of GPS radio navigational field for achieving extreme accuracy and spatial resolution in evaluation of altitude dependence of meteorological and ionospheric parameters from results of radio occultation measurements.

4.2. Radio holographic technique

The application of the radio holographic approach to this objective consists in using focused synthetic aperture method. This approach combines trajectory data and the refractive index model to obtain the maximal spatial compression of the main beam separately from the other rays trajectories. This makes possible to evaluate the intensity of radio waves at each beam trajectory and the corresponding angular displacement from a reference beam.

The aim of this section is to test the radio holographic concept by using the results of radio occultation measurements provided at wavelengths 19 and 24 cm (GPS/MET data) and to show possibility of application combined phase and amplitude radio occultation data for observing wave structures in the upper atmosphere.

The scheme of radio occultation observation is shown in Fig. 4.1. The terrestrial atmosphere is modeled locally as being spherically symmetrical, with a local centre of curvature at O. One of the “ray paths” followed by radio signals propagating from GPS to LEO satellites (points G and T, respectively) lies in the plane of Fig. 4.1, which also contains the point O. The ray has impact parameter p and corresponding refraction angle $\xi(p)$. The next connections are existing between $\xi(p)$ and p for the case of spherical symmetry:

$$\beta = \pi + \xi(p) - \theta - \mu - \arcsin[p/(R_g)], \qquad p = R_T \sin(\beta + \mu), \tag{4.1}$$

where R_T, R_g is the distances TO and GO. Since the functions $\theta(t)$, $R_T(t)$, $R_g(t)$ are known from trajectory data, equations (4.1) give impact parameter p if the refraction angle $\xi(p)$ or angle β are measured. In the case of multibeam propagation the determination of $\xi(p)$ is difficult

because the main beam GT is observed on the phone of the sum of the fields of secondary beams that are together with the main beam components of the angular spectrum of radio waves $A_s(\beta)$. The angular spectrum presents the radio field $E(\mathbf{r},t)$ as a superposition of waves having complex amplitude $A_{sj}(\beta)$ propagating at different angles β_j relative to the line TO:

$$E(\mathbf{r},t)=\sum_{j=1}^{M} A_{s\,j}(\beta_j)\, exp[i(\omega_o t-k\Phi(\beta_j,t))];$$

$$\Phi(\beta_j,t)=\int_{R_T}^{R_g} n_j dl; \qquad (4.2)$$

$$\Phi(\beta_j,t)= S_b(t)+S(\beta_j); \quad k=2\pi/\lambda,$$

where $\omega_o=2\pi f_o$, f_o-carrier frequency of radio field, n_j-is the refractive index distribution along j-th ray trajectory, M is a number of the ray trajectories connecting points T and G (M may be a function of time depending on physical conditions in the atmosphere), $\Phi(\beta_j,t)$ is the eikonal defined according to *Kravtsov and Orlov* [1990]. The function $\Phi(\beta_j,t)$ includes the free space $S_b(t)$ and combined ionospheric and atmospheric contributions $S(\beta_j)$ to the eikonal. The rays observed at point T may have different origin due to refraction in the atmosphere and ionosphere, scattering on irregularities, diffraction phenomena near caustics, etc. The eikonals $S(\beta_j)$ arising owing to refraction mechanisms have a common property expressed by the next relation derived under assumptions of spherical symmetry of the atmosphere and circular orbits of LEO and GPS satellites [*Pavelyev and Yeliseyev*, 1988]:

$$F_{dj} =\lambda^{-1}(dS(\beta_j,t)/dt)= -\lambda^{-1}p_j(d\theta/dt). \qquad (4.3)$$

Relation (4.3) describes connection of Doppler frequency excess F_{dj} with impact parameter p_j of j-th ray.

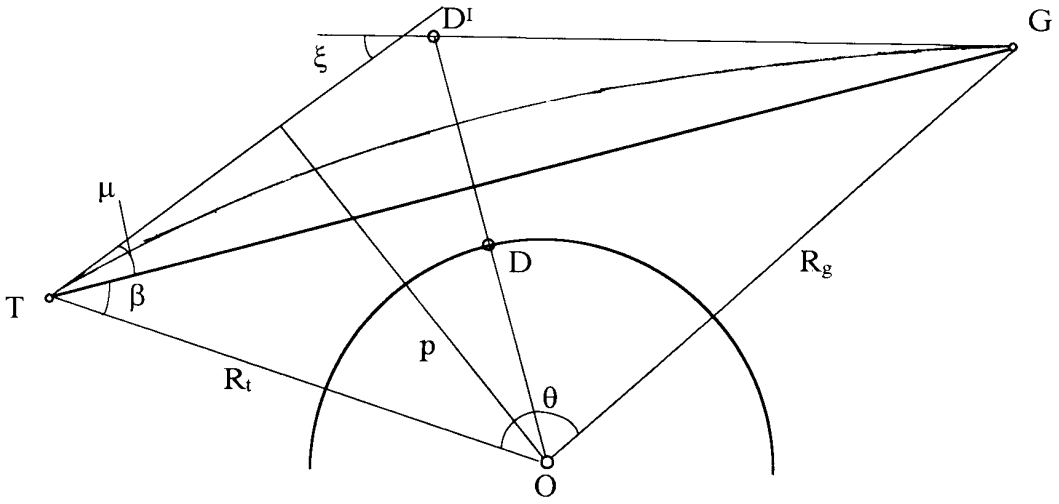

Fig. 4.1. Scheme of radio occultation

Record of complex radio signals along the LEO trajectory is the radio hologram's envelope that contains the amplitude $A(t)$ and phase path excess $\psi(t)= kS_e(t)$ of the radio field as functions of time which may be combined in the complex form:

$$E(t) =A(t) \exp[-i\psi(t)]. \qquad (4.4)$$

Temporal dependencies of the amplitude $A(t)$ and eikonal $S_e(t)$ are given in the GPS-MET radio occultation data. Dependence $E(t)$ on time contains information on the spatial distribution of the radio field. The radio field $E(\mathbf{r},t)$ from (4.2) is equal to $E(t)$ from (4.4) if ω_o =0, $S_b(t)$=0 (the free space term in eikonal is usually removed from radio occultation data) and $\mathbf{r}(t)$ describes the orbital motion of LEO satellite. A reference wave field $E_m(t)$=exp$[i\psi_m(t)]$, $\psi_m(t)= kS_m(t)$ may be used to reveal the angular spectra $A_{sj}(\beta_j)$ from radio hologram, where $\psi_m(t)$ and $S_m(t)$ are the expected phase path excess and eikonal for radio occultation region. The ray corresponding to the phase function $\psi_m(t)$ begins in the point G and intersects the direction TO at angle $\beta_m(t)$ in the point T. The form of the eikonal $S_m(t)$ may be different depending on the atmosphere properties according to season, geographic position and expected weather conditions in the radio occultation region. The function $S_m(t)$ may be evaluated using various models of the atmosphere and ionosphere, for example, the models proposed by *Pavelyev et al.,* [1996]. The next equation may be found after multiplication both sides (4.2) by the reference field $E_m(t)$:

$$E(t)\, E_m(t)=A(t) \exp\{-i[\psi(t)-\psi_m(t)]\}= \sum_{j=1}^{M} A_{s\,j}(\beta_j) \exp[-ik(S(\beta_j,t)-S_m(t))]. \qquad (4.5)$$

Using relation (4.3) the difference $S(\beta,t)-S_m(t)$ may be presented inside the time interval $-T/2<t<T/2$ in the form (under assumption $d\theta/dt$=const which is fulfilled for the case of circular orbits of LEO and GPS satellites):

$$S(\beta_j,t)-S_m(t)=S_{oj}+d\theta/dt[(p_j-p_m)t+d(p_j-p_m)/dt\, t^2/2!+...+d^{n-1}(p_j-p_m)/dt^{n-1}t^n/n!], \qquad (4.6)$$

where all derivatives in (4.6) are corresponding to the time instant t=0 that determines the spatial position of the phase center of the focused synthetic aperture. Equation (4.6) gives the phase distribution along the focused synthetic aperture for j-th ray relatively to the reference

beam. It is convenient to apply a spectral method for solution (4.5). For this aim it is necessary to multiply both parts of (4.5) by factor $\exp(-i\omega t)$, and integrate on time in the interval $-T/2 \le t \le T/2$. In the result the main power will correspond to the rays that are matched with function $S_m(t)$ in the sense that only two terms in the right side of (4.5) may be retained. For such rays after integration the next equation describing radio hologram's spectrum $W(\omega)$ may be obtained:

$$W(\omega)=\int_{-T/2}^{T/2} dt E(t)\, E_m(t)\exp(-i\omega t)=\sum_{J=1}^{M_1} A_s(\beta_j)d\beta f(\omega,\omega_j); \qquad \omega_j = k\, d\theta/dt\, (p_j-p_m)_o\,; \tag{4.7}$$

$$f(\omega,\omega_j)=\exp(-ikS_{oj})(\sin X_j)/X_j; \quad X_j = T(\omega-\omega_j)/2, \tag{4.8}$$

where M_1 is a number of rays that are in coherence with the reference beam.

According to (4.8), the module of function $f(\omega,\omega_j)$ has a sharp maximum at value of angle β_j, equal to:

$$\beta_j=\arcsin[\omega/kv+\sin(\beta_m+\mu_o)] - \mu_o; \qquad v=R_T(d\theta/dt), \tag{4.9}$$

Thus there is correspondence between angle β_j and the angular frequency ω described by (4.9). The measured value of the angle β_j is corresponding to the time instant t=0. According to (4.7)-(4.9) the angular spectrum $A_{sj}(\beta_j(\omega))$ may be found from approximate equation:

$$|A_{s\,j}(\beta_j(\omega))| \approx |W(\omega)|/\pi. \tag{4.10}$$

The angular width of the maximum $\Delta\beta$ depends on T. If T increases, the angular resolution in the angular spectrum increases and $\Delta\beta$ diminishes. Resulting resolution in the angular spectrum $\Delta\beta$ and corresponding vertical resolution Δh can be found from:

$$\Delta\beta=\lambda\Delta f/(2v); \quad \Delta f=1/T; \quad \Delta\beta=\pi/(Tkv); \quad \Delta h=L\Delta\beta; \quad L\approx(r^2-p^2)^{1/2}, \tag{4.11}$$

where $k=2\pi/\lambda$, T is the time of coherent data handling. According to Eq. (4.11) the accuracy of the radio holographic method increases when v and T are growing and the wavelength is diminishing. The wavelength dependence of angular resolution, Eq. (4.11), is distinct from the Fresnel one: $\Delta\beta$(radioholographic)~λ and $\Delta\beta$(Fresnel)~$\lambda^{1/2}$. Due to this difference, the radio holographic method seems to be an effective tool for radio occultation data analysis. The

angular position of the main beam β according to (4.1) is related to the impact parameter p and bending angle $\xi(p)$. After estimating dependence $\xi(p)$ the standard Abel inversion procedure may be used for determination the refractive index altitude profile as described by *Gorbunov et al.* [1996]. The analysis of errors connected with possible influence of the choice of the data window length is discussed by *Hocke et al.* [1999]. It follows from this analysis that the angular resolution of the radio holographic method may achieve 3-5 microradians. The angular spectrum may be prolonged along the rays up to any plane disposed near the atmosphere. In this case the angular spectrum may be interpreted as "radio image" or "radio brightness distribution" of the atmosphere and ionosphere as seen from the LEO orbit.

It may be noted that there exists a deep analogy between the focused synthetic aperture method applied to high resolution radar imaging (see, for example, *Wehner,* [1987], section 6.4 SAR Theory (Focused Aperture)) and the radio holographic approach, except the only difference: a target in the radio occultation case is a ray, moving through the atmosphere. The main requirement in the both cases is to find such function $\psi_m(t)$ that gives minimum angular width of the main maximum in the angular spectrum. This may be considered as maximum spatial compression of the radio occultation signal. For fulfilling this requirement the refractivity altitude dependence used in the radio physical model must be close to the real height dependence of the refractive index in the radio occultation region. If the used model of a target is accurate then extreme instrumental spatial resolution may be achieved (one half of the real antenna's aperture in the radar case as it described by *Wehner,* [1987], the angular accuracy $\Delta\beta$ and vertical resolution Δh from Eq. (4.11) in the radio occultation case). Really the resolution may be lower owing to influence of turbulence, horizontal irregularity of the atmosphere and other effects that can't be predicted by reference model. Thus spectral radio holographic method reveals only the rays in the angular spectrum that are in coherence (or matched in the sense of high resolution radar imaging technology) with the reference beam.

The angular spectrum may be prolonged along the corresponding rays in the plane PGO up to any straight line disposed near the atmosphere (for example, DD' in Fig. 4.1). In this case the angular spectrum may be interpreted as the "radio image" or "radio brightness distribution" of the atmosphere and ionosphere as seen from the LEO satellite's orbit. As an example, the results of an application of the radio holographic approach to the analysis of GPS/MET radio occultation data (event No.0392, February 05, 1997) are shown in Fig. 4.2. The vertical

distribution of radio brightness reveals a high vertical resolution of about 70-80 m in the mesosphere (upper left panel of Fig. 4.2). The radio brightness distribution in the troposphere at a level of 2 km is shown in Fig. 4.2 (at upper right panel and the two lower panels). The two prominent features, representing the main beam and the signal, reflected from the sea's surface, were observed with a vertical resolution of about 80 m. Fig. 4.2 demonstrates that the radio holographic method may be capable of resolving some details in one-dimensional vertical radio images of the atmosphere, on the scale of 30-50 meters, and this corresponds to a spatial resolution of about 1/10 of the size Fresnel zone. This value is somewhat higher than the magnitude of the expected spatial resolution of about 100 m that corresponds to the backward propagation method as modified by *Mortensen et al,.* [1999]. Analysis of the radio hologram gives the angular spectrum of the radio waves at point P and the distribution of radio brightness along the line DD' (Fig. 4.1). The angular position of the main beam β determines the impact parameter p and the bending angle $\xi(p)$ (Fig. 4.1). After the dependence $\xi(p)$ on p has been estimated, the standard Abel inversion procedure may be used for determination of the refractive index altitude profile [*Gorbunov et al.,*1996].

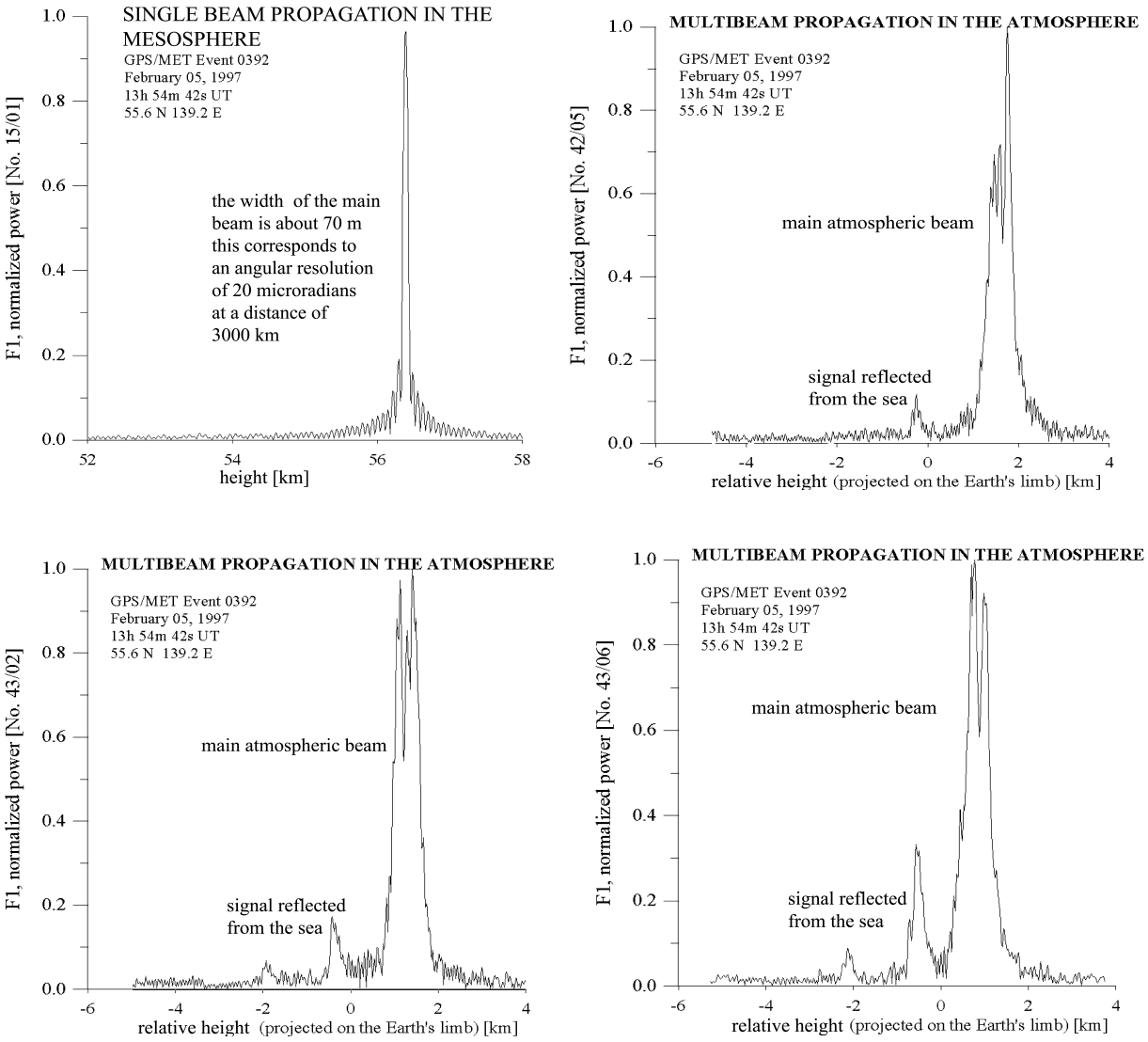

Fig. 4.2. Radio brightness distribution in the Earth's atmosphere as seen from the LEO satellite. Top left panel: mesosphere, single beam propagation, a vertical resolution of about 70 m. Top right and two lower panels: the signal, that has been reflected from the sea, is very well resolved relative to the main beam in the troposphere. The time interval between successive plots is about 0.48 seconds. Comparing the position of the reflected signal in neighboring panels shows the motion of the main beam. The vertical resolution is about 80 m.

4.3. Revealing multibeam propagation

Application of radio holographic principle to preliminary analysis of radio occultation data ("MIR"-GEO, at wavelength 32 cm; GPS/MET at wavelength 19 and 24 cm) led to direct observation multibeam propagation in the troposphere. An example of multibeam propagation in troposphere (at level H=3 km) obtained from radio occultation experiment MIR/GEO is shown in Fig. 4.3 (left part). The time interval between neighbouring spectra is equal to 1/32 sec. This value corresponds to distance nearly 250 m along the LEO trajectory. The time increases from lower left corner in upward direction to right top corner in Fig. 4.3 (left part). The width of main beam in angular spectrum at the half power level is about 40 microradian. This value corresponds to vertical extent of the beam in troposphere of the order 80 m. The power in the secondary beam and its vertical size is some times of the order of the corresponding values of the main beam. The changes in angular spectrum are connected with spatial distribution of radio field. Usually only one maximum corresponding to single ray trajectory (connecting transmitter installed on orbital station "MIR" and receiver on geo stationary satellite (GEO)) is seen, for example, - the spectrum in the left lower corner in Fig. 4.3. However the gradual transition from one to three beam propagation mode is noticeable in Fig. 4.3. This effect is connected with intersection of caustic boundary. Details of this process are important for fundamental theory of radio wave propagation in layered atmosphere. Results obtained by radio holographic method and shown in Fig. 4.3 give the first experimental evidence of caustics surface intersection observed from space and reveal connected diffraction phenomena. High vertical resolution of radio holographic method is also evident from analysis of GPS/MET radio occultation data. The resulting vertical radio brightness distributions are shown in Fig. 4.3 (right part). This data are relating with one radio occultation event 07 February 1997 (No. 0158). The upper curve describes experimental angular spectrum at height equal to 84 km. The width of the maximum is about 20 microradian and its vertical size is near 60 m. The broadening of angular spectrum in upper atmosphere may be connected with possible turbulence effects. Radio brightness distribution in the troposphere at level H=11.8 km is shown in right lower corner of Fig. 4.3. One pixel in angular spectrum corresponds to 0.004 mrad variation in arrival angle and 12 m change in height of ray perihelion. It follows from Fig. 4.3 that radio holographic method may resolve details in one-dimensional vertical radio image of the atmosphere with scale 12-50 metres, which corresponds to spatial resolution ~ 1/10 of Fresnel's zone size. This value is some

higher than magnitude of expected spatial resolution ~ 100 m corresponding to modified version of backward propagation method as described by *Mortensen and Hoeg* [1998]. The value of vertical resolution may be greater by choosing more heighten values of time interval T according to equation (4.11).

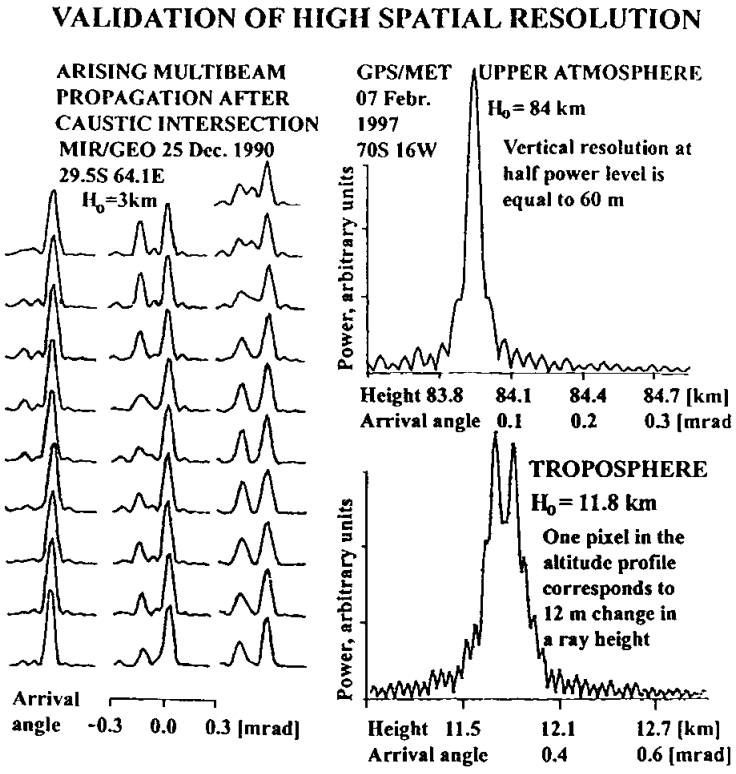

Fig. 4.3. Evidence of multibeam propagation from data of MIR/GEO and GPS/LEO radio occultation experiments.

4.4. Comparison of temperature profiles

Measurements of the arrival angle β permit to find dependence of the bending angle $\xi(p)$ on impact parameter p. The linear correction of bending angle must be applied in according with *Vorob'ev and Krasil'nilokova* [1994] for finding contribution of un-ionised part of atmosphere to the bending angle. Deflection of the impact parameters $\Delta p_{L1}=p_{L1}-p_m$ and $\Delta p_{L2}=p_{L2}-p_m$ from value p_m calculated using refractivity model described by *Pavelyev* [1998] are determined from the position of major peak in the spectrum of L1 and L2 signal of the same time interval. Than ionospheric corrected impact parameter p and bending angle ξ are given by

$$\Delta p=(f_1^2\Delta p_{L1}-f_2^2\Delta p_{L2})/(f_1^2-f_2^2);\quad p=p_m+\Delta p;\ \Delta\xi=\Delta p/(r\cos\varphi);\ \xi=\xi_m+\Delta\xi.. \qquad (4.12)$$

Hocke [1997], *Schreiner et al.* [1999], *Feng and Herman* [1999] described all details how the temperature profiles may be retrieved from the ionospheric corrected bending angle altitude dependence by using Abel inversion, dry air assumption, hydrostatic equilibrium and equation of state. For accuracy checking of the results of radio holographic temperature profile restoring *Hocke et al.* [1999] applied UCAR data retrievals. Removing diffraction/multipath effects was achieved in UCAR retrieval by means of backward propagation approach. In Fig. 4.4 the temperature difference of both retrievals is shown on the left hand side. In the middle, the absolute temperature profiles are shown (solid line: radio holographic retrieval, dash-dotted line:-UCAR retrieval). Vertical gradients of temperature (e.g., at tropopause) are mostly accompanied by significant structures of signal/noise ratio CASNR (SNR of coarse-acquisition ranging code, L1 wave) that is depicted on the right hand side. The average values of the standard deviation between both retrievals have been calculated for the selected occultation's events for heights below 30 km. The mean difference is 1.6 - 1.7 K for Fig. 4.4. The relative large differences between the temperature profiles of our retrieval and the UCAR retrieval in the middle and upper stratosphere (above 35 km) are caused by different data filtering as well as by small differences in upper boundary condition and statistical optimisation procedure which are required for the Abel inversion [*Hocke*, 1997].

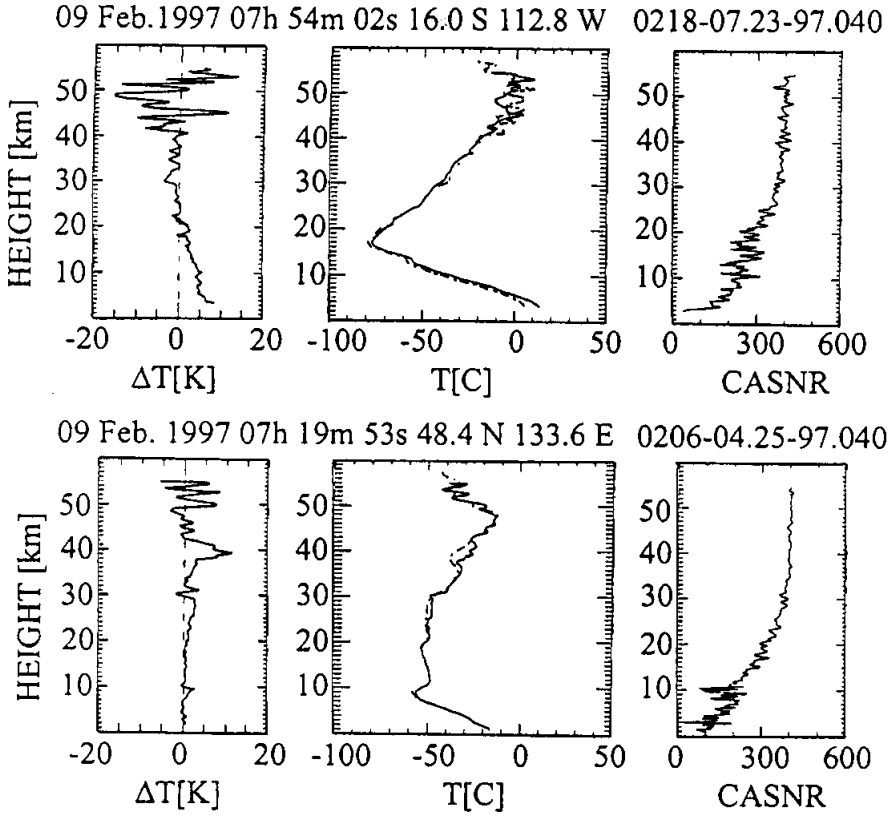

Fig. 4.4. Comparing the temperature profiles (solid lines) with UCAR data

4.5. Analysis of the radio holograms of D - and E-layer of the ionosphere

Usually single beam propagation mode exists in the mesosphere region. In this case it is convenient to divide the radio hologram into two independent amplitude and phase information channels. The amplitude channel is the main source for observing small spatial periods. The phase channel may be used to retrieve vertical periods with greater values if the contribution of the upper ionosphere has been subtracted. The accuracy in resolution of different spatial periods of wave structures is restricted on both channels by the vertical size of the radio hologram. There is also a filtration effect because of the finite size of the Fresnel zone (~1 km) at frequencies F1 and F2. This limits the possibilities for short-period observations to values of around 200 - 300 meters. The amplitude and phase components of radio holograms of the D-region of the ionosphere that correspond to two GPS/MET occultation events (07 February 1997, No. 0447, 0158) are shown in Fig. 4.5 (left and right panel respectively). Occultation event No. 0447 took place near Japan (Okinawa) in the middle of nighttime. The time-spatial coordinate of the main ray's minimal height H was close to 25.5^{o}N 231.7^{o}W, 15h 53m 23s UT. The second event (07 February 1997, No. 0158) corresponds to summer daytime in the Antarctic region. The time-spatial coordinates of ray minimal height H varied from 71.2^{o}S 18.2^{o}W, H=95 km, 14h 51m 05s UT to 70.5^{o}S 16.4^{o}W, H=60 km, 14h 51m 25s UT. The two curves in the middle of both panels of Fig. 4.5 correspond to the experimental phase excess variations at the first frequency F1, S_1 (upper curve), and at the second frequency F2, S_2, as functions of height. These curves have been multiplied by 20 and curve S_1 has been displaced by 0.4 m to make more visible the variations, that are connected with the wave structures. The upper ionospheric contribution was subtracted from the phase excess data by using the IRI-95 F-layer model for time and region of radio occultation. The variations in amplitude (top and bottom pairs of curves in Fig. 4.5) are also strongly correlated. The level of variations in the phase-path excess and in amplitudes at the two frequencies is proportional to the ratio f_2^2/f_1^2, and this demonstrates that the variations originate due to fluctuations in the electron density. The phase excess that are connected with wave structures change in the interval ±1 cm, with a random noise contribution of about ±1 mm. Spatial periods in the 1-3 km range can clearly be seen in the phase excess data of Fig. 4.5. A spatial period of 5 km can more clearly be seen in the phase excess data for Antarctic event than in the data for Okinawa event. In the amplitude data (top

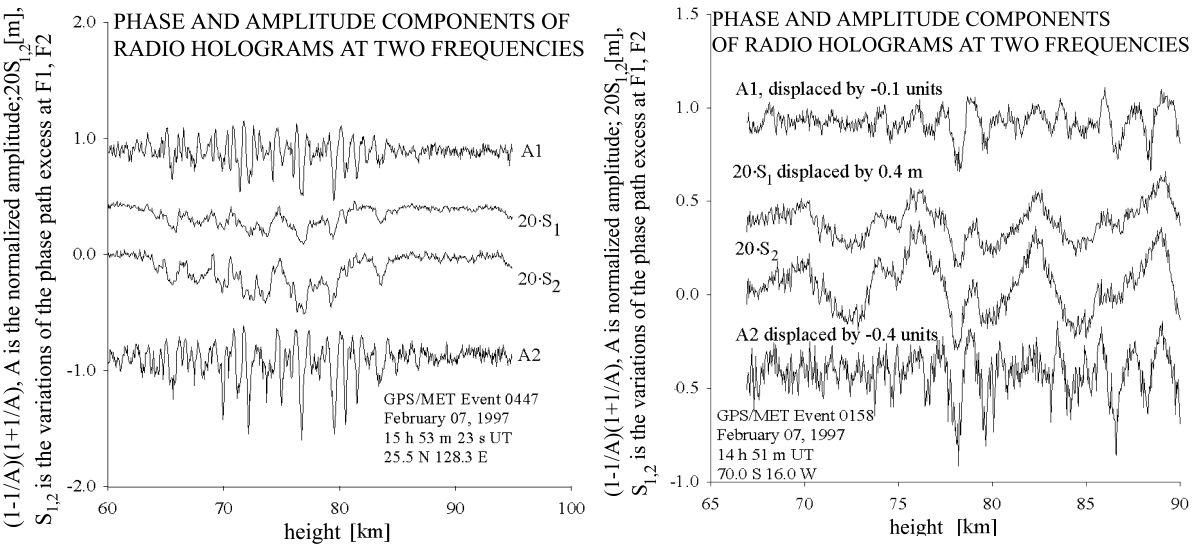

Fig. 4.5. Comparing two radio holograms of the D -layer of the ionosphere.

and bottom pairs of curves in Fig. 4.5) spatial periods in the 0.5-2 km range can also be seen. A feature at the height of 78 km is seen in both the phase excess and amplitude data. Analysis of Fig. 4.5 indicates that the amplitude data are more sensitive to high spatial frequency components in the refractive index while the phase excess data are more sensitive to low frequency components. These variations correspond to wave structures in the electrons density distribution in the D-layer of the ionosphere. The vertical gradient of electron density may be retrieved from the amplitude data by a method, which has been described by *Igarashi et al.* [2000]. The results of the restoration $dN_e(H)/dH$ for events 0158 and 0447 are shown in Fig. 4.6 (left and right panel, respectively). For ease of comparison, the curve F1 has been displaced by 19 th.el/cm^{3}km^{-1} in Fig. 4.6. The vertical distributions of $dN_e(H)/dH$ have nearly the same amplitude at both frequencies F1 and F2. The spatial periods for the Okinawian event are somewhat shorter by a factor of about two than the periods for the Antarctic event. The amplitude of the waves over Okinawa are also greater, indicating a more intense process. The maximum value of the positive gradient is at a height of about 76 km. The vertical gradients may be integrated to obtain waves in the electron densities altitudinal distribution. The amplitude spatial spectra of the vertical gradient of refractivity (*N*-units/km) that correspond to the variations in the gradients of electron density are shown in Fig. 4.7, left and right panels respectively. The upper two curves (displaced for ease of comparison) show the separate spatial spectra for frequencies F1 and F2. The lower curves show the spatial spectra that result from summation of the data at the two frequencies. A comparison of the two events reveals two maxima in the spatial spectrum with spatial periods of about 1 and 5 km. The period of 5 km is more clearly visible for Antarctic event. Periods of 1 km or less have a greater intensity in the Okinawan event. The origin of the waves observed in the vertical profiles of electron density might have a different origin. These waves may be connected with temperature waves caused by gravity waves which amplitude grows with height. Another cause may be connected with waves in ion's vertical distribution depending on the different concentration of water vapor (or due to different recombination rate). The strong feature, which is seen in the height ranges 70-80 km (Okinawan event) and 75-80 km (Antarctic event), may correspond to breaking of gravity waves in a region near the temperature inversion that is usually observed at this altitude by Earth-based radar and lidar tools [*Hauchecorne et al.,* 1987]. In Fig. 4.8, the impact parameter excess is shown for radio occultation event No. 0046. The sporadic E-layer caused sharp changes in the impact parameter at the height interval 95.5-98 km. The retrieved vertical profile of the electron density in E-layer is presented in Fig. 4.9. The expected electron density distribution

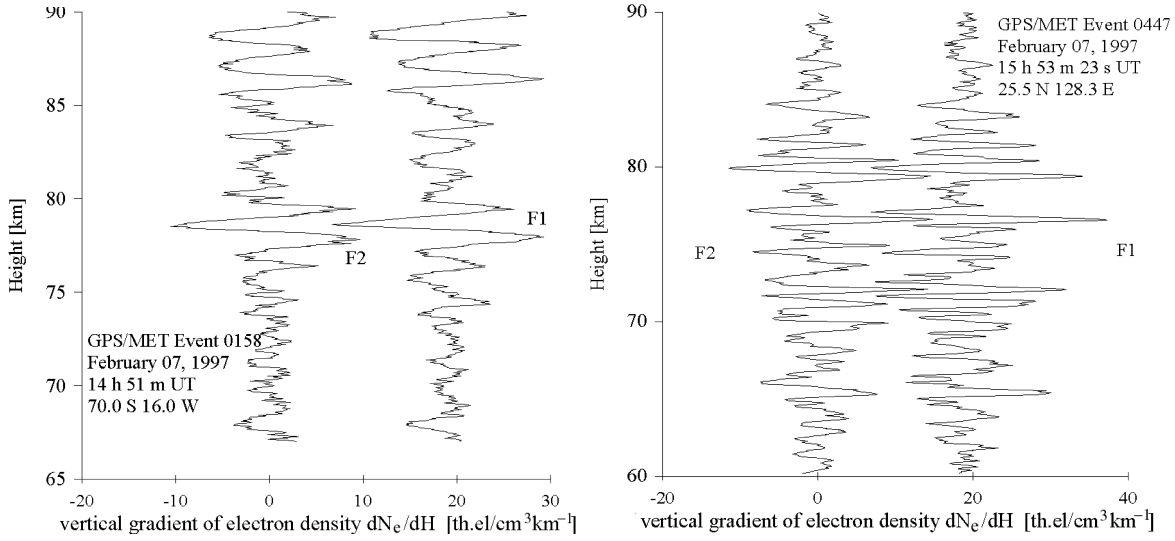

Fig. 4.6. Features in vertical gradients of electron density in D-layer. Wave structures in the vertical gradient may be connected with the breaking of gravity waves in the region of temperature inversion.

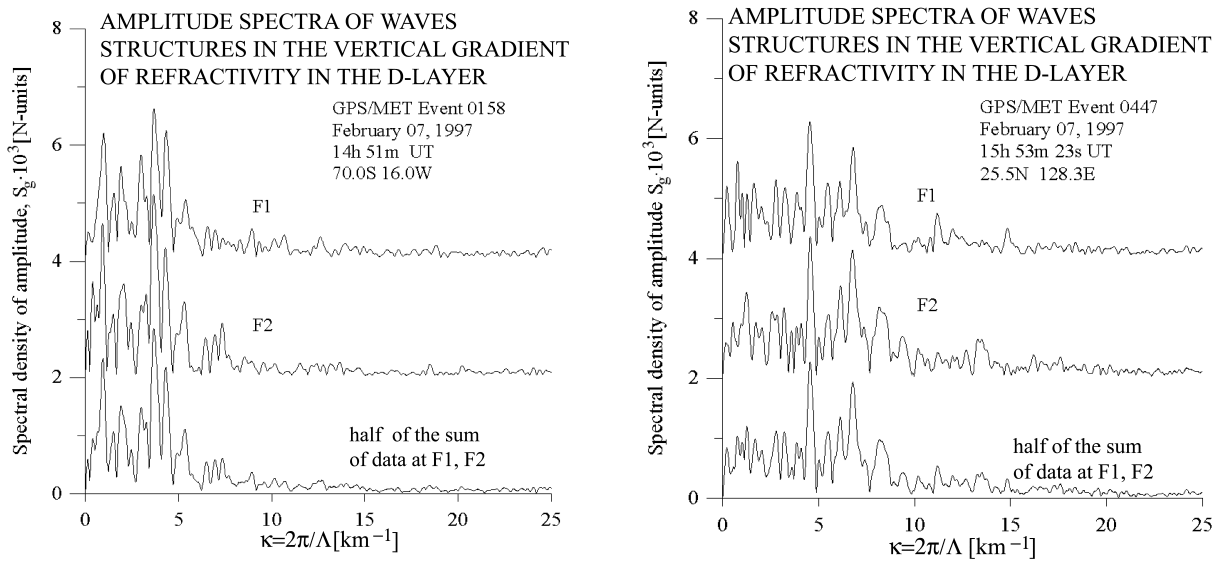

Fig. 4.7. Different spatial spectra of wave structures in the D-layer for the Antarctic (left panel) and Okinawan events.

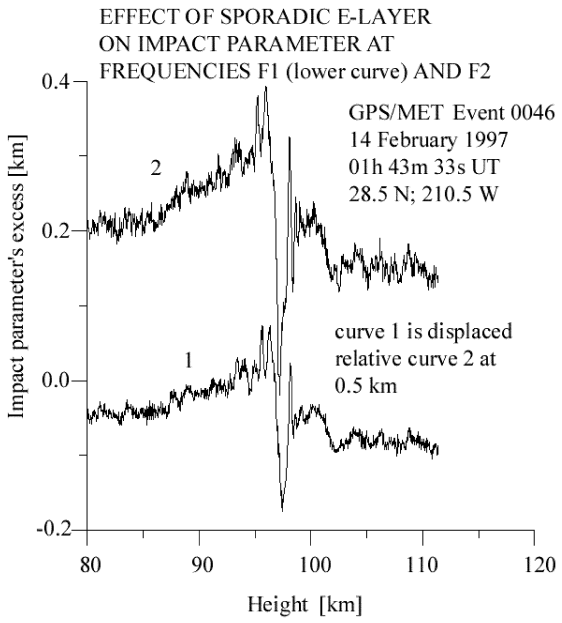

Fig. 4.8. Plasma convergence region at a height of 96-98 km as seen in radio occultation data.

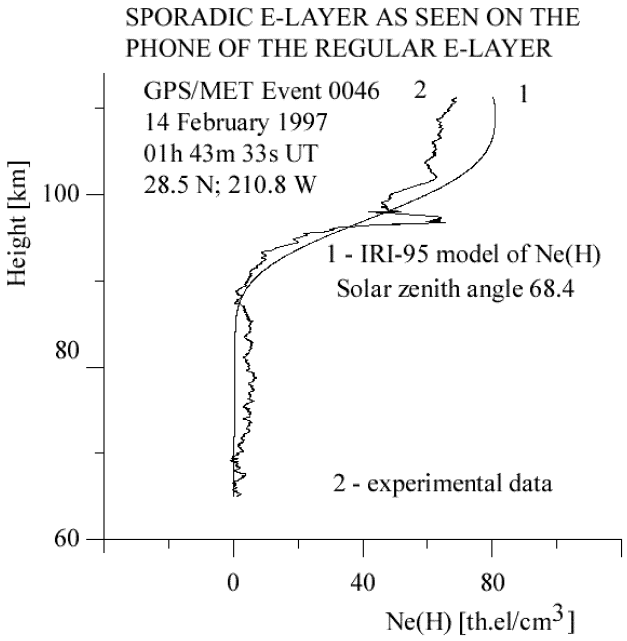

Fig. 4.9. Vertical distribution of the electron density revealed from radio occultation data (curve 2) and IRI-95 model (curve 1).

calculated using IRI-95 for the radio occultation time February 14, 1997 01h 43m 33s UT, coordinates 28.5º N; 210.5º W, is also presented (curve 1). The peak in electron density profile was about $6 \cdot 10^4$ cm^{-3} at level 97.5 km. The possible origin of the sporadic E-layer may be connected with convergence in the vertical-velocity of the neutral component of the mesosphere. This type of convergence may have been also the main cause of the wave structures observed in the D-layer (Fig. 4.8). Another possible explanation of the origin of sporadic E-layer is a specific convergence effect connected with the influence of the Earth's magnetic field on ion motion. In this case, the vertical convergence of the plasma's motion arose due to the horizontal divergence of the velocity of the neutral component of the ionosphere. According to *Whitehead* [1961] and *Kelly* [1989], this is a wind shear effect arising from the gravity waves in the neutral atmosphere.

4.6. Description of convergence effect of the wind velocity on the vertical distribution of the electron density

The main question here is what kind of information may be revealed from the electron density vertical distribution in the sporadic E-layer. According to *Whitehead* [1961] and *Kelley* [1989], the theory of wind shear allows us to connect electron density altitude distribution with a vertical profile of the horizontal neutral-wind velocity. The ion mass balance equation may be used to this aim. A connection of the vertical ion velocity $V(H,t)$ and the altitude distribution of the electron density $\rho(H,t)$ may be found from:

$$\partial(\ln\rho)/\partial t + V(H,t)\,\partial(\ln\rho)/\partial H = -dV(H,t)/dH. \qquad (4.13)$$

Dependence of the ion velocity $V(H,t)$ on the time t and height H is assumed in the form:

$$V(H,t) = v(H)T(t) \text{ for } t>0; \qquad V(H,t)=0 \text{ for } t<0. \qquad (4.14)$$

If the functions $\rho(H,t)$, $\rho(H,0)$ and $\partial(\ln\rho)/\partial H$ are known from experimental and model data then the time integral of the ions velocity $Ti(t)v(H)$ may be found as the solution of a differential equation of the first order:

$$\ln[\rho(H,t)/\rho(H,0)] = -Ti(t)dv(H)/dH - v(H)\int_{o}^{t} T(\tau)\partial(\ln\rho(H,\tau))/\partial H\, d\tau, \quad (4.15)$$

$$Ti(t) = \int_{o}^{t} T(\tau)d\tau. \quad (4.16)$$

Linear approximation may be used for estimation the time dependence $\partial(\ln\rho(H,\tau))/\partial H$:

$$\partial(\ln\rho(H,\tau)/\partial H \approx \{\tau\partial(\ln\rho(H,t)/\partial H + \partial(\ln\rho(H,0)/\partial H](t-\tau)\}/t. \quad (4.17)$$

Approximation (4.17) may be used for solution differential equation (4.15) and the function $Ti(t)v(H)$ may be found if the function $\ln\rho(H,t)$, $\ln\rho(H,0)$ is known from experimental data. Near the maximum of electron density $H=H_m$ $\partial(\ln\rho)/\partial H = 0$ and the time integral of the vertical gradient of the plasma velocity $dv(H)/dH$ is equal to:

$$-Ti(t)dv(H_m)/dH = \ln[\rho(H_m,t)/\rho(H_m,0)].$$

According to this equation the plasma concentration is increased relative initial value when magnitude of $-Ti(t)d(v(H_m))/dH$ is positive and diminishes in the opposite case. So position of maximum plasma density corresponds to maximal values of magnitude of vertical gradient of ion velocity. Thus position of maximums of electron density profiles corresponds to zone of convergence of vertical motion of ions in the D- and E-layer of the ionosphere. In the case of wind shear effect, according to *Whitehead* [1961] and *Kelly* [1989], the next connection exists between the vertical ion velocity $v(H)$ and horizontal neutral-wind velocity $U_{\perp}(H)$:

$$Ti(t)dU_{\perp}/dH = (1-b_z^2)^{-1/2}[\kappa_i/(1+\kappa_i^2)]^{-1} Ti(t)dv(H)/dH, \quad (4.18)$$

where κ_i is the ratio of the ions gyro frequency to collision frequency, U is the neutral-wind velocity, $U_{\perp}$ is the horizontal-wind component which is perpendicular to horizontal direction of the terrestrial magnetic field, B_* is an unit vector describing direction of the Earth's magnetic field, b_z is vertical component of the unit vector B_*. Equations (4.14)-(4.18) may be used to estimate the horizontal-wind velocity vertical profile. According to Eqs. (4.14)-(4.18), only time integral of vertical-velocity $W(H) = Ti(t)v(H)$ may be defined using known electron density vertical profile $\rho(H,\tau)$. Details of the structure of the sporadic E-layer and initial distribution of electron density $N_e(H,0)$ assumed for the search of the horizontal-wind velocity

vertical profile in a sporadic E-layer are given in Fig. 4.10. The results of qualitative retrieving vertical profiles of horizontal-wind velocity and its gradient are shown in Fig. 4.11. The maximum value of the horizontal-wind velocity vertical gradient is observed at height 96.9 km. The wind velocity at this height shows changes from an eastward to a westward direction. Preliminary results of the first radio occultation observation of the wind shear indicated the possibility of qualitative measurements of the vertical gradient of horizontal-wind velocity in a sporadic E-layer. Thus, there are some arguments that the technique of using high-accuracy radio occultation to measure parameters of an ionospheric E-layer may be applied in the future for observations of wind shear parameters and positions in the upper atmosphere.

The radio occultation data obtained may be compared with results of direct rocket measurements provided by *Igarashi et al.* [1998], *Yamamoto et. al.* [1998] in August, 1996. Their experimental results compare the altitude-electron density and neutral-wind velocity profiles as it can be seen in Fig.4.12. The sharp E-layer having a peak of electron density near $9\ 10^4$ cm^{-3} in Fig. 4.12 is similar to the E-layer form shown in Fig. 4.9. The width of the E-layer in both cases is near 4 km and the heights of the main peaks are located in the interval 95-104 km. The direct measurements of wind velocity show a tense connection of the levels with sharp vertical-velocity gradient (wind shear) and the locations of the maximums of electron density distribution. For determination of absolute values of wind velocity it is necessary to calibrate the radio occultation observations with earth-based ionosonds data.

4.7. Analysis of a possibility of revealing features in humidity vertical distribution

The amplitude data contain important information on the refractivity vertical gradient *dN(h)/dh*. This information may be used for restoration vertical gradient of temperature and in the case of some information on the radio occultation region, vertical humidity profile. In this section a short analysis of possibility of determination of humidity features will be discussed. For analysis the formula of hydrostatic equilibrium may be used. Equation of the hydrostatic equilibrium connects the temperature *T(h)* in K, pressure *P(h)* in mb, and water vapor pressure *e(h)* [mb] profiles:

$$P=P_o \exp\{-\int_{h_o}^{h} T_x\, dh/[T(1+0.378\, e/P)]\}, \qquad (4.19)$$

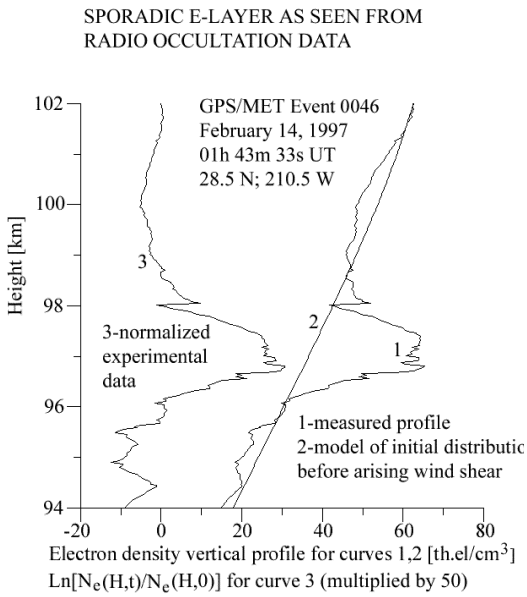

Fig. 4.10. Distribution of electron density in sporadic E-layer

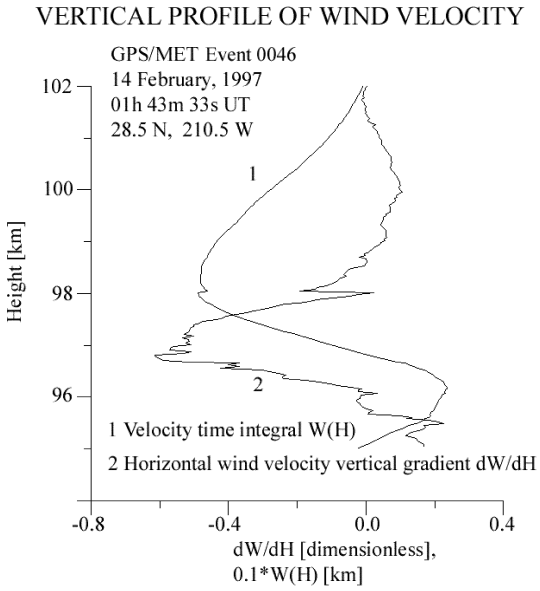

Fig. 4.11. Qualitative information on the vertical profile of the horizontal wind velocity

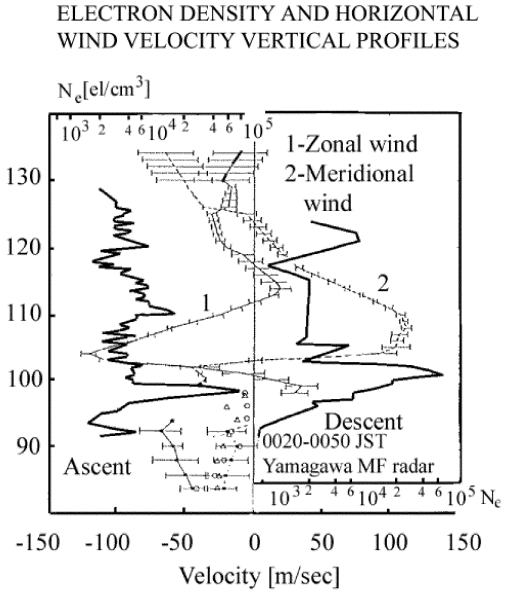

Fig. 4.12. Comparing results of rocket measurements of vertical profile of the electron density and Earth-based measurements of altitude profile of horizontal wind velocity

$$T_x = g m_1 / k, \tag{4.20}$$

where h, h_o are the heights above the sea level, m_1- molecular mass of dry air, k-Boltzman constant, g- Earth gravity acceleration:

$$g = g_o(1-0.0002644\cos 2\varphi)(1-0.000314\, h), \tag{4.21}$$

where T_x [K/km] is the main physical parameter of the temperature profile in the atmosphere depending on the molecular mass of dry air m_1, acceleration of the earth-gravity g and Boltzman constant k, h – is the height above the sea level [km]; g_o = 9.80616 m/sec^2 at latitude φ=45^o, φ=0^o at equator. The ratio m_1/k is equal to gas constant R=2.8704·10^6 [erg g^{-1}K^{-1}]. For ratio $g_o m_1/k$ one may obtain $g_o m_1/k$=34.16 K/km. So T_x is equal to $g(g_o m_1/k)/g_o$ = 34.16 g/g_o K/km. Thus, T_x is slow changing function of height and has physical sense of the vertical temperature gradient. Equation (4.19) gives connection between the atmospheric pressure, humidity and temperature vertical profiles.

The temperature $T(h)$, pressure $P(h)$, and water vapor pressure $e(h)$ profiles are connected with refractivity altitude dependence $N(h)$:

$$N(h) = 77.6P(1+4810e/PT)/T. \tag{4.22}$$

It may be shown using (4.19), (4.22) that connection exists between the vertical gradients of the temperature and refractivity:

$$\beta = -[N(h)]^{-1} dN(h)/dh = T^{*-1} dT^*/dh + T_x/T_a, \tag{4.23}$$

$$T^* = T/[1+4810e/(PT)]; \quad T_a = T(1+0.378e/P). \tag{4.24}$$

The equation (4.24) connects the vertical gradient of logarithm of the refractivity with vertical gradient of logarithm of the equivalent temperature $T^*(h)$. The first term in the right part of (4.23) has high level of the oscillations with height. The second term in (4.23) has slow variations and may be determined from known average meteorological conditions in the radio occultation region. The influence of humidity on the second term in equation (4.23) is smaller by a factor ~ 50 than influence in the first term in equation (4.23). Thus equation (4.23) contains separately “dry” and “wet” terms. This may be used for evaluation features in the humidity vertical profile. For this aim some a priory data may be used on the atmospheric conditions in the radio occultation region. From the a priory information a model of the

temperature vertical profile $T_m(h)$ may be reconstructed and corresponding refractivity profile $N(h)$ may be found. Then the altitude dependence $\beta_m(h)$ may determined. The function $\beta_m(h)$ is connected with „dry“ temperature model $T_m(h)$ profile by equation:

$$\beta_m(h) = -[N_m(h)]^{-1}(dN_m(h)/dh) = T_m^{-1}(h)(dT_m(h)/dh) + T_x/T_m(h). \quad (4.25)$$

The difference of the experimental and model dependencies $\beta(h)$ and $\beta_m(h)$ may be used for finding humidity profile:

$$\beta(h) - \beta_m(h) = [N_m(h)]^{-1}(dN_m(h)/dh) - [N(h)]^{-1}(dN(h)/dh) = d[lnT^*(h)/T_m(h)]/dh + T_x[T_a^{-1}(h) - T_m^{-1}(h)] \quad (4.26)$$

The function $\beta(h)$ contains important information on the humidity distribution in the atmosphere. Equation (4.26) may be used for revealing features in the humidity profile from measuring of the amplitude of the two radio occultation signals. The concrete implementation of this method is a task for future work.

CONCLUSION

The carried analysis of the amplitude fluctuations allowed to reveal the features permitting to study the turbulence of the atmosphere from the surface up to the altitude ~30 km. The observation results of star flickers at their occultation by the atmosphere, obtained on the station MIR and given in [*Aleksandrov et. al.,* 1990*; Gurvich and Kan,* 1997*; Grechko et. al.,* 1997], have shown the efficiency of this method for studying the stratospheric turbulence at the altitudes of 20 ÷ 50 km. The comparison of our radio occultation data and observations of star flickers [*Gurvich and Kan,* 1997], indicate to the agreement of the results of a turbulence parameter definition in the field of overlapping the experimental data. It is necessary to mark, that atmospheric inhomogeneities are anisotropic, and their separating into classical turbulence and atmospheric “layering” is conditional. This difficulty is shown at the radio occultation measurement of the atmosphere, where the separation of the field strength fluctuations, caused by turbulence, from amplitude fadings and spikes because of thin regular stratums is subjective. The analysis of field strength fluctuations of centimetre radio waves in the radio occultation experiments has shown the possibility of studying statistical irregularities of the refractive index. Thus the spectral index p of a spatial spectrum of inhomogeneities is determined for the height interval from 0.3 up to 35 km. In the troposphere, at altitudes lower

than 7 km, p is close to the value 11/3, corresponding to the Kolmogorov spectrum of the turbulence in ~50% observations. In the stratosphere, at the altitudes more than 15 km p=4.6 in ~50% of cases and $p \approx 11/3$ only in 13% of observations.

Thus the expected values of the rms decimetre wave scintillations on a board CHAMP will reach from 0.04 up to 0.14 at H_0=5 km, from 0.04 up to 0.1 at H_0=15 km, and from 0.03 up to 0.09 at H_0=20 km. Exponent n of spectrum of the field strength scintillation will same as on Fig. 1.8 of Chapter 1. The characteristic frequency of amplitude fluctuations will to ~3 times lower than for centimetre range and it will reach from 1 up to 3 Hz in dependence from the geometry of radio occultation. The amplitude measurements on a board CHAMP will allow to receive information about turbulence or stability of the atmosphere for the height range from 3 up to 20 km.

The determination of altitude profiles for density, pressure, and temperature by radio occultation technique is based on the idea that the refractive index altitude distribution $N(h)$ has the property of local spherical symmetry. Refractive index inhomogeneities form a random field $\delta N(h, t)$ superimposed on the regular function $N(h)$. It is refractive index fluctuations that limit the potentially attainable accuracy of determining atmospheric parameters by the radio occultation technique. By the potentially attainable accuracy we mean the limit of accuracy set by atmospheric inhomogeneities in the absence of other sources of error. The potentially attainable accuracy can be estimated from the ratio between the fluctuation and regular components of frequency changes due to the influence of the atmosphere. Let us compare σ_f with regular changes in frequency, ΔF, due to the atmosphere. To this aim, we use the values of ΔF from [*Yakovlev et al.,* 1995b]. Most accurately, altitude profiles of the refractive index, $N(h)$, and, consequently, of temperature are recovered at altitudes of 4 to 10 km. At $h < 3$ km, an additional interference comes from atmospheric humidity, whereas at $h > 20$ km, the net effect of frequency change is too small. By comparing σ_f with ΔF for the altitude range h = 4 to 10 km, we find that $\sigma_f/\Delta F \approx 4 \times 10^{-3}$. The potentially attainable accuracy of the radio occultation method can be estimated by comparing known data on fluctuations of reduced refractive index δN of radio waves with its mean value $N = (n - 1) \times 10^6$. As will be recalled, fluctuations of δN equal to one or two N units are always present at altitudes of 3 or 4 km. The mean reduced refractive coefficient for these altitudes is N = 200 to 180 N-units. Hence, $\delta N/N \approx 0.005$. In order of magnitude, this figure is about the same as the radio $\sigma_f/\Delta F$. At $h > 5$ km, refractive index fluctuations are

mainly associated with temperature fluctuations, that is, $\delta N/N = \delta T/T$. This simple relation likewise permits determining the potentially attainable accuracy for the recovery of the temperature altitude profile by the radio occultation method. To sum up, $\sigma_f/\Delta F \approx \delta N/N \approx \delta T/T \approx 0.003$ to 0.005. This estimate implies that at $h = 3$ to 8 km the temperature can be determined to within an accuracy of $\delta T \approx 1$ K.

For the first time, experimental data on the actual accuracy of temperature determination by the radio occultation method were reported by *Ware et al.,* [1996]. Accordingly, at $h = 5$ to 10 km, the temperature can be determined to within an accuracy of 2 or 3 K.

It was shown in Chapter 1 that analysis of amplitude fluctuations allows to obtain information on vertical distribution of statistical parameters of atmospheric inhomogeneities. It is shown in this report that analysis of the phase fluctuations gives additional information on turbulence degree of the atmosphere. Joint analysis of the phase and amplitude fluctuations gives most reliable information on vertical distribution of the atmospheric inhomogeneities degree described by parameter $C_n(h)$.

For elaboration of program module in antispoofing regime the radio holographic program module may be used. Instead F1 and F2 phase data this module must use the phase difference F1-F2 as function of time for finding dependence of refraction angle difference ξ_1-ξ_2 on the height in the ionosphere region. For measuring atmospheric parameters this module must use the amplitude A1(t) temporal dependence and method proposed by *Hajj et al.,*[1994] for restoration the refractivity altitude profile on the radio occultation amplitude data. The practical accuracy and instrumental error of this approach may be found in future work using GPS/MET antispoofing data.

For practical implementation of the ionospheric contribution correction the method of *Vorob'ev and Krasilnikova* [1994] is effective in the present time for excluding ionospheric contribution at levels lower than 40 km. Nowadays this method is successfully applied to analysis of radio occultation data for measuring the temperature altitude profiles in the atmosphere under spherical symmetry assumption. However to find the influence of the horizontal gradients and magnetic field one may use more general approach based on the calculus of variations. The analytic radio physical model is needing for more precise ionospheric correction. This model must describe the connections between the phase path, bending angle and amplitude in an analytical form and use existing models of the ionosphere

for quickly reconstructing stationary radio wave path in radio occultation region, finding expected dependencies of the phase excess, impact parameter for subtracting ionospheric contribution from experimental radio occultation data. In frame of calculus variations method this model may be used for estimation small correction caused by magnetic field and horizontal gradients of the refractivity in the ionosphere. An analytic radio physical model is developed for subtracting ionospheric influence from radio occultation data. This model may be applied to description ionospheric contribution in the phase and amplitude of radio occultation signal by using special ionospheric correction program tool. The preliminary validation of the program module shown its effectiveness for calculating expected altitude dependencies of the phase excess, impact parameter and bending angle corresponding to the upper ionosphere contribution. The further elaboration is needing to include existing ionospheric models in radio physical program module according to region of radio occultation.

The possibility of the experimental radio occultation measurement of the upper ionosphere's contribution has been considered. The main assumption is global spherical symmetry of the ionosphere above the LEO satellite in the radio occultation region. Despite this the methodology may be used in practice for the first approximation of the ionospheric contribution. The described methodology may be used in the case when the time of radio occultation measurements are prolonged by factor 2-3 to obtain data for evaluation of the bending angle in the upper ionosphere.

Practically the possibility exists to consider the contribution of the upper ionosphere as a slow changing temporal trend that may be excluded by extrapolation or by low noise filtration methods. The practical implementation of this approach is demonstrated by means of analysis of phase path excess and the amplitude radio occultation data for finding features in the E- and D- layers of the ionosphere. Comparing the time dependencies of the phase-residuals and amplitudes at the both frequencies revealed a difference in sensitivity for identifying wave structures in the upper atmosphere. The phase path excess is more sensitive to large-scale structures, while the amplitude variations are connected with inhomogeneities having smaller spatial periods. For considered two radio occultation events combined analysis of the phase and amplitude data reveals spatial periods from 1-2 km up to 8-10 km at altitudes of 72-108 km. Accurate measurements of electron density altitude profiles and its gradient in E-layer of the ionosphere show effectiveness of the approach for observing wave structure in the upper atmosphere.

The main point of radio holographic concept is to introduce radio optics and holographic principles derived in high resolution radar imaging technology into the radio occultation problem. The radio holographic method consists in combining phase and amplitude data to achieve high vertical resolution (more than the Fresnel zone size) and thereby reveal fine structures in meteorological parameters and electron density altitude profiles with short spatial periods (0.2-0.5 km). As a result extreme values of a vertical resolution (higher than the size of the Fresnel zone) and more accurate estimates of the parameters of the natural phenomena in the atmosphere and ionosphere may be achieved. Radio holography method produced the first successful observation in GPS/MET radio occultation data signals, reflected from the sea surface. This demonstrates its high-technology level and opened new perspectives for radio occultation experiments. Combined amplitude and phase analysis opened new possibilities for radio occultation observation wave structures in the lower ionosphere and qualitative measurement wind velocity vertical profile in the mesosphere.

Radio holographic method is an effective tool for investigation of atmosphere and ionosphere of the Earth. This method has high spatial and angular resolution. The vertical resolution of radio holographic method increases as λ^{-1} comparing to $\lambda^{-1/2}$ in existing method. The limit of principal resolution is bounded only by time of coherent data handling (it is not higher then the time interval of hologram registration) and physical uncertainties in atmospheric conditions which do not be predicted by radio physical model applied for phase-locking signal generating. In multibeam propagation condition radio holographic method may be used for measuring parameters of different rays and for restoration relative physical parameters of atmospheric features. The efficiency of radio holographic method was confirmed by direct revealing multibeam propagation and testing high spatial resolution using MIR/GEO and GPS/MET radio occultation data. The value of vertical resolution 50-60 m was achieved which corresponds to 1/10 of the Fresnel zone size. The radio holographic method may be applied for measuring physical parameters of natural processes in the upper atmosphere caused by different types of waves (planetary, gravitational etc.) and for precise revealing electron density profile in the ionosphere.

ACKNOWLEDGMENTS

We are grateful to UCAR for access to the GPS/MET data.

References

Aleksandrov, A. P., G. M. Grechko, A. S. Gurvich, V. S. Kan, M. K. Manarov, A. I. Pakhomov, Y. V. Romanenko, S. A. Savchenko, S. I. Serova, and V. G. Titov, Stratosphere temperature variation spectra determined from observations of star stintillations from spacecraft, Izv. Akad. Nauk SSSR, Fiz. Atmos. i Okeana, 26, 5–16, 1990 (in Russian).

Armand, N.A., Frequency fluctuations of radio wave propagating in the turbulence atmosphere, Radiotekh. and Elektron., v. 27, N 9, p. 1683, 1982 (in Russian).

Armand, N.A., A.I. Efimov, and O.I. Yakovlev, Frequency fluctuations of the decimeter and centimeter radio waves, Radiotekh. and Elektron., v. 33, N 8, p. 1574, 1988 (in Russian).

Anthes R. A., Ch. Rocken, Ying-Hwa Kuo. Applications of COSMIC to Meteorology and Climate. To appear in special issue on COSMIC of Terrestrial, Atmospheric and Oceanic Sciences (TAO), March 2000.

Fante, R. L., Electromagnetic beam propagation in turbulent media, Proc. IEEE, 63, 1669–1692, 1975.

Fante, R.L., Electromagnetic beam propagation in turbulent media, Proc. IEEE, 68,. 75, 1980.

Feng, D.D. and B.M. Herman, Remotely sensing the Earth's atmosphere using the Global Positioning System (GPS)-the GPS/MET data analysis. Journal of Atmospheric and Ocean Technology 16, 990-1002, 1999.

Gaikovich K.P., A.S. Gurvich, and A.P. Naumov, On determination of meteorological parameters from inside-atmosphere measurements of optical refraction of space sources. Reprint NIRFI № 153, Gorkii, 1982, 28 p. (in Russian).

Gorbunov, M.E., A.S. Gurvich, and L. Bengtsson, Advanced algorithms of inversion of GPS/MET satellite data and their application to reconstruction of temperature and humidity. Report 211 Max-Planck-Institute for Meteorology ISSN 0937-1060, 1996.

Gorbunov, M.E., S.V. Sokolovskiy, and L. Bengtsson Space Refractive Tomography of the Atmosphere: Modelling of Direct and Inverse Problems Report 210 Max-Planck-Institute for Meteorology ISSN 0937-1060, 1996.

Gorbunov, M.E. and A.S. Gurvich, Microlab-1 experiment: Multipath effects in the lower troposphere. J. Geophys. Res., 103, 13,819-13,826, 1998.

Grechko, G. M., A. S. Gurvich, V. Kan, A. I. Pakhomov, Yan P. Podvyazny, and S. A. Savchenko, Observations of atmospheric turbulence at altitudes of 20 – 70 km (in Russian), Dokl. Akad. Nauk, 357, 683–686, 1997.

Gu, M., and F.K. Brunner, Theory of the two frequency dispersive range correction.

Manuscripta Geodetica, 15, 357-361, 1990.

Gurvich, A. S., Star scintillation spectra during occultations by the Earth's atmosphere (in Russian), Optika atmos., 2, 239–245, 1989.

Gurvich A. S., and V. Kan, Radio wave fluctuations in satellite–atmosphere–satellite links: Estimates from stellar scintillation observations and their comparison with experimental data (in Russian), Izv. Akad. Nauk, Fiz. Atmos. i Okeana, 33, 314–323, 1997.

Hajj, G.A.,and L.J. Romans, Ionospheric electron density profiles obtained with the Global Positioning System: Results from GPS/MET experiment, Radio Sci.,33(1), 175-190, 1998.

Hajj, G.A., E.R. Kursinski, W.I. Bertiger et al, Assessment of GPS occultations for atmospheric profiling. Proceedings, Seventh Symposium on Satellite Meteorology and Oceanography, Amer. Meteorol. Soc., 1994.

Hocke, K., Inversion of GPS meteorology data. Annales Geophysicae 15, 443-450, 1997.

Hocke, K., A. Pavelyev, O. Yakovlev, L. Barthes and N. Jakowski, Radio occultation data analysis by radio holographic method. JASTP, 61, 1169-1177, 1999.

Hofmann-Wellnhof, B., H.L. Lichtenegger and J. Collins, Global Positioning System Theory and Practice, Springer-Verlag New York, 586 p., 1992.

Igarashi, K., Y. Murayama, K. Hocke, R. Yamazaki, M. Kunitake, M. Nagayama, and I. Nishimuta, Coordinated observations of the dynamics and coupling processes of mesosphere and lower thermosphere winds with MF radars at the middle-high latitude. Earth Planets Space 51, 657-664, 1999.

Igarashi, K., T. Ogawa, Y. Murayama, I. Nishimuta, M.E. Larsen, M. Yamamoto, and S. Fukao, Simultaneous observations of mesospheric winds and sporadic E-layer at Yamagawa during the SEEK campaign. Reprint ISAS – Report No. 38 75-82, March 1998.

K. Igarashi, N.A. Armand, A.G. Pavelyev, Ch. Reigber, J. Wickert, K. Hocke, G. Beyerle, S.S. Matyugov, O.I.Yakovlev. Application of small satellites for high precision measuring effects of radio wave propagation. Submitted to Digest of the 3rd IAA Symposium on Small Satellites for Earth Observation. April 2-6, 2001, Berlin, Germany. 2000. No. IAA B3 0207P, P.1-4.

Ishimaru, A., Wave propagation and scattering in random media, Academic Press, v. 2, 1978.

Kalashnikov I.E., S.S. Matyugov, A.G. Pavelyev and O.I. Yakovlev Analysis of features of radio occultation method. In the book: "Electromagnetic waves in the atmosphere and space". Ed. by A.V.Sokolov and A.A. Semenov. Moskow, Nauka, 1986, p. 208-218 (in Russian).

Karayel, E.T., and D.P. Hinson, Sub-Fresnel-scale vertical resolution in atmospheric profiles from radio occultation. Radio science,.32, No.2, P.411-428, 1997.

Kelley M.C. The Earth's Ionosphere. Plasma Physics and Electrodynamics. Academic Press, inc. ISBN 0-12-404012-8, 484 pp., 1989.

Kravtsov, Yu., and Yu. N. Orlov, Geometrical Optics of Inhomogeneous Media, Springer-Verlag, New york, 1990.

Kucherjavenkov A., O. Yakovlev, I. Kucherjavenkova, and L. Samoznaev, Regular variations of the frequency and amplitude of radio waves on data of MIR/GEO radio occultation experiments, Radioteknika i elektronika, 43, No. 8, 945-951, 1998 (in Russian).

Kursinski, E.R., et al., Initial results of radio occultation observations of Earth's atmosphere: using the Global Positioning System, Science, 271, 1107-1110, 1996.

Kursinski, E.R., G.A. Hajj, J.T. Schofield, R.P. Linfield, and K.R. Hardy, Observing Earth's atmosphere with radio occultation measurements using the Global Positioning System, J. Geophys. Res. 102, D19, 23429-23465, 1997

Leitinger, R., H.-P. Ladreiter, and G. Kirchengast, Ionospheric tomography with data from satellite receiption of Global Navigation Satellite System signals and ground receiption of Navy Navigation Satellite System signals, Radio Sci., 32(4), 1657-1669, 1997.

Lindal, G.F., J.R. Lyons, D.N. Sweetnam, V.R. Eshleman, D.P. Hinson and G.L. Tyler, The atmosphere of Uranus: results of radio occultation measurements with Voyager 2. J. Geophys. Res. 92, 14,987-15,001, 1987.

Lindal, G.F. The atmosphere of Neptune: An analysis of radio occultation data acquired with Voyager 2. Astron. J., 103, 967-982, 1992.

Lucia, D.J., J.M. Anderson, Analysis and Recommendation for Reuse of the L1 and L2 GPS Spectrum, Navigation Journal of the Institute of Navigation, v. 45, N 4, p. 251, 1998.

Marouf, E.A., G.L. Tyler, and P.A. Rosen, Profiling Saturn rings by radio occultation, Icarus, 68, 120-166, 1986.

Melbourne W.G., E.S. Davis, C.B. Duncan, G.A. Hajj, K.R. Hardy, E.R. Kursinski, T.K. Meehan, L.E. Young, and T.P. Yunck The Application of Spaceborne GPS to Atmospheric Limb Sounding and Global Change Monitoring, JPL Publication 94-18, 147 pp., April 1994.

Mortensen, M.D. and P. H○eg. Inversion of GPS occultation measurements using Fresnel diffraction theory. Geophys. Res. Letters, 25, No.13, 2441-2449, 1998.

Mortensen, M.D., R.P. Linfield, and E.R. Kursinski Vertical resolution approaching 100 m for GPS occultations of the Earth's atmosphere. Radio Science, 34, No.6, 1475-1483, 1999.

Orlyanskii A.D., E.N. Lesnovsky, A.F. Kovalev, O.F. Kluev, Yu.K. Chasovitin, N.M. Klueva, S.E. Ivanova, L.S. Mironova, T.N. Sykilinda, and T.A. Lobanova, Gos-standard of Russian Federation. Ionosphere and plasmosphere of the Earth. Model of global distribution of the electron density and collision frequency in the height interval 45…20000 km. Ed. by Gosstandard of Russia.728 pp. Moscow, 1997, (in Russian).

Pavelyev A.G. and A.I. Kucherjavenkov, Refraction attenuation of radio waves in the planetary atmospheres, Radioteknika i Elektronika, 23, N 7, 1123-1130, 1978a. (in Russian)

Pavelyev A.G., and A.I.Kucherjavenkov, Theory of refraction attenuation of radio wave in planetary atmospheres. Radio Engineering and Electronic Physics. 23, No. 7, 1345-1351, 1978b.

Pavelyev A.G., and S.D. Yeliseyev, Study of the Atmospheric Layer near the Ground using Bistatic Radar. Journal of Communication Technology and Electronics. No 9. P. 124-130. 1989.

Pavelyev A., A.V. Volkov, A.I. Zakharov, S.A. Krytikh, and Kucherjavenkov A.I., Bistatic Radar as a Tool for Earth Investigation Using Small Satellites. Acta Astronautica, 39, 721-730, 1996.

Pavelyev A., On the possibility of radio holographic investigation on communication link satellite-to-satellite. Radioteknika i elektronika, 43, No. 8, 939-944, 1998 (in Russian).

Pavelyev A., K. Hocke, O. Yakovlev, N. Jakowski, J. Wickert, S. Matugov, A. Kucherjavenkov, A. Wehrenpfennig, and A. Zakharov, Radio holographic method for atmosphere sounding using small satellite. Small satellites for Earth Observation. Digest of the 2-nd International Symposium of the International Academy of Astronautics. Ed. H.P.Roser, R. Sandau, A. Valenzuella. Wissenschaft und Technik Verlag. 199-202. Berlin, 1999.

Rocken C. et al., Analysis and validation of GPS/MET data in the neutral atmosphere, J. Geophys. Res.,102(D25), 29,849-29,866, 1997.

Rubashkin, S.G., A.G. Pavelyev, O.I. Yakovlev et al., Reflection of radar waves by the ocean surface for bistatic radar using two satellites, J. Communications Technology and Electronics, v. 38, N 9, p. 64, 1993.

Schreiner, W.S., S.V. Sokolovskij, C. Rocken and D.C. Hunt, Analysis and validation of GPS/MET radio occultation data in the ionosphere. Radio Science 34, No. 4, 949-966, 1999.

Tyler G.L., et al., Voyager radio science observations of Neptune and Triton. Science, 246, 1466-1473, 1989.

Vorob'ev, V.V. and T.G. Krasil'nikova, Estimation of accuracy of the atmosphere refractive index recovery from Doppler shift measurements at frequencies used in the NAVSTAR system. Izv. Russ. Acad. Sci., Physics of the Atmosphere and Ocean,

Engl. Transl. 29(5), 602-609, 1994.

Vorob'ev, V.V., A.S. Gurvich, V. Kan, S.V. Sokolovskiy, O.V. Fedorova, and A.V. Shmakov. Structure of the Ionosphere from the Radio-Occultation GPS-"Microlab-1' Satellite Data: Preliminary Results, Earth Observations and Remote Sensing, 15, p. 609-622, 1999.

Ware, R., M. Exner, D. Feng, M. Gorbunov, K. Hardy, B. Herman, et al., GPS sounding of the atmosphere from low Earth orbit – Preliminary results, Bull. Am. Meteorol. Soc., 77, 19-40, 1996

Wehner, D. R. High Resolution Radar. Ed. Artech House, inc. 685 Canton Street Norwood, MA 02062, International Standard Book Number: 0-89006-194-7. Library of Congress Catalog Card Number: 8-931. 1987

Whitehead J.D. The formation of the sporadic-E layer in the temperate zones. Journal of Atmospheric and Solar Terrestrial Physics, Vol. 20, No.1, 49-58, 1961.

Woo, R., A. Ishimaru, and F.–Ch. Yang , Radio scintillations during occultations by turbulent planetary atmosphers, Radio Sci.,15, 695–703, 1980a.

Woo, R., J. W. Armstrong, and A. Ishimaru, Radio occultation measurements of turbulence in the Venus atmosphere by Pioneer Venus, J. Geophys. Res., 85, 8031–8038, 1980b.

Yakovlev, O.I., Space radio science, Ed. Gordon and Breach Science Publishers, 2001.

Yakovlev, O.I., S.S. Matyugov, and I.A. Vilkov, Attenuation and scintillation of radio waves in Earth's atmosphere from radio occultation experiments on satellite-to-satellite links, Radio Sci., 30, N 3, p. 591, 1995a.

Yakovlev ,O.I., I.A. Vilkov, A.I. Zakharov et al., Frequency shift, time delay, and refraction of radio waves in eclipse experiments along satellite-to-satellite path, J. Communications Technology and Electronics., 40, N 12, p. 73, 1995b.

Yamamoto M., T. Ono, H. Oya, R.T. Tsunoda, M.F. Larsen, S. Fukao, M. Yamomoto, Structures in sporadic -E observed with an impedance probe during the SEEK campaign: Comparison with neutral-wind and radar echo observations. Geophysical Research Letters. 25, No.11, 1781-1792, 1998

Zverev, V.A., Radio optics. Ed. by Soviet Radio. Moscow. 1975 (in Russian).